THE UNIVERSITY OF MICHIGAN

INDUSTRY PROGRAM OF THE COLLEGE OF ENGINEERING

THERMODYNAMIC PROPERTIES OF METHANE AND NITROGEN AT LOW TEMPERATURES AND HIGH PRESSURES

Millard L. Jones, Jr.

A dissertation submitted in partial fulfillment
of the requirements for the degree of
Doctor of Philosophy in The
University of Michigan
Department of Chemical and Metallurgical Engineering
1961

December, 1961

IP-541

ACKNOWLEDGEMENTS

I wish to express my gratitude to the many people and organizations who have assisted me in their research:

I especially want to thank Professor Donald L. Katz, my thesis committee chairman, for his guidance and assistance.

I want to thank the members of my thesis committee, Professors Joseph J. Martin, Gordon J. Van Wylen, Edgar F. Westrum and G. Brymer Williams, for their advice and assistance.

I am indebted to a number of persons who assisted me in construction of equipment, treatment of the data and the many problems encountered. They are: Pratip Bandyopadhyay, graduate student; Edward Rupke and Herbert Senecal of the UMRI Instrument Shop; and Frank Drogosz and Cletus Bollen of the Chemical and Metallurgical Engineering Department. I especially want to thank David T. Mage, who assisted me throughout the course of my research, and Dr. Richard C. Faulkner, Jr., whose work provided a foundation for the present research.

I want to thank the people and organizations who provided materials and technical and financial assistance:

The Phillips Petroleum Company, for the gift of a large quantity of isopentane and pure methane.

The Tennessee Gas Transmission Company, for the gift of a large quantity of pure methane.

Dr. Riki Kobayashi and the Gulf Oil Company, for their aid in obtaining the methane.

The National Bureau of Standards, for advice and aid in the special calibration of thermocouples.

The Computing Center for providing computer time to process the voluminous data of this research.

The National Science Foundation, for a grant without which the present research could not have been undertaken.

The American Chemical Society, for grants for the support of personnel and purchase of equipment.

The Continental Oil Company, for a research fellowship.

TABLE OF CONTENTS

TABLE OF CONTENTS (CONT'D)

LIST OF TABLES

LIST OF TABLES (CONT'D)

LIST OF FIGURES

LIST OF FIGURES (CONT'D)

ABSTRACT

The main objects of this experiment are (1) to refine presently existing flow calorimetric equipment such that it is capable of measurements of isobaric heat capacities (C_p) and latent heats of vaporization of light hydrocarbon gases and their mixtures to accuracy of better than $\pm 1\%$ in the temperature range -250°F to 50°F at pressures to 2000 psia, (2) to determine the heat capacities and latent heats of vaporization of methane, and (3) to use the measured thermodynamic data to construct a new pressure-enthalpy-temperature diagram for methane.

The perfected flow calorimetric equipment utilizes a three stage compressor for circulation. The gas is cooled to the measuring temperature by a series of cooling baths which in turn are cooled by either dry ice or liquid nitrogen. The actual measurement of heat capacity or latent heat is accomplished in a flow calorimeter which is maintained at the measuring pressure and temperature in a constant temperature measuring bath. The primary measurements made are the quantity of heat added to the fluid passing through the calorimeter, the temperature rise of the fluid, and the rate of flow of the fluid. Small corrections are made for heat leakage and pressure drop through the calorimeter.

In the course of refining the measurements and experimental techniques, several measurements of heat capacity and latent heat of vaporization of nitrogen were obtained at low temperatures and high

pressure. Upon perfection of the equipment, thermodynamic properties of methane were determined throughout the region -250 to 50°F, 150 to 2000 psia, except that experimental difficulties made measurements of liquid heat capacity and latent heat below 300 psia impossible. Particular emphasis was placed on measurements of heat capacity near the critical point and in other regions where heat capacity changes rapidly with pressure and temperature. Except that some latent heats of vaporization of methane under pressure have been measured by previous investigators, the data of the present experiment is the first of its type in the low temperature high pressure region. The methane data allows the first accurate calculation of enthalpy properties of compressed liquid or gaseous methane in the critical region.

The results of the methane measurements were used to construct a new pressure-enthalpy-temperature diagram for methane. Since no accurate measurements of the change of enthalpy with pressure or Joule-Thomson coefficients of methane were available from the literature in the range of the experiments, and no such measurements were made, the Benedict-Webb-Rubin equation of state was used to calculate enthalpy as a function of pressure at 50°F, the highest temperature of the chart. Statistical heat capacities were used to extend the diagram to low pressures.

The main conclusions of this experiment are: (1) the experimental equipment allows measurement of latent heats of vaporization to better than $\pm 1\%$ and heat capacities to $\pm 0.5\%$. (2) Equations of state which fit the volumetric data allow calculation of gaseous enthalpies and heat capacities under pressure with fair accuracy at moderate pressure and at higher

reduced temperatures; however, they give results of poor accuracy for gases of high reduced densities, particularly in the critical region. (3) The pressure-enthalpy-temperature diagram presented for methane allows calculation of enthalpy differences to about 1%, and constitutes a considerable improvement in accuracy over recent compilations, where the extension of enthalpy as a function of pressure is based upon equation of state or other treatment of the volumetric data, or upon previous measurements of isothermal expansions. These compilations are shown to be reasonably accurate at higher temperatures and moderate pressures, but allow errors of up to 5 or 10% at higher pressures and low temperatures, and in the region of the critical point.

NOMENCLATURE

a	linear flow meter calibration constant.
a	constant in the Benedict equation of state.
a	constant in the Bloomer-Rao equation of state.
$a_0 \ldots a_3$	calibration constants in the modified flow metering equation.
A	thermocouple calibration constant.
A_o	constant in the Benedict equation of state.
A_o	constant in the Bloomer-Rao equation of state.
$A_2 \ldots A_5$	constants in the Martin-Hou equation of state.
b	linear flow meter calibration constant.
b	constant in the Benedict equation of state.
b	constant in the Bloomer-Rao equation of state.
b	constant in the Martin-Hou equation of state.
B	thermocouple calibration constant.
B_o	constant in the Benedict equation of state.
B_o	constant in the Bloomer-Rao equation of state.
B_1	second virial coefficient.
B_2, B_3, B_5	constants in the Martin-Hou equation of state.
c	constant in the Benedict equation of state.
c	constant in the Bloomer-Rao equation of state.
C	thermocouple calibration constant.
C_o	constant in the Benedict equation of state.
C_o	constant in the Bloomer-Rao equation of state.
C_1	third virial coefficient.

C_1 temperature correction factor for metering pressure.

C_2 temperature correction for the barometer reading.

C_2, C_3, C_5 constants in the Martin-Hou equation of state.

C_P isobaric heat capacity.

C_{PF} apparent isobaric heat capacity at flow rate F.

C_P° ideal isobaric heat capacity.

C_S heat capacity of a saturated fluid.

C_{SL} heat capacity of a saturated liquid.

C_{SV} heat capacity of a saturated vapor.

C_V constant volume heat capacity.

D thermocouple calibration constant.

D_o constant in the Bloomer-Rao equation of state.

D_1 third virial coefficient.

E voltage

E_c voltage across the calorimeter heater.

E_T thermocouple voltage with one set of junctions at the ice point and the other at temperature T.

$E_{L1} \ldots E_{L11}$ voltage corresponding to potentiometer switch positions L1, L2... L11.

F mass flow rate.

g gravitational acceleration.

g_c standard gravitational acceleration.

H enthalpy.

H' enthalpy as a function of pressure at constant temperature.

H° enthalpy of a gas at zero pressure.

ΔH_V isobaric latent heat of vaporization.

Δh uncorrected pressure drop across the flow meter.

I	current.
I_c	current passing through the calorimeter heater.
k	constant in the Martin-Hou equation of state.
$Ll \ldots Lll$	potentiometer switch positions.
M	molecular weight.
P	pressure.
P_b	barometric pressure.
P_b'	barometric pressure reading.
P_{bal}	weight on pressure balance.
P_m	metering pressure.
P_m'	metering pressure reading.
ΔP_c	pressure drop through the flow meter.
Q	volumetric flow rate.
Q	heat input to the calorimeter.
δQ	heat leakage to or from the calorimeter.
δQ	incremental heat input to a system.
R	universal gas constant.
R_0	calibration constant for the platinum thermometer: resistance of the coil at the ice point.
$R_1 \ldots R_9$	standard resistor designations or values.
R_T	resistance at temperature T.
R_{PT}	resistance of the platinum thermometer at temperature T.
sat	indicates path or value along saturation curve.
T	temperature.
T_m	temperature of the gas in the flow meter.
T_r	room temperature.

T_r	reduced temperature.
T_R	temperature of the resistors.
T_s	temperature of the metering pressure manometer scale.
T_{Hg}	temperature of the metering pressure manometer mercury column.
ΔT	temperature difference.
ΔT_c	temperature rise through the calorimeter.
δT	temperature change through the calorimeter with no heat input.
U	internal energy.
V	volume.
V	specific volume of a fluid.
V_G	specific volume of gas.
V_L	specific volume of a liquid.
W	weight of gas collected in a flow calibration run.
$x_1 \ldots x_n$	independent variables.
y	a function of one or more independent variables.
Z	compressibility factor of a gas.
Z_r	compressibility factor of the gas in the flow metering u-tube.
Z_m	compressibility factor of the gas in the flow meter.
α	calibration constants for standard resistors.
α	calibration constants for the platinum resistance thermometer.
α	constant in the Bloomer-Rao equation of state.
α	constant in the Benedict equation of state.
β	calibration constants for standard resistors.
β	calibration constants for the platinum resistance thermometers.
γ	constant in the Benedict equation of state.
γ	constant in the Bloomer-Rao equation of state.

δ	calibration constants for the platinum resistance thermometer.
δ	constant in the Bloomer-Rao equation of state.
θ	time interval for collection of a sample in a flow meter calibration run.
ρ	density.
ρ_r	density of gas in the flow metering u-tube.
ρ_m	density of gas in the flow meter.
ρ_w	density of water in the flow metering u-tube.
σ	estimated uncertainties in measurements.
μ	viscosity.
μ^*	Joule-Thomson coefficient.

INTRODUCTION

In the design of low temperature gas separation or liquefaction plants involving the light hydrocarbon gases and their mixtures, accurate knowledge of the enthalpy properties of the gases involved is of great importance.

With respect to the pure components, the engineer in general has a choice of graphs or tabulations which combine some experimental work with derived properties. In general these works have not been subjected to verification by direct experimental measurement. When dealing with mixtures of light gases the dearth of reliable thermodynamic data makes it necessary for him to rely upon generalized charts or methods of calculation which are of poor or at least unknown accuracy, and which may introduce considerable error into the design. The safety factors which must necessarily be added because of this uncertainty makes the economic design of these plants difficult and adds considerably to the plant installation cost.

It is understandable, then, that with the wider application of low temperature processes considerable effort should be made to resolve the problem of accurate calculation of the enthalpy properties of light hydrocarbon gases and their mixtures in the low temperature range. With this in mind, the goal of the engineer is to provide correlations which will allow him to calculate these properties reliably to a high degree of accuracy. In order to do this it is necessary to obtain experimental data of high accuracy for both pure components and a wide

variety of mixtures with which to test the proposed correlations. There are several methods which may be used to obtain the necessary data. The method chosen is felt to be the most direct and the most accurate of those available, and perhaps involves the most complicated and difficult experimental problems. It consists of the direct measurement of enthalpy differences at constant pressure - heat capacities and latent heats of vaporization - by means of a constant flow calorimeter which may be operated throughout the pressure-temperature range of interest.

The specific objectives of the present experiment are:

1. To refine and perfect existing calorimetric equipment to the extent that it is capable of measurement of isobaric specific heats and latent heats of light hydrocarbon gases and their mixtures to better than 1% in the range -250 to 50°F, at pressuresto 2000 psia.

2. To measure the specific heats and latent heats of methane in the aforementioned temperature-pressure range.

3. To use the measured methane data to construct a new pressure-enthalpy-temperature diagram for methane.

This investigation of methane constitutes the first thermodynamic data obtained in a broad program to determine and correlate the thermodynamic properties of light hydrocarbon gases and their mixtures in the low temperature, high pressure region.

EXPERIENCE OF PREVIOUS INVESTIGATORS

The literature will be reviewed under a series of topics covered in this research beginning with thermodynamic theory.

Theoretical Background

The thermodynamic theory of pure fluids is well developed and is presented in a number of textbooks such as that of Dodge.[17] The reader is referred to such texts for the derivations of the following equations which are applicable to the present investigation.

The enthalpy of a pure fluid is defined by the equation,

$$H = U + PV \qquad (1)$$

where U is the internal energy of the substance, and P and V are the independent variables, pressure and volume. The value of enthalpy is dependent only upon the state of the substance, and is not dependent upon the path traversed in reaching that state. In all but a few special systems the effect of magnetic fields, gravitational fields, etc. are negligible and the enthalpy of a single phase, single component substance may be expressed in terms of any two of the variables, temperature, pressure, and volume. Using pressure and temperature, the following exact differential equation may be written:

$$dH = \left(\frac{\partial H}{\partial T}\right)_P dT + \left(\frac{\partial H}{\partial P}\right)_T dP \qquad (2)$$

The quantity $(\partial H/\partial T)_P$ is defined as the isobaric heat capacity, C_P.

The change of enthalpy with pressure, $(\partial H/\partial P)_T$, may be expressed in terms of the heat capacity at constant pressure and the Joule-Thomson

coefficient in the equation

$$\left(\frac{\partial H}{\partial P}\right)_T = -\left(\frac{\partial H}{\partial T}\right)_P \left(\frac{\partial T}{\partial P}\right)_H = -C_P \mu^* \tag{3}$$

or in terms of temperature, pressure and volume.

$$\left(\frac{\partial H}{\partial P}\right)_T = V - T\left(\frac{\partial V}{\partial T}\right)_P \tag{4}$$

Thus, enthalpy changes between any two states may be determined by integration along any path, using isobaric heat capacities and either values of $(\partial H/\partial P)_T$, Joule-Thomson coefficients, or volumetric data. Practically, integration is usually done along constant pressure and constant temperature paths. The completed equation, then, is

$$H_2 - H_1 = \int_{T_1}^{T_2} C_P dT + \int_{P_1}^{P_2} \left(\frac{\partial H}{\partial P}\right)_T dP \tag{5}$$

Similar equations may be derived for internal energy,

$$dU = \left(\frac{\partial U}{\partial T}\right)_V dT + \left(\frac{\partial U}{\partial V}\right)_T dV \tag{6}$$

where $(\partial U/\partial T)_V$ is the heat capacity at constant volume, C_V. The change of U with volume at constant temperature is expressed by the equation,

$$\left(\frac{\partial U}{\partial V}\right)_T = -P + T\left(\frac{\partial P}{\partial T}\right)_V \tag{7}$$

The heat capacities, C_P and C_V are related by the equation,

$$C_P - C_V = T\left(\frac{\partial P}{\partial T}\right)_V \left(\frac{\partial V}{\partial T}\right)_P \tag{8}$$

which reduces to

$$C_P - C_V = R \tag{9}$$

at low pressure where gases approach the ideal condition.

The dependance of C_P and C_V on pressure and volume, respectively, are given by the equations

$$\left(\frac{\partial C_P}{\partial P}\right)_T = -T\left(\frac{\partial^2 V}{\partial T^2}\right)_P \tag{10}$$

$$\left(\frac{\partial C_V}{\partial V}\right)_T = T\left(\frac{\partial^2 P}{\partial T^2}\right)_V \tag{11}$$

Equation (5) may be modified to include paths through the two phase liquid-vapor region by adding the term ΔH_V, the isobaric latent heat of vaporization to the right side, giving

$$H_2 - H_1 = \int_{T_1}^{T_2} C_P dT + \int_{P_1}^{P_2} \left(\frac{\partial H}{\partial P}\right)_T dP + \Delta H_V \tag{12}$$

This equation implies a constant pressure path through the two phase region, but any path could be used with modification of the term ΔH_V to designate the enthalpy difference.

The isobaric latent heat of vaporization may be related to other saturated properties by the familiar Clapeyron equation,

$$\left(\frac{dP}{dT}\right)_{sat} = \frac{\Delta H_V}{T(V_G - V_L)} \tag{13}$$

or the equation,

$$C_{SV} - C_{SL} = \frac{d(\Delta H_V)}{dT} - \frac{\Delta H_V}{T} \tag{14}$$

where C_S is defined as

$$C_S = \left(\frac{\delta Q}{\delta T}\right)_{sat} \tag{15}$$

and is related to the isobaric heat capacity and the slope of the vapor-pressure curve by the equation,

$$C_S = C_P - T\left(\frac{\partial V}{\partial T}\right)_P \left(\frac{dP}{dT}\right)_{sat} \tag{16}$$

The enthalpy change along the saturation line may be calculated by the equation,

$$dH_{sat} = C_S dT + VdP \tag{17}$$

Heat Capacities of Gases

The heat capacity is one of the most important quantities in the determination of the enthalpy of a gas. It may be calculated at zero pressure from molecular data or it may be measured experimentally by a number of direct or indirect methods. Partington and Shilling's book, "The Specific Heats of Gases"[61] constitutes a fine summary of experiments and data published before 1924, and includes a detailed description of the classical methods used in the measurement of C_P, C_V, and C_P/C_V. Measurements were usually at low pressure, and seldom covered a large temperature range. However, in the early 1900's some experiments were undertaken to determine the effect of pressure and temperature on heat capacity. The works of Scheele and Heuse[31,69,70] and Holborn and Jacob[32] are good examples of early investigations of the effects of temperature and pressure, respectively, on heat capacity.

The experimental methods used recently in the measurement of heat capacity are (1) Flow calorimetry, (2) Constant volume calorimetry, (3) Heat Exchanger, (4) Explosion, (5) Isentropic expansion, (6) Velocity

of sound, (7) Resonance, (8) Self-sustained oscillation, (9) Flow comparison, (10) Constant volume comparison, and (11) Heat exchanger using a different fluid.

Masi[50] reviews the first ten methods in some detail, and lists the measurements made with them in the period 1924-1954. Method eleven was used by Brown and others[23,37,41,44,55,62,73] to compare the heat capacities of various hydrocarbons to that of water.

The more indirect methods of extending heat capacity as a function of pressure might be added. Joule-Thomson coefficients, direct measurements of $(\frac{\partial H}{\partial P})_T$, or equations of state may be used in this respect.

The Constant Flow Calorimetric Method

Of the many methods used in determining heat capacities the most versatile and useful method, particularly for light gases, is the constant flow calorimetric method developed by Callendar[9]. It consists of a device for moving gas through a vessel at a constant measurable rate, with the addition of a measured quantity of electrical heat and measurement of the temperature rise produced in the fluid.

While quite simple in theory it should be noted that the design and construction of flow calorimetric apparatus for precision work is exceedingly complicated. Extreme care must be exercised in order to (1) Reduce heat leakage due to convection, conduction and radiation to a minimum, (2) Assure the accomplishment and accurate measurement of very steady flow, and (3) Accomplish accurate measurement of the true temperatures of the fluid. Extension to extreme pressure and temperature accentuates these problems and adds many more.

The experimental difficulty of the constant flow method, however, is offset by certain advantages. It yields direct measurements and does not depend upon equations of state or upon the relative heat capacities of other gases. The corrections due to heat leakage are easily made and are usually quite small. The degree of accuracy obtainable is high, and depends primarily upon the amount of effort put into the design and construction of the apparatus and the refinement of technique. With respect to constant volume calorimetry, a direct method used primarily for specific heats of liquids and solids, the constant flow method has one outstanding advantage. The heat capacity of the calorimeter in no way enters into the heat capacity calculations. This makes the constant flow method especially suitable for the measurement of heat capacities of light gases under pressure, where the corrections for the heat capacity of a constant volume apparatus would be large compared to that of the gas contained.

A number of excellent investigations using the constant flow method have been undertaken in the past. The apparatus used and the materials investigated have been reviewed by Partington[61], Masi[50] and Faulkner[22]. Faulkner also gives a detailed description of the apparatus used as a basis for the apparatus of the present investigation along with the details of its design and operation.

The Isobaric Latent Heat of Vaporization

The constant flow calorimetric method lends itself readily to the measurement of the isobaric latent heat. Almost any calorimeter of this type which will allow liquids to be circulated may be modified to measure latent heats. Constant volume apparatus may also be easily adapted to the measurement of latent heat, by removing the evaporated gas at constant pressure.

Osborne and Ginnings[59] and Hesterman and White[30] have adapted this method to the measurement of latent heats under pressure.

The latent heat of vaporization of a pure compound may also be calculated using the Clapeyron Equation (13) if the vapor pressure data and the saturated volumetric data of the substance are known. The work of Bloomer and Rao[6] on the thermodynamic properties of nitrogen is a good example of this method.

Enthalpy Properties of Methane and Nitrogen

A review of the literature was undertaken in order to determine the degree to which the enthalpy properties of methane and nitrogen had been investigated in the pressure-temperature range of the present experiment, and to provide data for comparison with that of the present experiment.

Gaseous Heat Capacities

Experimental determinations of low pressure gaseous heat capacities have been reported in the literature for both methane [21,31,43,54,67] and nitrogen[7,16,21,29,31,72]. Flow calorimetry, isentropic expansion, velocity of sound and other methods have been used with good results over wide temperature ranges. The flow calorimetric determinations of Scheele and Heuse[31] in the range - 180 to 20°C and the isentropic expansion determination of Eucken and Lude[21] in the range 0 to 200°C are among the best atmospheric determinations. A number of statistical determinations of the zero pressure heat capacity have been made for both methane[2,14,63] and nitrogen[27,28,33,74] which are felt to be of the same order of accuracy as the best experimental measurements.

Determinations of the gaseous heat capacity of methane or nitrogen under pressure are few. Lussana[45,46] made measurements on methane in the range 20 to 90°C, at pressures of from 6 to 35 atmospheres, and Katz[34] used the resonance method at 23°C at pressures up to 5 atmospheres. Macky and Krase[47] investigated the heat capacity of nitrogen from 30 to 150°C at pressures up to 800 atmospheres using a flow calorimeter and Workman[78] used the heat exchanger method to measure the heat capacity of nitrogen from 20 to 60°C at pressures up to 60 atmospheres. The explosion method was used by Newitt[57] to investigate the constant volume heat capacity of nitrogen at high temperatures. Clark and Katz[11] used the resonance method to obtain the heat capacity ratio of nitrogen at 23°C up to 25 atmospheres.

No previous experimental measurements of the heat capacity of gaseous methane or nitrogen at low temperature and high pressure were found.

Liquid Heat Capacities

A number of measurements of the saturated liquid heat capacity, C_{SL} have been made for both methane[12,20] and nitrogen[12,18,27,36] below their boiling points, usually in coordination with measurements on the heat capacity of solidified gases or latent heats of phase transition. Wiebe and Brevoort[76] measured the saturated liquid heat capacity of both methane and nitrogen from their boiling points to their critical point. Hesterman and White[30] measured the saturated liquid heat capacity of methane from its boiling point to its critical point.

Latent Heats of Vaporization

A number of early determinations of the latent heat of vaporization of nitrogen at atmospheric pressure have been accomplished[1,13,15,18,27,71], with considerable disagreement as to the true value. It appears that the most recent and reliable investigation is that of Giaque and Clayton[27] who also measured liquid heat capacities and heats of transition of nitrogen.

The only experimental determinations of the latent heat of vaporization of methane to date are those of Frank and Clusius[24] who measured it at 5 psia, and Hesterman and White[30] who used a constant volume calorimeter to measure latent heat at a number of pressures between one atmosphere and the critical pressure. The latter constitutes the only experimental determination of the latent heat of methane or nitrogen under pressure previous to the present investigation.

Derived Properties

Since the experimental data for methane and nitrogen is sparse in the low temperature, high pressure range covered by the present investigation, it is desirable to refer to compilations of derived and experimental data which cover the desired range, and to methods which may be used to calculate properties of comparison.

The most recent and complete compilations of the thermodynamic properties of methane and nitrogen are those of Matthews and Hurd[52] and Keesom[35] for methane and Bloomer and Rao[6] for nitrogen. The properties of gaseous nitrogen have been presented recently in NBS Circular 564[74]. The change of enthalpy or heat capacity with pressure may be calculated

either graphically from volumetric data, or from equations of state which fit the volumetric data such as those of Benedict, Webb and Rubin[4] or Martin and Hou[49].

APPARATUS

The apparatus used in this experiment was essentially the same as that used by R. C. Faulkner[22] in his experiments on nitrogen. It was improved in some ways to eliminate the problems he encountered. This section is intended to give the reader a general knowledge of the apparatus as it now stands, and a detailed description of the major equipment which has been added, including the elaborate flow rate calibration apparatus. A detailed description of the many important aspects of design of the original equipment is available in Dr. Faulkner's thesis.

The Flow System

A schematic diagram of the flow system is shown in Figure 1. The gas under consideration is first compressed to high pressure (1000-2500 psia) where the compressor oil and any remaining water are removed. It is then throttled to the approximate measuring pressure (150-2000 psia) and split into two streams, one being throttled into the intake of the compressor for recirculation. The other stream is passed through a dry ice cooler and a stirred bath cooler where it is brought to the approximate measuring bath temperature (-250° to 30°F), and then into the controlled temperature measuring bath where it is conditioned to the bath temperature by circulation through a coil of tubing. The gas then enters the calorimeter, which is immersed in the measuring bath. A measured quantity of heat is added and the temperature rise, pressure, and pressure drop are measured. After leaving the calorimeter the gas is warmed to room temperature, throttled to about 80 psig, rewarmed if needed and passed into the flow metering bath

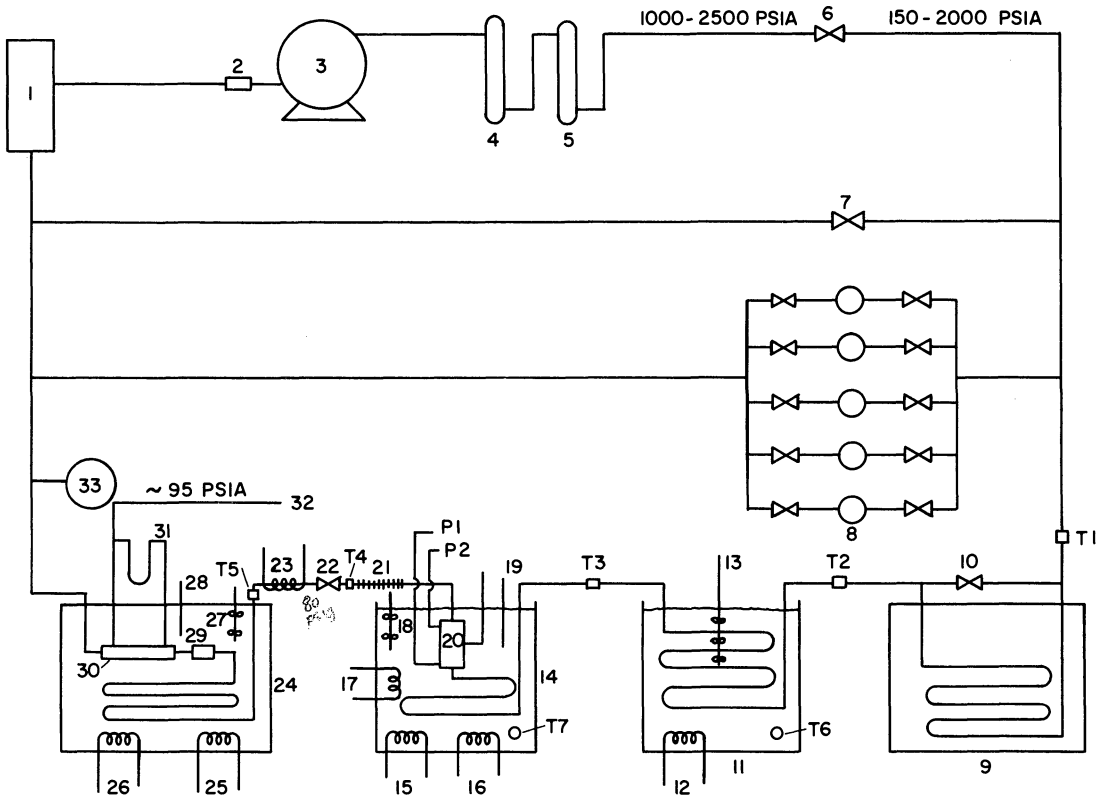

Figure 1. Flow Diagram of the Apparatus.

LEGEND FOR FIGURE 1

1. Compressor input buffer tank
2. Micron filter
3. Compressor, 4 SCFM
4. Oil removal unit (activated charcoal)
5. Water removal unit (anhydrous calcium sulphate)
6. Metering valves
7. Calorimeter bypass metering valves
8. Gas storage and buffering tanks
9. Dry ice cooler
10. Bypass valve
11. Low temperature cooling bath
12. Liquid nitrogen cooling
13. Stirrer
14. Low temperature measuring bath
15. Liquid nitrogen cooling
16. Controlled heat input
17. Nickel resistance-sensor for heat input controller
18. Stirrer
19. Platinum thermometer
20. Calorimeter
21. Finned tubing
22. Calorimeter metering valves
23. Line heater
24. Metering bath
25. Water cooling
26. Controlled heating
27. Centrifugal stirrer
28. Thermometer
29. Micron filter
30. Flow meter
31. U-Tube and cathetometer
32. Lead to 180" mercury manometer
33. Buffer tank

T1,T2, ... T7 System thermocouples

where it is brought to bath temperature in a large coil of tubing. It is then passed through the flow meter where the flow rate is determined. The gas then returns to the intake of the compressor to be recycled. Stability of both flow rate and pressure is aided by the buffer tanks shown, and by the volumes of the purification units on the output of the compressor. When needed, gas may be let in or out of the flow system via the storage tanks. The system temperatures are monitored by means of a Honeywell indicating potentiometer and the system pressures by means of various pressure gages.

The main difference between the present flow system and that of Faulkner's is the substitution of the presently used stirred bath cooler, which is cooled by liquid nitrogen, for direct liquid nitrogen cooling. This makes the cooling of the gas to measuring bath temperature much easier and more reliable, and eliminates the instability problems which he encountered.

The Flow Calorimeter

The calorimeter used in this experiment was a modification of that used in the experiments of R. C. Faulkner, Jr.[22] and is shown in Figure 2. The gas, after being brought to the temperature of the measuring bath, enters the calorimeter through the tubing in the lower section, passes through the thermocouple well, through the coil of tubing which goes into the upper section of the calorimeter, and into the calorimeter heating capsule. A measured amount of electrical energy is added here by passing direct current through a nichrome wire resistance heater enclosed in the capsule, and the gas is passed out of the capsule, through the second thermocouple well and

1. ENTRANCE THERMOCOUPLE WELL
2. MECHANICAL PARTITION
3. CALORIMETER HEATER CAPSULE
4. CALORIMETER HEATER BAFFLES
5. CALORIMETER CONDITIONING BAFFLES
6. EXIT THEROCOUPLE WELL
7. MAIN RADIATION SHIELD
8. RADIATION SHIELD
9. LINE OF SIGHT RADIATION SHIELD
10. CONAX MIDGET THERMOCOUPLE GLAND
11. CALORIMETER HEATER LEADS
12. ENTRANCE PRESSURE TAP
13. EXIT PRESSURE TAP
14. VACUUM LINE

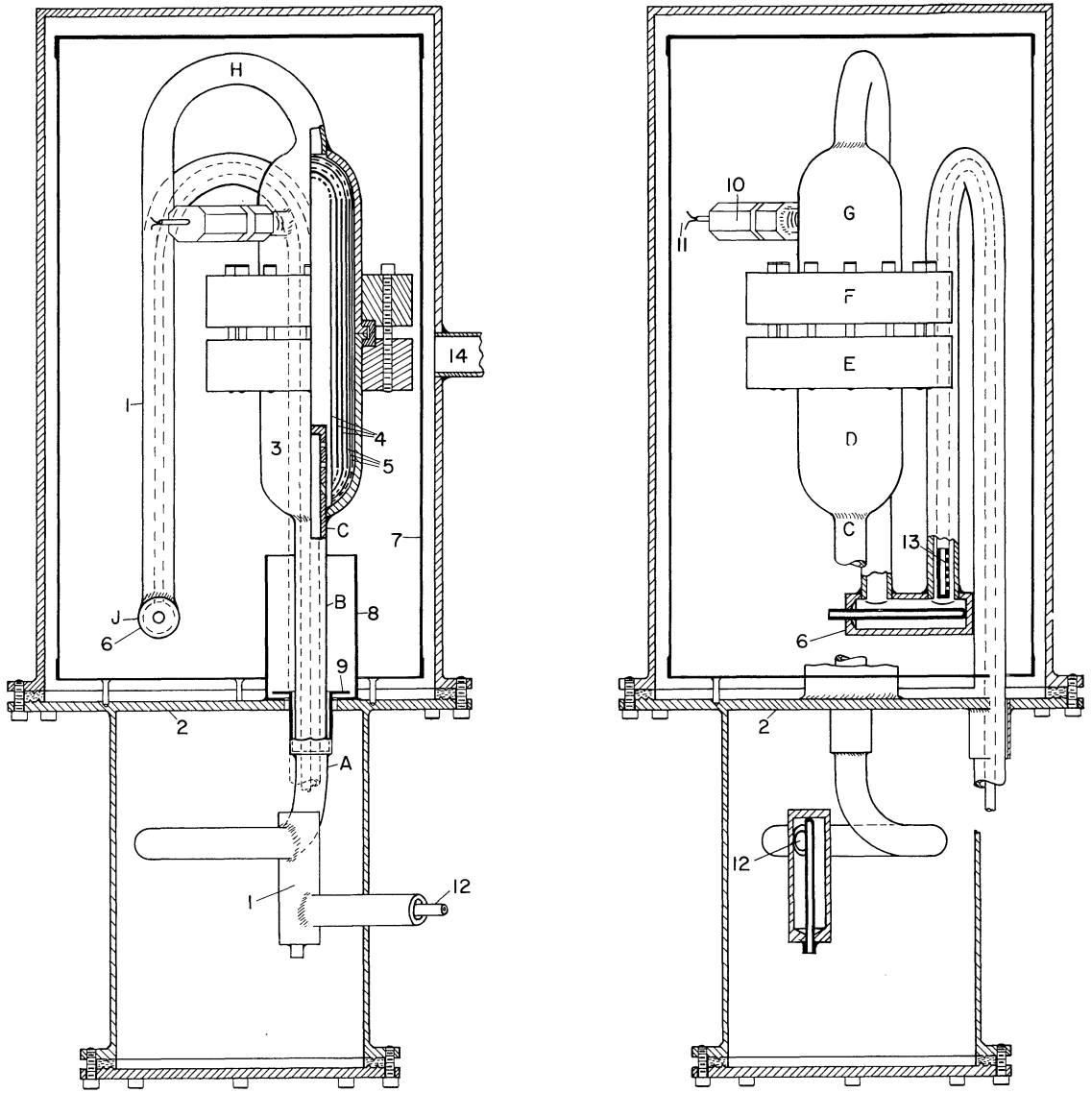

Figure 2. Constant Flow Calorimeter.

TABLE I

TEMPERATURE PROFILE OF THE CALORIMETER

Location (Figure 2)	Percent Measured Temperature Rise	
	High Flow Rate	Low Flow Rate
A	0.00	0.00
B	0.25	0.50
C	52.1	63.2
D	94.7	94.0
E	98.0	96.0
F	99.0	98.6
G	99.2	99.1
H	100.15	100.6
I	100.23	101.1
J	100.00	100.0

out of the calorimeter through the vacuum insulated exit tube. The temperature rise is measured by a six-junction, copper-constantan thermocouple between the two thermocouple wells, and provision is made for installation of difference thermocouples to measure temperature differences between any two points in the calorimeter.

Inspection of Figure 2 shows that the calorimeter consists of two distinct sections. Both are kept under high vacuum to minimize heat loss due to conduction and convection. The lower section which contains the inlet thermocouple well is maintained at the inlet or bath temperature, "T_1". The upper section, containing the heater capsule and the exit thermocouple well is maintained at the temperature of the gas after the heat has been added, "T_2". The lower section is separated thermally from the upper by the mechanical partition which remains at the bath temperature. The upper section is separated thermally from the bath surroundings and the mechanical partition by the calorimeter guard, which is maintained at the exit temperature. It acts as a shield against heat loss from the heater capsule via radiation and conduction.

In order to reduce heat leakage as much as possible, it is desirable to have the skin of the calorimeter entrance tube change sharply from T_1 to T_2 in the region between the partition and the heater capsule. This is accomplished by the internal baffling of the calorimeter heater capsule. Firstly, the incoming gas scavenges the heat conducted from the calorimeter capsule at T_2 to the entrance tube at T_1, raising the gas temperature slightly. Then the gas is heated to a temperature slightly above T_2 by passage over the nichrome wires on the inner baffles, circulated through the outer baffles to even out its temperature, and passed along the inside of the

shell of the heater capsule from its base to its exit. In this last operation the gas is cooled to T_2, replacing the heat lost to the entrance tube. This results in an extremely sharp temperature gradient at the base of the calorimeter, as desired. Table I shows the temperature profile of the calorimeter at both high and low flow rates. The letters A, B, etc., refer to locations where thermocouples were placed and are shown in Figure 2.

The calorimeter was modified in the following ways to eliminate most of the problems present in previous experiments.

1. A Conax thermocouple gland with lava sealant was installed as the seal for the calorimeter power input leads. This eliminated leakage from the high pressure calorimeter to the vacuum system under all conditions.

2. The vacuum seals and piping were replaced and/or improved such that vacuum of one micron or better was achieved for most data runs.

3. The calorimeter was modified to remove as much weight as possible, and to further eliminate possible heat leaks. Heater and thermocouple leads, and the six-junction thermocouple were brought into thermal contact with appropriate parts of the calorimeter and calorimeter guard in order to minimize errors due to heat transfer through these wires. The wires were first tied in place and then brought into thermal contact by use of either Apiezon grease or epoxy resin. Both methods seemed to work satisfactorily.

Measuring Instruments

The major measurements of this experiment were (1) Temperature of the controlled bath, (2) Temperature rise through the calorimeter, (3) Heat input to the calorimeter, (4) Pressure of the measurement,

(5) Pressure drop through the calorimeter, and (6) Flow rate. The instruments used in these measurements are discussed in the following. A discussion of the accuracy factors involved is given in Appendix A.

Electrical Measurements

The measurements of bath temperature, temperature rise through the calorimeter, and heat input to the calorimeter involve the measurement of small emfs generated by thermocouples or produced by current flow through calibrated resistors. The instrument used in these measurements was a calibrated Leeds and Northrup Type K-3 potentiometer, connected to the various quantities to be measured through a multiposition switch. The potentiometer is capable of measuring emfs of the range of those of the present experiment to $\pm$ 0.01%. Its complete calibration characteristics are shown in Table XXXII, Appendix E.

Leeds and Northrup National Bureau of Standards type resistors were used where needed to scale large voltages to potentiometer range, or where needed to measure current. The resistors used were immersed in a stirred oil bath in order to keep them at a known temperature. The values of resistance are given by the equation,

$$R_T = R_{25}(1 + \alpha(T_R-25) + \beta(T_R-25)^2) \qquad (18)$$

where T_R is the temperature of the bath, degrees Centigrade, and R_T is the resistance at that temperature. The resistance at 25°C, R_{25}, and the calibration constants α and β were determined by the Leeds and Northrup Company. Values of these constants for the resistors used in this

experiment are given in Table XXXIII, Appendix E. The resistances calculated by Equation (18) are stated to be accurate to 0.01% by the manufacturers.

Heat Input

Figures 3 and 4 are schematic diagrams of the two sets of apparatus which were used to supply and measure the heat input to the calorimeter. The apparatus in Figure 3 was used in most of the experiments on nitrogen, but was replaced by the apparatus in Figure 4 to give higher heat input with better regulation and stability.

The original direct current power supply used was a Lambda Model 65 M, delivering up to 0.6amps direct current at 100 volts with 0.25% regulation. Although satisfactory results were obtained with this instrument operation was very difficult due to its instability. The power supply which replaced this unit was a Kepco Model SM325-2MX transistorized supply capable of delivering up to 2.0 amps at 325 volts, with 0.01% regulation. The characteristics of these two power supplies are given in Table XXXVI, Appendix E.

Bath Temperature Measurement

The temperature of the calorimeter bath was determined by passing a small direct current through a platinum resistance thermometer immersed in the bath and measuring the current through and voltage across it. The resistance calculated was then used to give the temperature of the bath by use of the modified form of the Callendar equation,

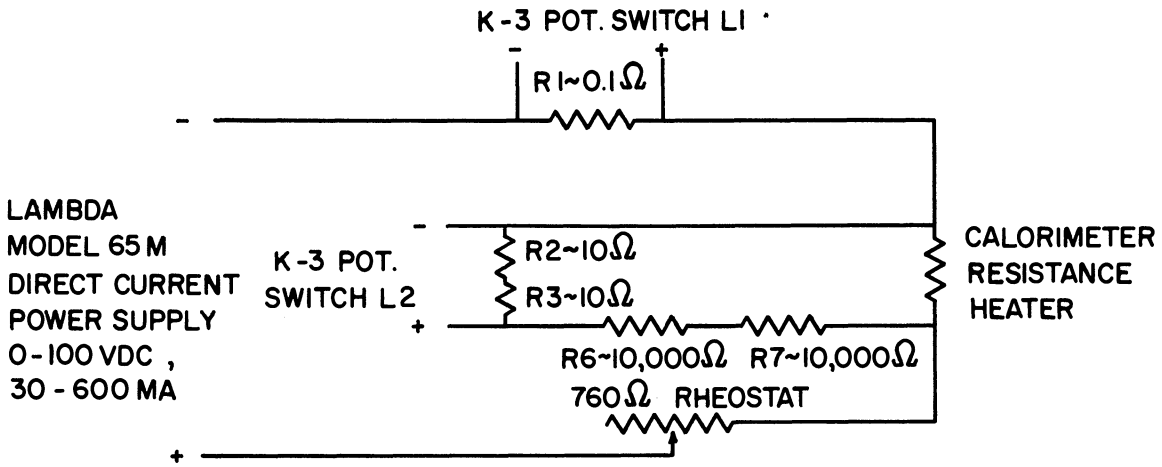

Figure 3. Heat Input Wiring Diagram, Initial Power Supply.

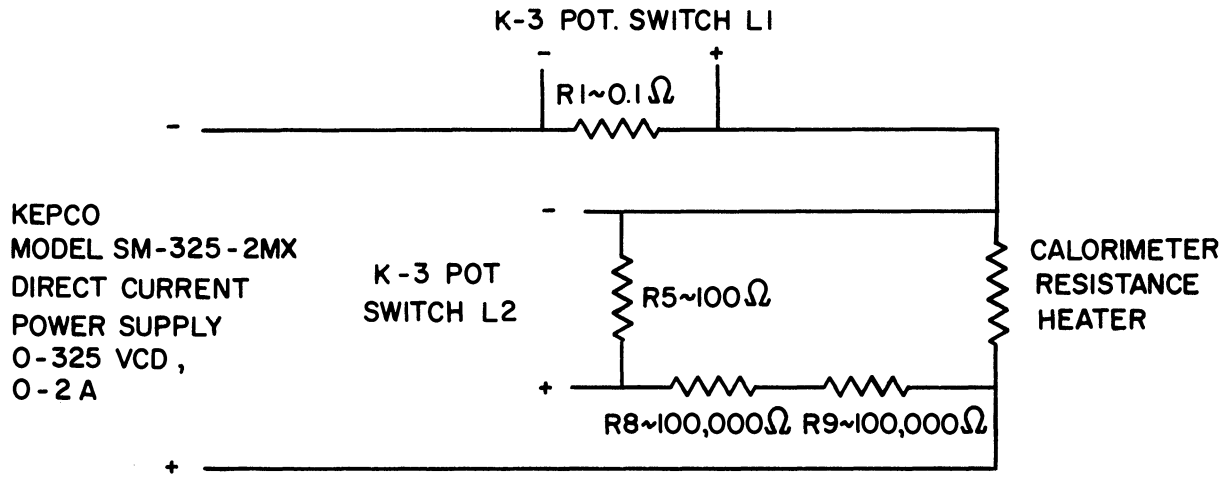

Figure 4. Heat Input Wiring Diagram, Improved Power Supply.

$$T = \frac{R_{PT}-R_0}{\alpha R_0} + \delta\left(\frac{T}{100} - 1\right)\left(\frac{T}{100}\right) + \beta\left(\frac{T}{100} - 1\right)\left(\frac{T}{100}\right)^3$$

where T is the temperature of the bath, degrees Centigrade and R_{PT} is the resistance of the platinum coil at T°C. The resistance of the platinum coil at 0°C, R_0 and the three calibration constants, α, δ and β were determined by the Leeds and Northrup Co. for the first thermometer used, and by the National Bureau of Standards for the second. In both cases, R_0, α and δ were determined from calibrations at the ice, steam, and sulphur points. The constant β, which is used only at temperatures below the ice point, was determined by calibration at the boiling point of oxygen.

Figure 5 shows the wiring diagram for the platinum thermometer, and the calibration constants are listed in Table XXXIV, Appendix E.

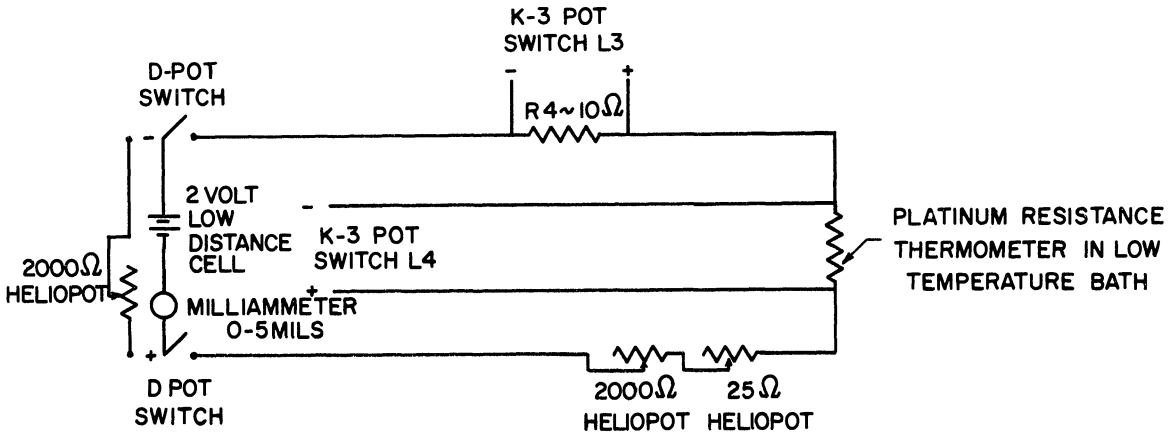

Figure 5. Platinum Thermometer Wiring Diagram for Calorimeter Bath Temperature.

Measurement of Temperature Rise

The temperature rise through the calorimeter was measured by use of a calibrated six-junction copper-constantan thermocouple. Two thermocouples were made as carefully as possible from B. and S. gage #36 copper and #30 constantan wire. They were calibrated at the National Bureau of Standards by comparison with a platinum thermometer every 20°C from 0°C to 120°C, and at the liquid oxygen and liquid nitrogen points. The values of emf obtained were smoothed by fitting them to a cubic equation in temperature

$$E_T = A + BT + CT^2 + DT^3 \qquad (20)$$

where E_T is the emf produced by the thermocouple between 0 degree Centigrade and T degrees Centigrade, and the constants A, B, C, and D are determined by the method of least squares. The results of this treatment are shown in Table XXXI, Appendix E, which lists the measured and calculated emfs, the deviations, and the calibration curve constants for the two thermocouples used. Thermocouple G25691T is the better of the two, and was used in all but the very early experiments.

As previously stated in the description of the calorimeter, the thermocouple was brought into thermal contact with the calorimeter in such a way as to eliminate error due to heat transfer through the thermocouple wires.

It is estimated that the error in the measurement of temperature rise using thermocouple G25691T as described is within 0.2% for temperature rises of the order of 10°C or 20°F.

Pressure Measurement

The pressure of each measurement was taken as the mean pressure,

$$P = \frac{P_1 + P_2}{2} = P_1 + \frac{\Delta P_{ic}}{2} \qquad (21)$$

where P_1 is the pressure at the inlet thermocouple well and ΔP_{ic} is the pressure drop across the calorimeter (measured at the thermocouple wells).

The inlet pressure, P_1 was measured by a dead weight pressure balance of the rotating piston type designed by Roebuck(64) for Joule-Thomson measurements. The diameter of the piston was found to be 0.2479± 0.0001 inches, which corresponds to an area of 0.048266± 0.0004 square inches or a pressure of 20.717 psi ± 0.1% per pound of weight. The weights used conformed to Class C standards. Any deviation within these standards is negligible with respect to the error caused by the piston diameter.

Pressure drop across the calorimeter was measured by means of a 40 inch high pressure bottom well mercury manometer built by the Meriam Instrument Company, Inc.

Flow Metering

The flow meter used in the present experiment was a "Linear Flow Meter," manufactured by the National Instrument Laboratories for measurement of flow rates of light gases under pressures from 60 to 130 psia. It consists of a flow restriction designed for flow in the laminar flow range coupled with a U-tube and cathetometer to measure pressure drop and a 180" mercury manometer to measure pressure. The temperature of the measurement was set by flowing the gas through a length of tubing immersed in the constant temperature metering bath, and then into the flow restriction which was also immersed in the bath, as shown in Figure 1.

Although the precision of this equipment was excellent, being about 0.1%, accurate calibration was obtained only with great difficulty. The flow restriction was calibrated by the manufacturer at pressures from 60 to 130 psia as a function of flow rate, and the calibration given in the form,

$$\rho_m \Delta P_m = b\mu F + aF^2 \qquad (22)$$

where ρ_m is the density of the gas in the flow meter, Lb/Ft^3, ΔP_m the pressure drop across the flow meter, standard inches of water, μ the viscosity of the gas, micropoises and F the mass flow rate, Lb/Min. The values a and b were calibration constants given as functions of pressure. The accuracy of flow rate measurements made using the above equipment and calibration was felt to be well within 0.5%, based on the manufacturers' claims.

In the early experiments on nitrogen attempts were made to measure values of heat capacity using flow rates calculated from the calibration constants provided by the manufacturer. Although the precision of the calculated heat capacities was excellent, the absolute values were unrealistic and could not be corrected for heat leakage by the usual processes (see Reduction of Data). It was apparent that some instrument was either out of calibration or functioning improperly, so all instruments and measurements were checked. The flow restriction was returned to the manufacturer for checking, and its calibration found to be unchanged.

Further measurements on nitrogen indicated that the same problem existed, and every possible source of error was investigated and cleared, with the exception of the flow rate measurement. At this point the manufacturers suggested that the flow restriction may have become contaminated,

so the author took the flow meter directly to the manufacturer and assisted personally in its cleaning and recalibration. In reducing the calibration data the author found that the methods used by the manufacturer in reducing the original data to give the original calibration curves were grievously in error.

The calibration curves had been obtained by use of a variation of Equation (22),

$$\frac{\Delta P_m}{\mu Q} = b + a\frac{\rho_m Q}{\mu} \qquad (22a)$$

where Q is the volumetric flow rate, and should be in units of ft^3/min. But the constant "a" which was determined as the slope of the line obtained by plotting $\frac{\Delta P_m}{Q\mu}$ versus $\frac{\rho_m Q}{\mu}$ had been obtained using units of grams per liter for the density, and reported unchanged for use with units of pounds per cubic foot. Further, the raw data which the manufacturers obtained in the recalibration was of such poor precision that the desired accuracy of 0.1% could not possibly be achieved.

At this point it was decided to construct a flow calibration apparatus capable of determining the calibration curves to better than 0.1%, and the subsequent calibration showed that the new calibration given by the manufacturers using the correct units was in error by about 2.5%. It also showed that the calibration data cannot be accurately fitted by the linear equations (22) or (22a), but that a cubic or higher order equation must be used.

The above activities added approximately one year to the length of the experiments, beyond the time which would have been required to take an uncalibrated meter, build calibration equipment, and calibrate it.

Calibration of the flow metering apparatus was achieved by the construction and use of the equipment shown schematically in Figure 6, attached to the exit of the flow meter. The high pressure sample tanks are of the type shown in Figure 7. This equipment is merely a device for collecting the timed throughput of the flowmeter in order to determine the rate of flow by direct weighing and correlate it with the flow variables. With the dewars full of liquid nitrogen, and the reservoir and sample tanks immersed, the metering pressure is set at the desired value using the pressure regulator, and the flow rate is set by adjusting the metering valve. The throughput of the flow meter is condensed in the reservoir tank until the flow comes to steady state. At this point the electrical switch is thrown, activating the timer and solenoid valve simultaneously, and diverting the flow to the aluminum sample tank. The major flow variables, pressure and pressure drop are then measured and monitored until the required quantity of gas is collected in the sample bottle, and the switch released. The sample bottle is then closed off, allowed to rise to room temperature and weighed to determine the throughput of the meter. The gas in the sample tank and the reservoir tank are both returned to the intake of the compressor for recompression.

Considerable attention was given to detail in both the design and operation of this calibration apparatus in order to obtain satisfactory accuracy. Sample calculations for a typical run are included in Appendix D, showing in detail the calculations and corrections used.

The flow meter was calibrated for both methane and nitrogen, and the results for each gas correlated by the equation,

1. Line from Compressor Output
2. Storage Tank
3. Pressure Regulator
4. Metering Bath
5. Conditioning Coil
6. Cooling Water
7. Controlled Heat Input
8. Micron Filter
9. Stirrer
10. Thermometer
11. Flow Meter
12. U-Tube and Cathetometer
13. Lead to 180" Mercury Manometer
14. Shut-Off Valve
15. Metering Valve
16. Vacuum Lead
17. Micron Filter
18. Three Way Solenoid Valve
19. Reservoir Tank
20. Liquid Nitrogen Dewar
21. High Pressure Sample Tank
22. Liquid Nitrogen Dewar
23. Timer
24. Electric Switch
25. Return to Compressor Intake

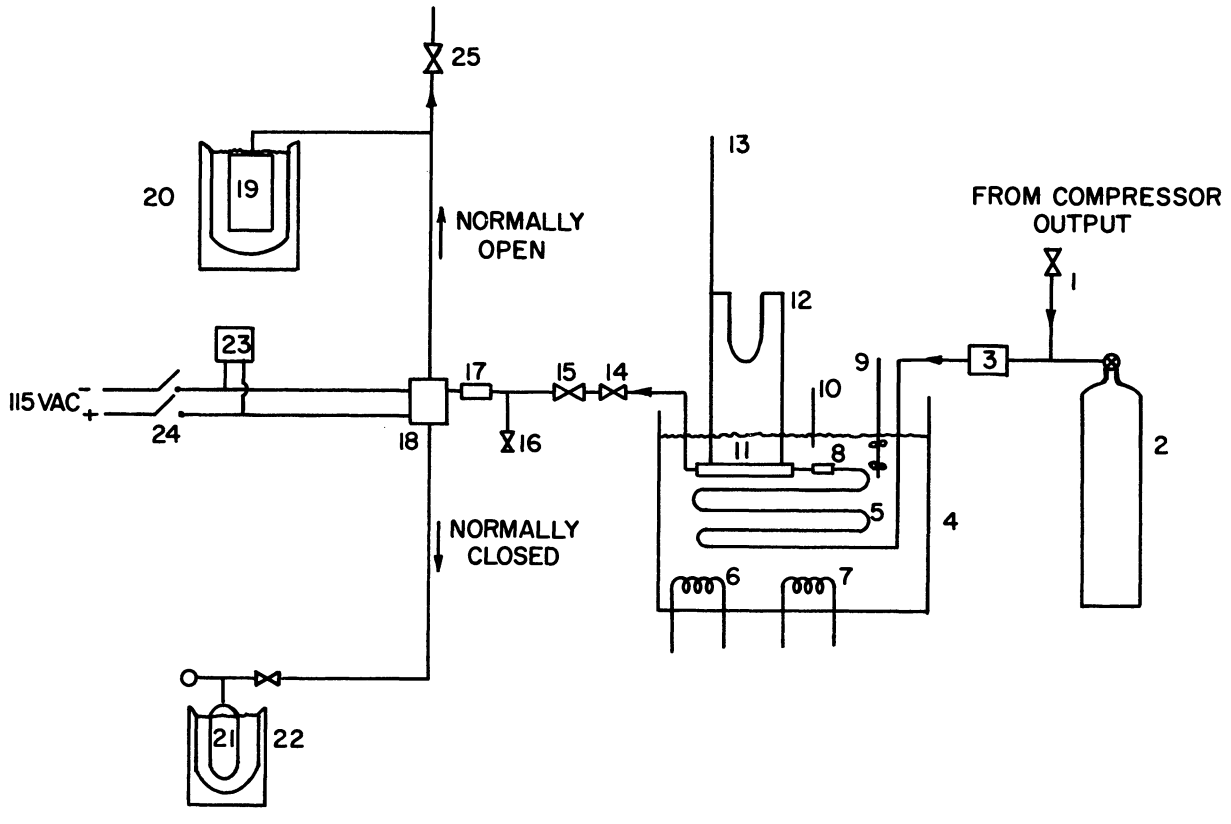

Figure 6. Mass Flow Calibration Apparatus

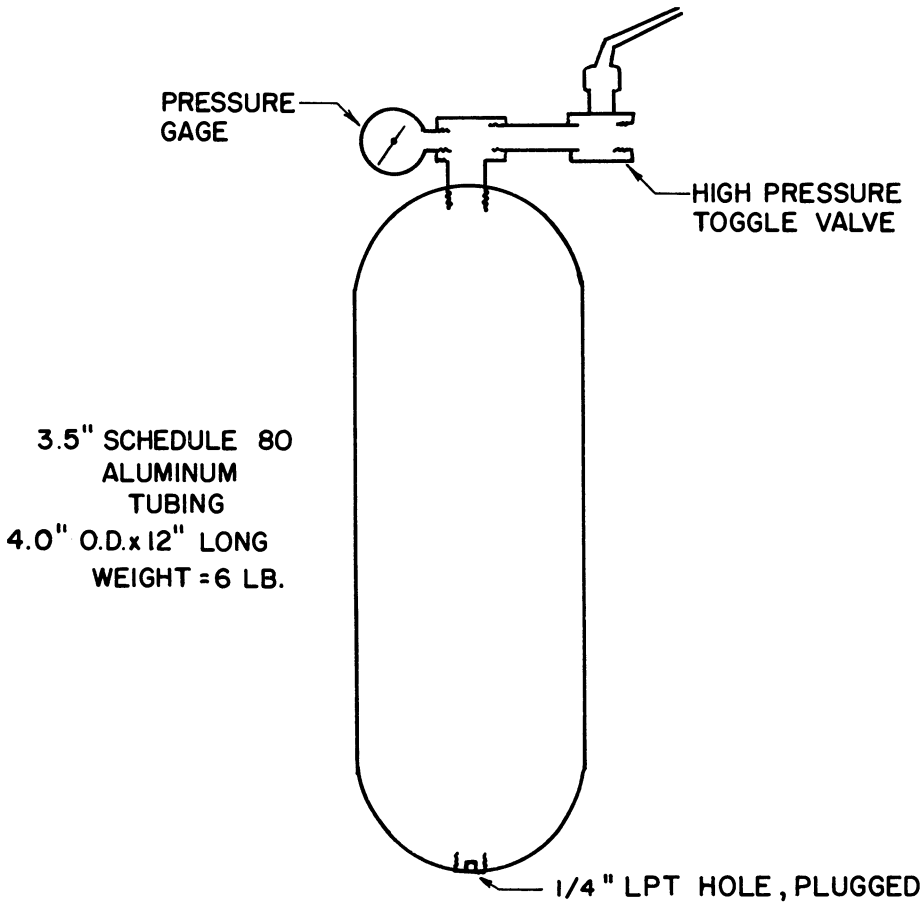

Figure 7. High Pressure Sample Tank.

$$\frac{\rho_m \Delta P_m}{\mu F} = a_0 + a_1 \frac{F}{\mu} + a_2 \left(\frac{F}{\mu}\right)^2 + a_3 \left(\frac{F}{\mu}\right)^3 \qquad (23)$$

where a_0, a_1, a_2, a_3 are the calibration constants obtained from a fit of the data by the method of least squares. Because of the non-linear behavior of this flow meter, and the increased difficulty of calibration, the meter was not calibrated as a function of pressure. Rather, pressure was eliminated as a major variable by calibrating and using the meter at the same pressure. Of course, since the exact pressure could not be obtained in each case, corrections were made for the small deviations. Temperature effect was eliminated by controlling the metering bath at the same temperature during both calibration and data runs.

Figure 8 gives the summary of mass-flow calibration data for nitrogen and methane, and the data used to construct this figure is tabulated in Tables XXV and XXXVI, Appendix B. The only runs not reported are those in which the sample bottles were known to have had leaks through the shut off valves. Indeed, a few methane runs which are above the calibration line are believed to have had leaks; however, the calibration line is changed little by discarding them. It is felt that the overall accuracy of the flow rate measurement is about 0.15%.

In this experiment the calibration curves of the flow meter were considered to be only a means of calculating flow rate. As such they are completely satisfactory, but for future work involving other gases and mixtures of gases it would be desirable to develop a correlation such that one calibration line could be used for all gases upon determination of the viscosity of each gas.

With this in mind the viscosity of methane was altered to place its calibration line on top of that of nitrogen. The results of this procedure are summarized in Figure 9. The generalized line approximates the results of each calibration to about 0.1%. However, it is felt that the best results are obtained by the use of the individual lines.

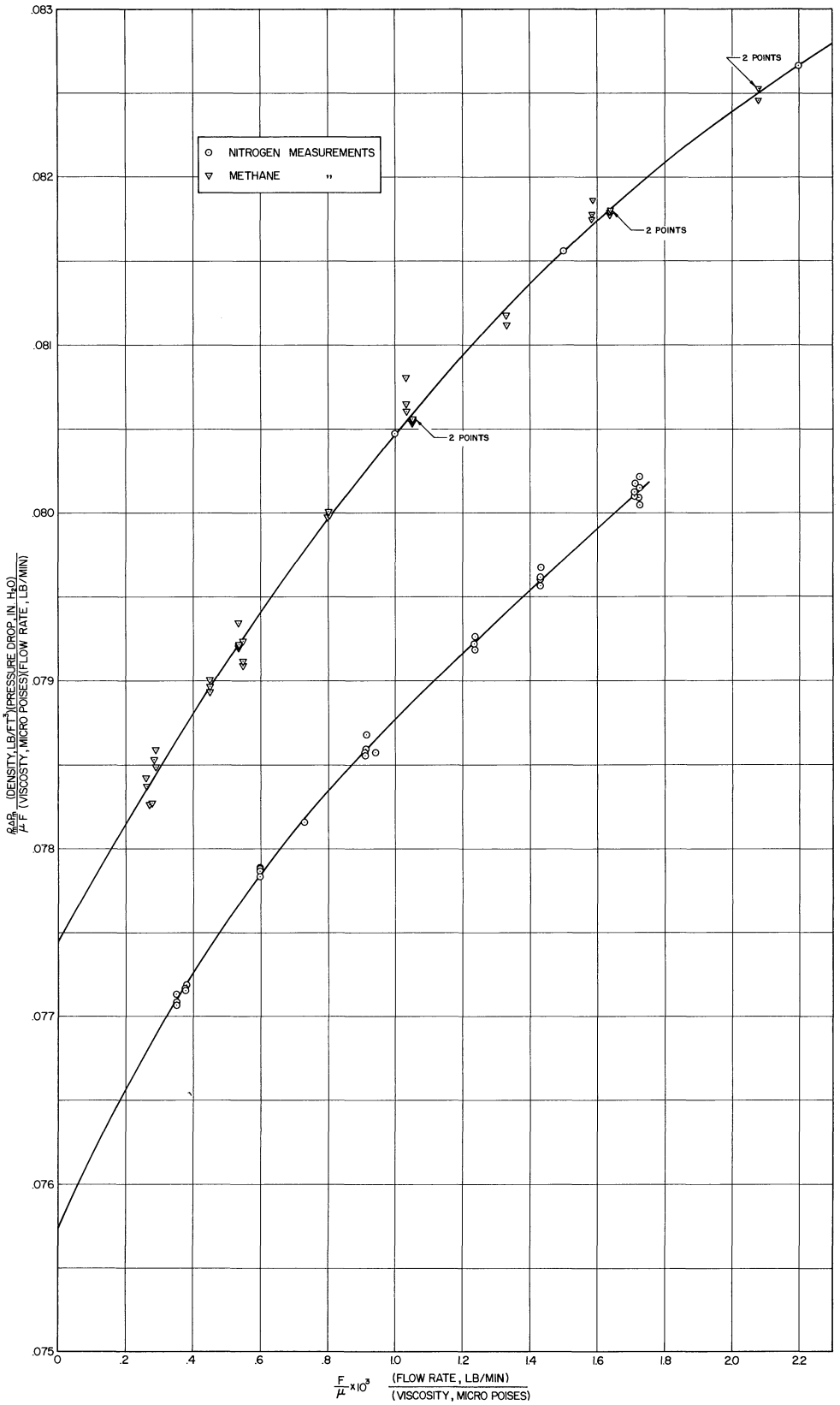

Figure 8. Flow Meter Calibration Data

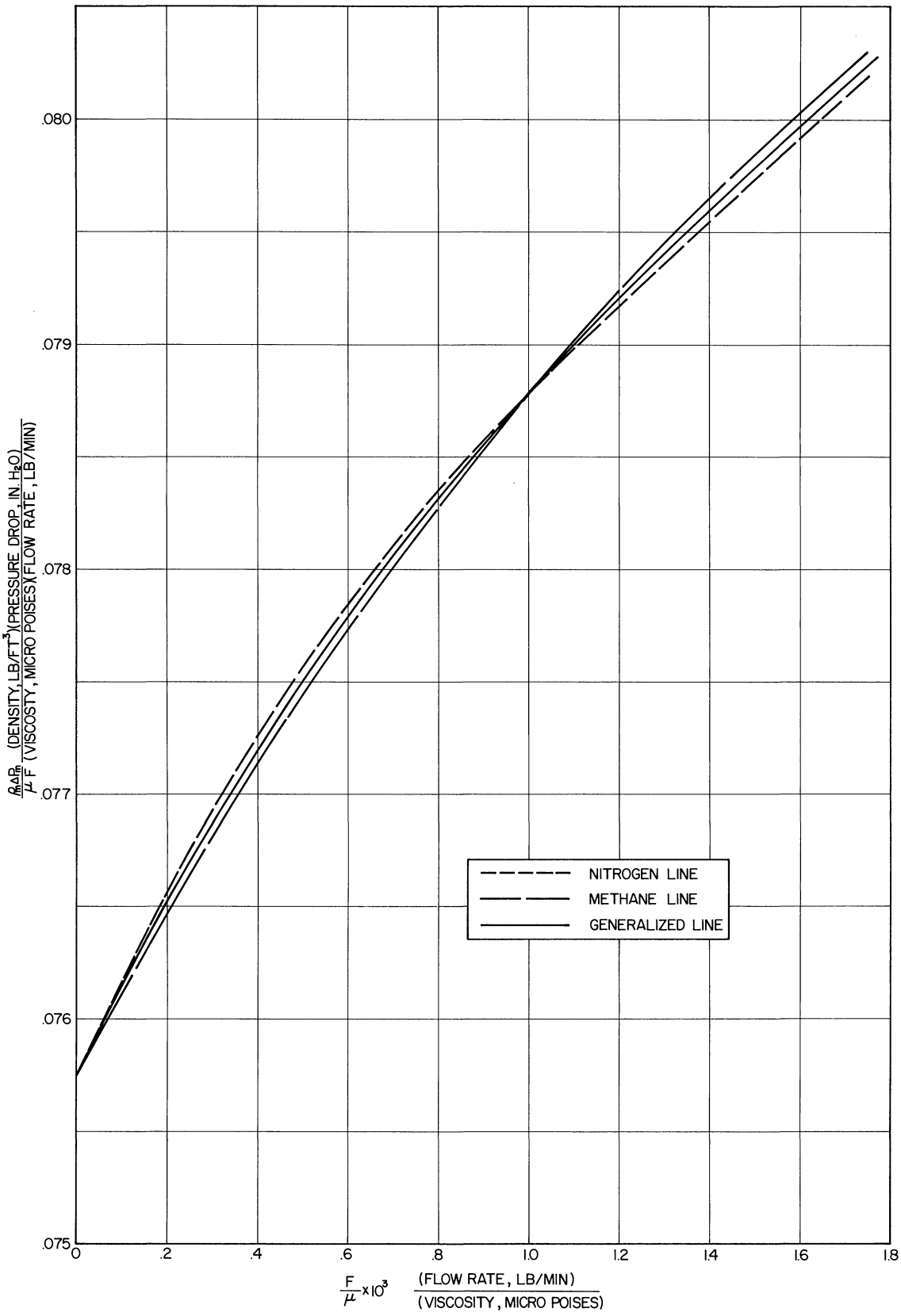

Figure 9. Generalized Flow Metering Calibration Curve.

EXPERIMENTAL DATA

The experimental apparatus was first used to measure isobaric heat capacities of gaseous nitrogen in order to test the equipment during its perfection. It was felt that the thermodynamic properties of nitrogen in the more ideal range could be calculated from equations of state and spectroscopic data accurately enough to give a good indication of the accuracy of the experimental apparatus. Furthermore, pure nitrogen was readily and cheaply available in the large quantities required during the period of equipment perfection.

When several isobaric specific heats had been measured and the performance of the apparatus was satisfactory with respect to operation, accuracy and precision, the apparatus was given an extreme physical test by using it to measure latent heat of vaporization and low temperature high pressure fluid heat capacities of nitrogen. Since the apparatus performed well in these tests investigation of the thermodynamic properties of methane was undertaken.

The experimental apparatus performed well in almost all of the experiments, allowing a high degree of precision along with stable, reliable operation. The exception was that in the measurement of heat capacities of compressed liquids and latent heats of vaporization at the lower pressures liquefaction and vaporization of the gas in the system caused pressure fluctuations which made measurements more difficult. In general these fluctuations could be reduced to acceptable magnitudes by reducing flow rate, but at pressures below 300 psia they became so large that measurements were impossible.

In the following sections the results of this experiment are presented and discussed with respect to the operating and calculating techniques required to obtain valid data.

Equipment Operation

Operation of the experimental apparatus may be separated into three areas:

1. Preparation, including the maintenance and checking of various components and the filling and setting of the various baths at the appropriate temperatures.

2. Start-up, which consists of initiating flow through the system, operation of all the system components and the accomplishment of approximate steady state.

3. Taking the measurement, which includes both the reading of the measuring instruments and the determination of steady state.

Preparation of the Apparatus

The apparatus is prepared for operation in exactly the same way as described by Faulkner[22] except that the cooling system consists of a dry ice cooler and a low temperature stirred cooling bath instead of the complex mixed flow system he used. The bath is filled with a fluid such as isopentane, which is cooled by flowing liquid nitrogen from a pressurized dewar through cooling coils immersed in the liquid. This is the same preparation as that given the low temperature calorimeter bath.

For a thorough, detailed description of the preparation required, the reader is referred to Dr. Faulkner's thesis. For the purpose of this manuscript let us say only that when the system is prepared for start-up,

1. The compressor is oiled and its cooling system working.

2. All valves and fittings are free of leaks.

3. All electrical instruments, including the potentiometer, platinum thermometer, calorimeter thermocouples, calorimeter guard heater, power supply and heat input system, low temperature bath controls and temperature indicator are checked for satisfactory operation.

4. The metering bath, low temperature cooling bath, and calorimeter bath are controlled at their proper temperatures.

5. The pressure balance is loaded with the necessary weights and connected to the system.

6. The vacuum system is working satisfactorily.

Start-up

The initial step in starting up the apparatus is the setting of the desired flow through the system such that the desired pressures are obtained throughout the system, and steady sate flow is approached. This is done by turning on the compressor and manually adjusting the metering valves (6,7 and 22 as shown in Figure 1) while adding gas to or withdrawing gas from the circulating system via the reservoir tanks when necessary.

When flow becomes reasonably steady the calorimeter power is turned on and set to the approximate value needed for the desired temperature rise, and the guard heater is adjusted to maintain the calorimeter

guard at the temperature of the gas leaving the calorimeter. As the system progresses toward steady state, fine adjustments must be made on the valves, calorimeter heater, and the quantity of gas in the system, in order to obtain the exact conditions desired. The line heater and low temperature cooling bath are adjusted such that the temperatures T_3 and T_5 approximate the temperatures in the measuring bath and metering bath, respectively.

Measurement of Properties at Steady State

In describing the process of measuring properties with the apparatus used in this experiment, it is necessary to point out that true steady state operation was seldom achieved. Rather, it was necessary for the operators to let the equipment approach steady state as closely as possible and then use their judgement to eliminate errors due to unsteady state.

With the equipment controlling properly and the metering valves set, experience shows that the finest approach to steady state is achieved by simply allowing the apparatus to run, while maintaining the calorimeter pressure at the predetermined value. Maintaining this pressure would set the flow rate through the calorimeter and the calorimeter bypass valves and allow the compressor output pressure, metering pressure and calorimeter exit temperature to approach their steady state values.

When steady state is approached, the main variables which must be essentially constant are:

1. The temperature rise through the calorimeter.
2. The calorimeter bath temperature.

3. The heat input to the calorimeter.

4. The pressure at the calorimeter.

5. The metering pressure.

6. The pressure drop across the flow restriction.

Each of these variables has a direct bearing upon the accuracy of the measurement.

Monitoring all of these variables, however, was not necessary in order to determine whether or not the system was at steady state. Constant monitoring of the temperature rise through the calorimeter was adequate to determine whether the mass of the calorimeter had been brought to temperature. In some experiments difference thermocouples were installed at various points on the calorimeter shell to measure the temperature profile of the calorimeter skin. It was found that a constant temperature profile could be predicted easily by monitoring the temperature rise alone. Small changes in calorimeter heat input, bath temperature, and flow rate could also be detected by the operator monitoring the temperature rise. The aforementioned technique of fixing the calorimeter pressure by the addition or removal of gas was adequate to set the metering pressure and the pressure drop across the flow restriction.

Thus, the progress toward steady state was watched by monitoring the dead weight pressure balance and the calorimeter thermocouple emf. When these two measurements indicated a high degree of steady state and the other control elements were functioning properly, the various measurements listed in Table II were taken. The apparatus was then monitored for fifteen or twenty minutes, and another set of readings taken in the same manner. The continuous monitoring between measurements showed whether or

TABLE II

INSTRUMENT READINGS FOR DATA MEASUREMENTS

Reading	Designation	Instrument	Units	Quantity Calculated
Heat input voltage	E_{L1}	Potentiometer	Volts	Heat input, Q
Heat input amperage	E_{L2}	Potentiometer	Volts	Heat input, Q
Resistor temperature	T_R	Thermometer	°F	Heat input, Q
Platinum thermometer voltage	E_{L3}	Potentiometer	°F	Measuring bath temp., T_1
Platinum thermometer	E_{L4}	Potentiometer	°F	Measuring bath temp., T_1
Main thermocouple voltage	E_{L11}	Potentiometer	°F	Temperature rise ΔT_c
Pressure drop across calorimeter	ΔP_c	High pressure mercury monometer	In. Hg.	Pressure drop corr. to C_p
Pressure balance load	P_{bal}	Weights	Lb.	Measurement Pressure, Psia
Flow meter bath temp.	T_m	Thermometer	°C	Flow rate, F
Flow meter pressure drop	Δh	Cathetometer	In. H_2O	Flow rate, F
Flow meter pressure	P'_m	180" Mercury manometer	In. Hg.	Flow rate, F
Manometer scale temp.	T_s	Thermometer	°F	Temp. corr. to 180" manometer
Manometer mercury temp.	T_{HG}	Thermometer	°F	Temp. corr. to 180" manometer
Room temp.	T_r	Thermometer	°C	Temp. corr. to Cathetometer
Room Pres.	P'_r	Barometer	In. Hg.	Convert pressures to

not changes had been taking place during the first reading. Comparison of the two readings showed the degree of precision obtained and was a good check on the degree of steady state obtained. When the two readings disagreed significantly or conditions indicated that something was unsatisfactory, more readings were taken until the operators were satisfied.

Reduction of Data

The raw data taken at each measurement of heat capacity or latent heat was transferred to punched cards for processing by the IBM Type 704 digital computer at the computing center on campus, to give calculated values of heat input, flow rate, temperature, temperature rise, pressure and heat capacity along with various combinations of these quantities which were useful in data reducing. Samples of the data input or raw data are listed in Tables XXVII and XXVIII in Appendix C, along with sample calculations for methane and nitrogen. The calculated data is tabulated in Tables XXI, XXII, XXIII, and XXIV in Appendix B, along with the reduced data obtained.

Heat Capacities

In order to obtain the true heat capacity at any pressure and temperature, it was necessary to correct the experimental measurements for heat leakage and for pressure drop through the calorimeter. The basic equation involved is the energy balance,

$$Q = FC_p(T_2-T_1) + F\left(\frac{\partial H}{\partial P}\right)_T (P_2-P_1) + \delta Q \qquad (24)$$

where Q is the measured heat input, Btu/min. °F is the flow rate, C_P is the average heat capacity between the temperatures of the gas at the calorimeter inlet, T_1, and at the calorimeter exit, T_2. The term $(\frac{\partial H}{\partial P})_T$ is the average value of the change of enthalpy with pressure at constant temperature, and P_1 and P_2 are the pressures of the measured gas at the inlet and exit of the calorimeter. The heat leakage, δQ is a combination of heat losses and gains due to radiation, conduction through the vacuum surrounding the heater capsule, and conduction through the calorimeter heater and thermocouple leads. However, the calorimeter was constructed in such a way that the amount of heat leakage should be dependent primarily upon the temperature rise through the calorimeter and the conditions in the calorimeter, and should not be dependent upon flow rate. Thus the heat leakage correction may be made by measuring several values of heat capacity at one pressure and temperature as a function of flow rate, using the same temperature rise, and maintaining the vacuum level and guard heater temperature constant. Equation (24) may be modified, then, to

$$C_{PF} = \frac{Q}{F\Delta T_c} - (\frac{\partial H}{\partial PT})\frac{\Delta P_c}{\Delta T_c} = C_P + \frac{\delta Q}{F\Delta T_c} \qquad (25)$$

where ΔT_c and ΔP_c refer to the temperature rise and pressure drop through the calorimeter. This equation gives a straight line relationship between the apparent heat capacity corrected for pressure drop through the calorimeter, C_{PF} and the reciprocal flow rate if the assumptions made about heat leakage are correct. Figure 10 is a series of measurements on nitrogen which shows that the straight line relationship holds. Heat capacity was measured at four flow rates in this case, to prove the assumption of

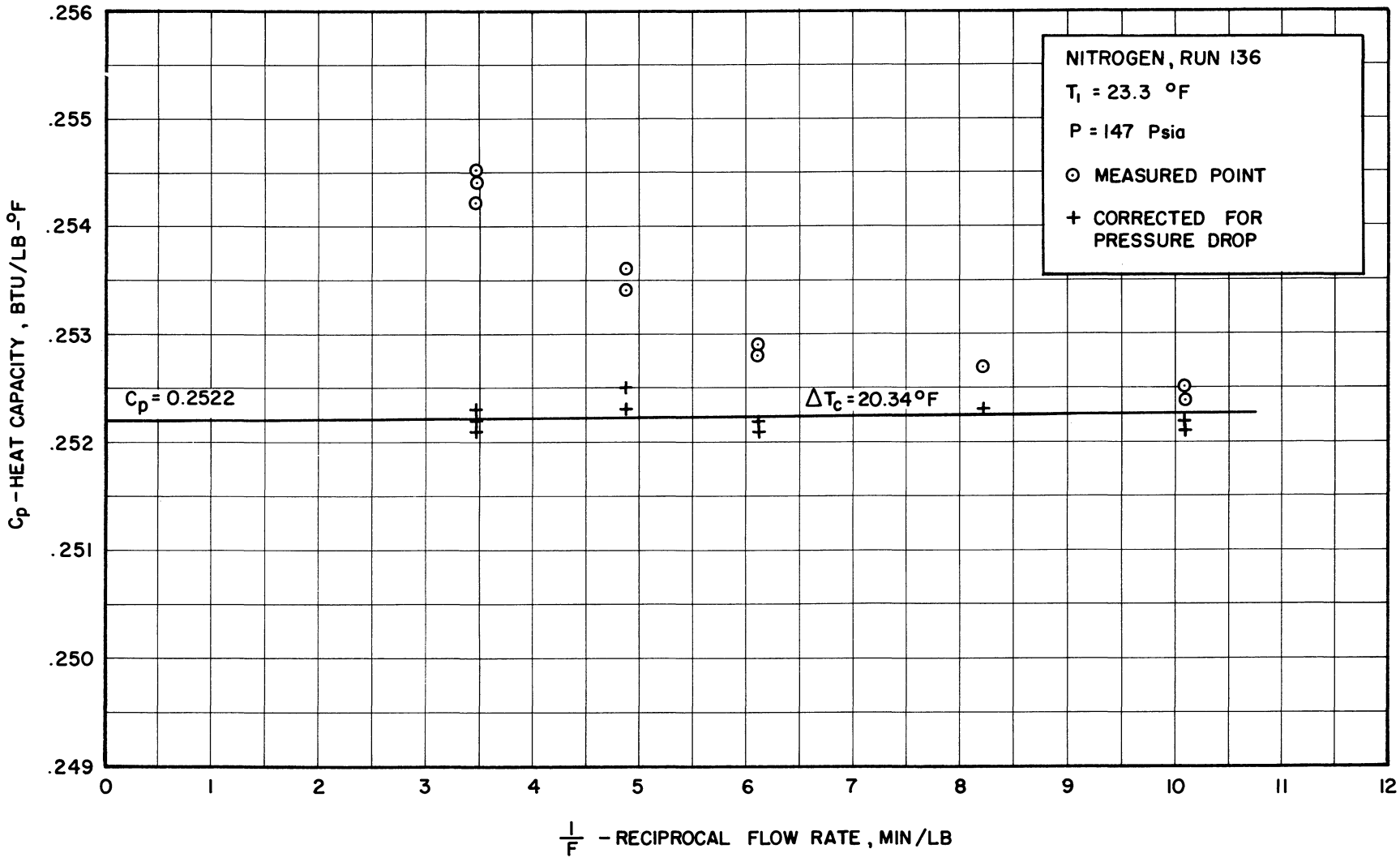

Figure 10. Heat Leakage Correction for Nitrogen Run No. 136 :32°F,147 psia.

linearity. However, it was felt that the performance of the equipment in this and similar instances justified the measurement of heat capacity at fewer flow rates. In general, measurements were taken at only two flow rates.

Three methods were readily available for making the correction for pressure drop through the calorimeter.

1. Equation (25) could be used directly, with use of values of $(\frac{\partial H}{\partial P})_T$ calculated from equations of state or thermodynamic charts.

2. Equation (25) could be modified by substituting Equation (3), $(\frac{\partial H}{\partial P})_T = -\mu^* C_P$ to give the equation,

$$C_{PF} = \frac{Q}{F\Delta T_c(1-\mu^*\frac{\Delta P}{\Delta T})} = C_P + \frac{\delta Q}{F\Delta T_c(1-\mu^*\frac{\Delta P}{\Delta T})} \qquad (26)$$

which is useful when Joule-Thomson coefficients are available.

3. The correction could be measured directly by running the calorimeter without heat input at the mean temperature of the run and measuring the temperature drop. This quantity could then be subtracted from the temperature rise of the heat capacity determination, using the equation,

$$C_{PF} = \frac{Q}{F(\Delta T_c - \delta T)} = C_P + \frac{\delta Q}{F(\Delta T_c - \delta T)} \qquad (27)$$

It was felt that the correction due to pressure drop through the calorimeter was small enough that inaccuracies in the calculation of $(\frac{\partial H}{\partial P})_T$ from equations of state, enthalpy tabulations or Joule-Thomson coefficients would be negligible with respect to the overall heat capacities, and probably smaller than the error involved in the direct measurement, so methods (1) and (2) were in general used. Some direct measurements using method (3) were made yielding equivalent results.

Corrections for nitrogen were made using the Joule-Thomson coefficients of Roebuck and Osterberg[65], or values of $(\frac{\partial H}{\partial P})_T$ calculated from the tabulation of enthalpy properties of Bloomer and Rao[6]. Several points were calculated both ways and found to give essentially identical results.

Corrections for methane were made employing method (1) and values of $(\frac{\partial H}{\partial P})_T$ calculated from the Benedict - Webb - Rubin[4] equation of state or from the charts of Matthews and Hurd[52] or Keesom[35].

In many instances heat capacities were measured in regions where the change of heat capacity with respect to temperature and pressure was high. The change with respect to pressure presented little problem in correction, since the system was held at constant pressure quite easily. However, it was desirable to determine the change of heat capacity with temperature, not only to aid in the construction of graphs of heat capacity versus temperature for enthalpy calculations, but to aid in making corrections for the small differences in temperature rise in each heat capacity measurement. The change of heat capacity with temperature, then, was determined by making measurements at each flow rate at two or more temperature rises. Maximum utility was made of this procedure by differencing each of the temperature rises with each other to give additional heat capacities. For example, measurements made with exit temperatures at 10°F and 20°F above the bath temperature could be differenced to give a heat capacity between 10°F and 20°F. This was facilitated by the fact that pressure drop through the calorimeter remained essentially constant at each flow rate while heat input was varied. Equation (24) may then be expanded to show that the straight line

relationship should hold for the differenced quantities. Writing Equation (24) for points measured between T_1 and T_2 and between T_1 and T_3, where T_3 is higher than T_2. We have,

$$Q_{1,2} = FC_{P1,2}(T_2-T_1) + F\left(\frac{\partial H}{\partial P}\right)_T (P_2-P_1) + \delta Q_{1,2} \qquad (24a)$$

$$Q_{1,3} = FC_{P1,3}(T_3-T_1) + F\left(\frac{\partial H}{\partial P}\right)_T (P_3-P_1) + \delta Q_{1,3} \qquad (24b)$$

Subtracting Equation (24a) from Equation (24b), assuming constant flow rate, constant pressure drop and constant $\left(\frac{\partial H}{\partial P}\right)_T$ we have

$$Q_{1,3} - Q_{1,2} = FC_{P1,3}(T_3-T_1) - FC_{P1,2}(T_2-T_1) + \delta Q_{1,3} - \delta Q_{1,2} \qquad (24d)$$

or since

$$C_{P1,3}(T_3-T_1) = C_{P1,2}(T_2-T_1) + C_{P2,3}(T_3-T_2) \qquad (28)$$

we may write an equation similar to Equation (25a),

$$C_{PF2,3} = \frac{Q_{2,3}}{F\Delta T_{2,3}} = C_{P2,3} + \frac{\delta Q_{2,3}}{F\Delta T_{2,3}} \qquad (25a)$$

Therefore the points obtained by differencing the data at each flow rate should also have a straight line relationship with respect to reciprocal flow rate, without including a correction for pressure drop. The assumptions involved in deriving Equation (25a) are not strictly valid, since pressure drop, $\left(\frac{\partial H}{\partial P}\right)_T$ and F do change when the temperature rise through the calorimeter is changed. However, the changes are usually small enough to be neglected.

Figure 11 is a series of measurements on methane which illustrates the linearity of the apparent heat capacities C_{p_F} for both measured and differenced data. It is important to note that the slopes of the lines drawn in Figure 11 are essentially the same. Since the slopes of the lines are the rates of heat leakage per degree of temperature rise through the calorimeter, $\frac{\delta Q}{\Delta T_c}$ BTU/Min. °F, this figure indicates not only that the apparent heat capacities are linear with respect to reciprocal flow rate, but that the heat leakage is directly proportional to the temperature rise through the calorimeter. This is important because temperature rise may vary slightly in the measurement of heat capacity as a function of flow rate for use in Equations (25), (26), or (27). If heat leakage were a strong function of temperature rise, this plus the change of heat capacity with temperature would make the correction for heat leakage much more complicated.

No attempt was made to correlate heat leakage as a function of measurement conditions. It appeared that it consisted, in general, of a small heat addition to the calorimeter of less than 0.002 BTU/Min. °F, which would be within the order of magnitude of the experimental error. However, in a few runs the heat leakage appeared to be quite large, indicating the possibility of error in the measurements versus flow rate, or that the vacuum level in the calorimeter was low. In each of these instances, the lines were drawn as usual, extrapolating to infinite flow rate. This puts emphasis on the measurements at high flow rate, which are least likely to be in error, and which are least affected by heat leakage. In only a few runs is it felt that this procedure could have given additional errors greater than 0.3%. Ordinarily the error involved is well within 0.1%.

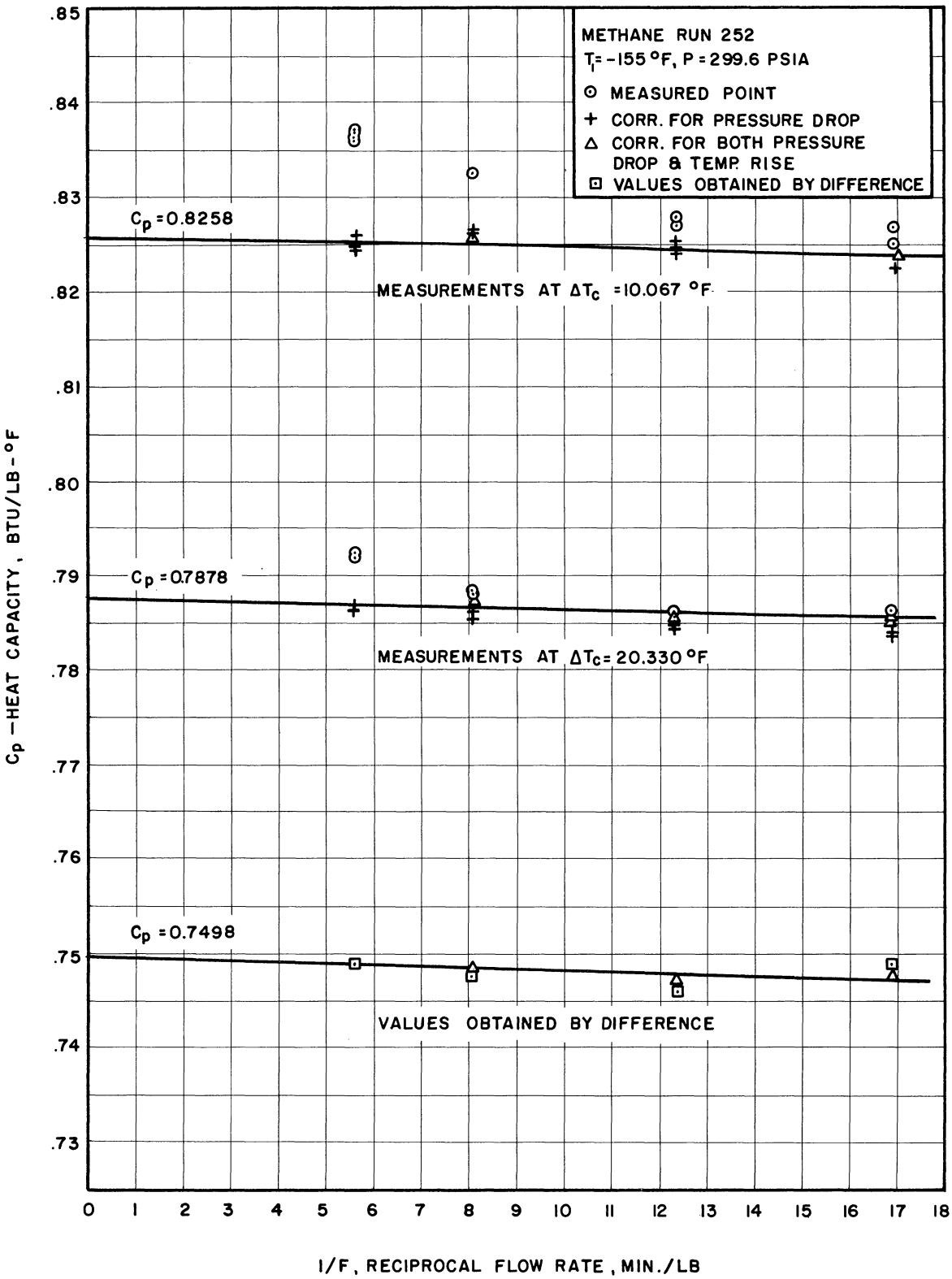

Figure 11. Heat Leakage Correction for Methane Run No. 252:-155°F,300 psia

Latent Heats of Vaporization

Latent heats of vaporization were determined by making a series of measurements of enthalpy differences at constant flow rate and constant bath temperature. The heat input was increased incrementally such that several liquid heat capacities would be measured initially, followed by measurements in the two phase region and finally by measurements in the superheated gas range. The temperature change is then plotted versus the heat input per pound for the series of measurements. The enthalpies of the gas at its dew and bubble points are found by extending the lines drawn through points in the gas and liquid regions until they intersect with the line drawn through the two phase region. Figure 12 shows this technique for two methane latent heats at 550 psia.

Since the temperature rise through the two phase region due to impurities is slight the heat leakage at the bubble point is essentially the same as that at the dew point, so heat leakage should not enter into the latent heat calculation. However, several points were measured at more than one flow rate to determine whether or not heat leakage had an effect. It appeared that any effect was within the accuracy of measurement. Since pressure drop was very small and remained essentially constant throughout the two-phase region, it may be eliminated as an important variable.

Experimental Measurements

The measurements of this investigation included isobaric heat capacities of nitrogen and methane, in the range -250 to 50°F, 150 psia to 2000 psia. Latent heats of vaporization of nitrogen were measured at 350, 400 and 450 psia, and those of methane at 350, 450, 550, and 625 psia.

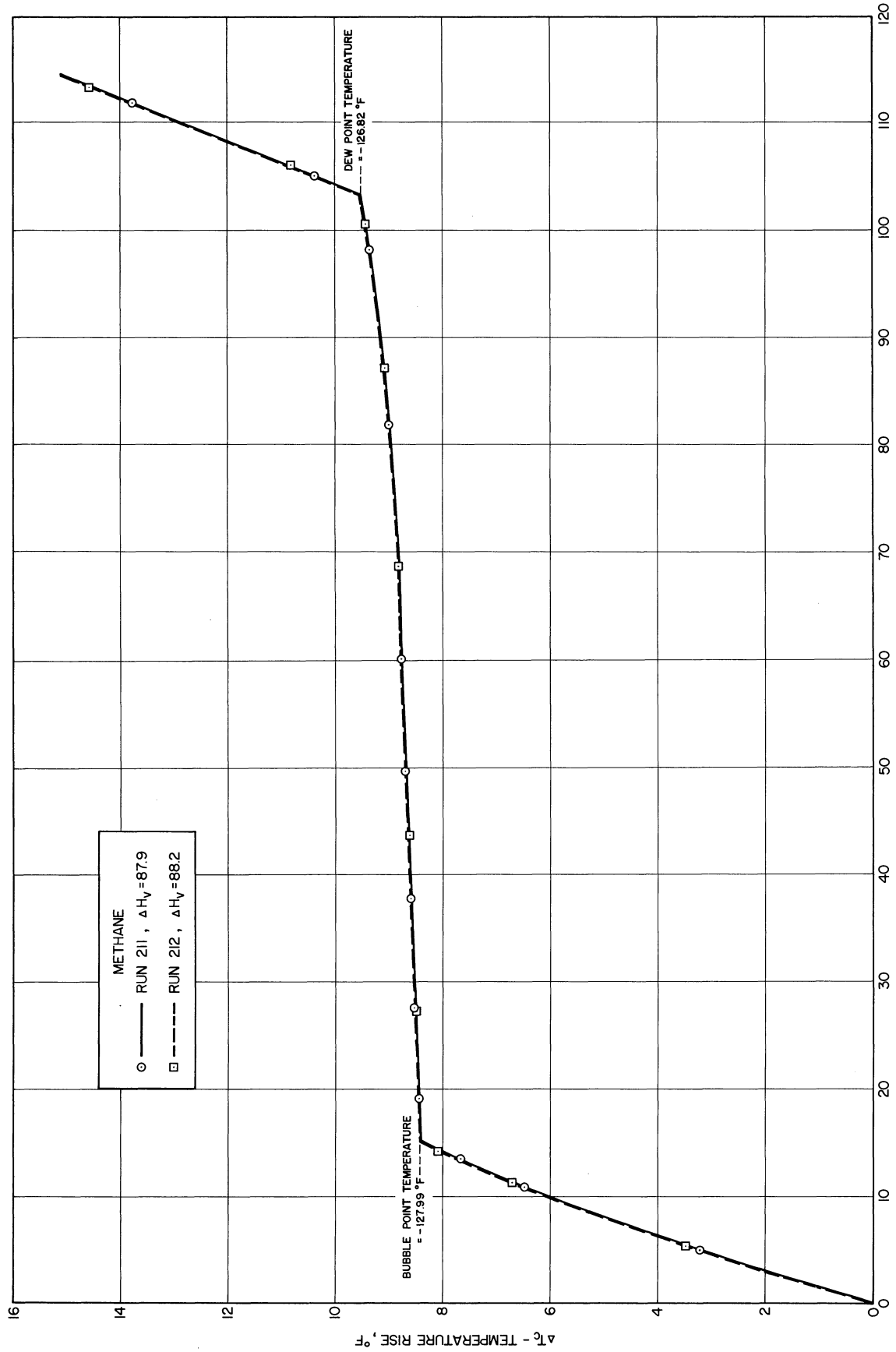

Figure 12. Graphical Determination of Latent Heat of Vaporization for Methane at 550 Psia, Showing Extrapolation of Measurements to the Saturation Curve.

The nitrogen used in these measurements was the extra pure, extra dry grade supplied by the Air Reduction Company. The methane used was supplied by the Tennessee Gas Transmission Company directly from the well, and was compressed and shipped to the University of Michigan by the Gulf Oil Company. The impurities in the gases used were determined by mass spectrometer analyses several times throughout the course of the experiments, and were found to be constant. The compositions of these gases are listed in Tables III and IV.

Measurements on Nitrogen

The experimental measurements made on nitrogen are summarized in Figure 13, a pressure-temperature chart which indicates the temperatures and pressures of each measurement made. Tables V and VI give the final values determined for the heat capacities and latent heats measured, respectively.

Measurements on Methane

Figure 14 is a pressure-temperature diagram which summarizes the pressures and temperatures of the measurements made on methane. Table VII gives a summary of the values of the heat capacities measured, including the gaseous, liquid and fluid heat capacities. Table VIII gives a summary of the values of latent heats measured.

TABLE III

NITROGEN COMPOSITION

Constitutent	Mole Percent
Nitrogen	99.95%
Argon	0.05%
Total	100.00%

TABLE IV

METHANE COMPOSITION

Constitutent	Mole Percent
Methane	99.45%
Nitrogen	0.25%
Ethane	0.20%
Propane	0.05%
Carbon Dioxide	.05%
Total	100.00%

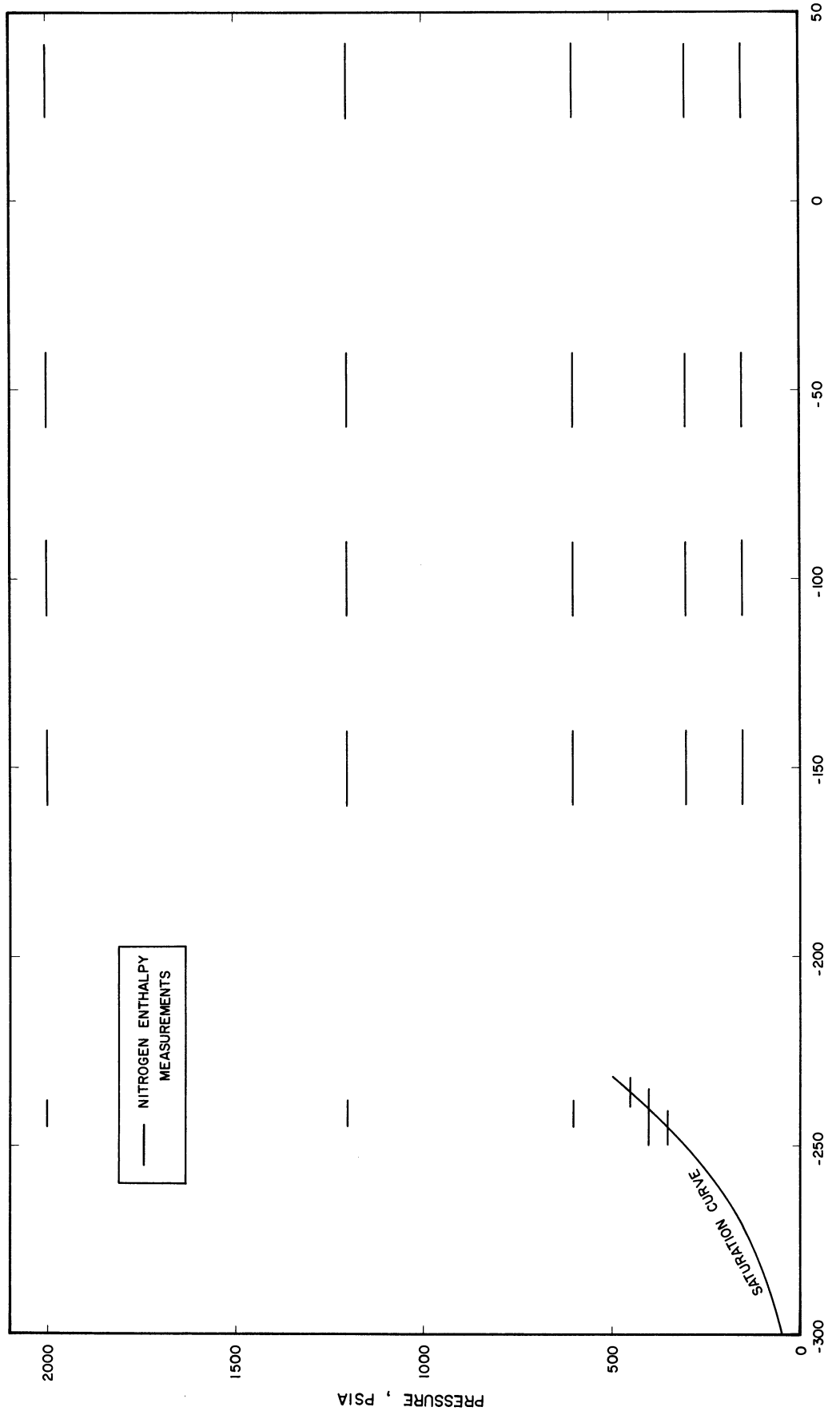

Figure 13. Pressure-Temperature Chart for Nitrogen Indicating Conditions of Enthalpy Measurements.

TABLE V

MEASURED HEAT CAPACITIES OF NITROGEN

Run	Pressure Psia	Initial Temperature, °F	Final Temperature, °F	Isobaric Heat Capacity, Cp Btu/lb °F
136	146.4	23.30	43.64	0.2522
120	147.0	-58.87	-38.65	0.2547
127	147.0	-109.93	-90.74	0.2577
130	147.0	-159.87	-139.83	0.2645
111	294.0	22.17	42.47	0.2574
121	294.0	-58.87	-38.72	0.2630
134	294.0	-110.03	-90.27	0.2696
131	294.0	-159.90	-140.00	0.2859
113	399.8	-250.00	-245.05	0.8079
110	588.0	22.39	42.59	0.2673
122	588.0	-58.88	-38.43	0.2802
133	588.0	-110.03	-90.28	0.2982
132	588.0	-159.90	-139.85	0.3398
114	588.0	-244.99	-234.54	0.8228
109	1176.0	22.39	42.90	0.2871
123	1176.0	-58.72	-38.29	0.3171
126	1176.0	-109.93	-90.11	0.3608
129	1176.0	-159.87	-139.92	0.4876
115	1176.0	-244.99	-234.55	0.5681
108	2000.0	22.35	42.55	0.3110
124	2000.0	-58.49	-38.25	0.3562
125	2000.0	-109.93	-90.08	0.4208
128	2000.0	-159.87	-140.02	0.5233
116	2000.0	-244.99	-234.52	0.4946

TABLE VI

MEASURED LATENT HEATS OF VAPORIZATION OF NITROGEN

Run	Temperature °F	Pressure Psia	Latent Heat Btu/lb
138	-245.10	349.7	41.5_0
139	-245.11	349.7	41.1_3
140	-240.25	399.4	34.1_0
142	-235.92	449.8	25.8_2
143	-245.16	349.8	41.6_9

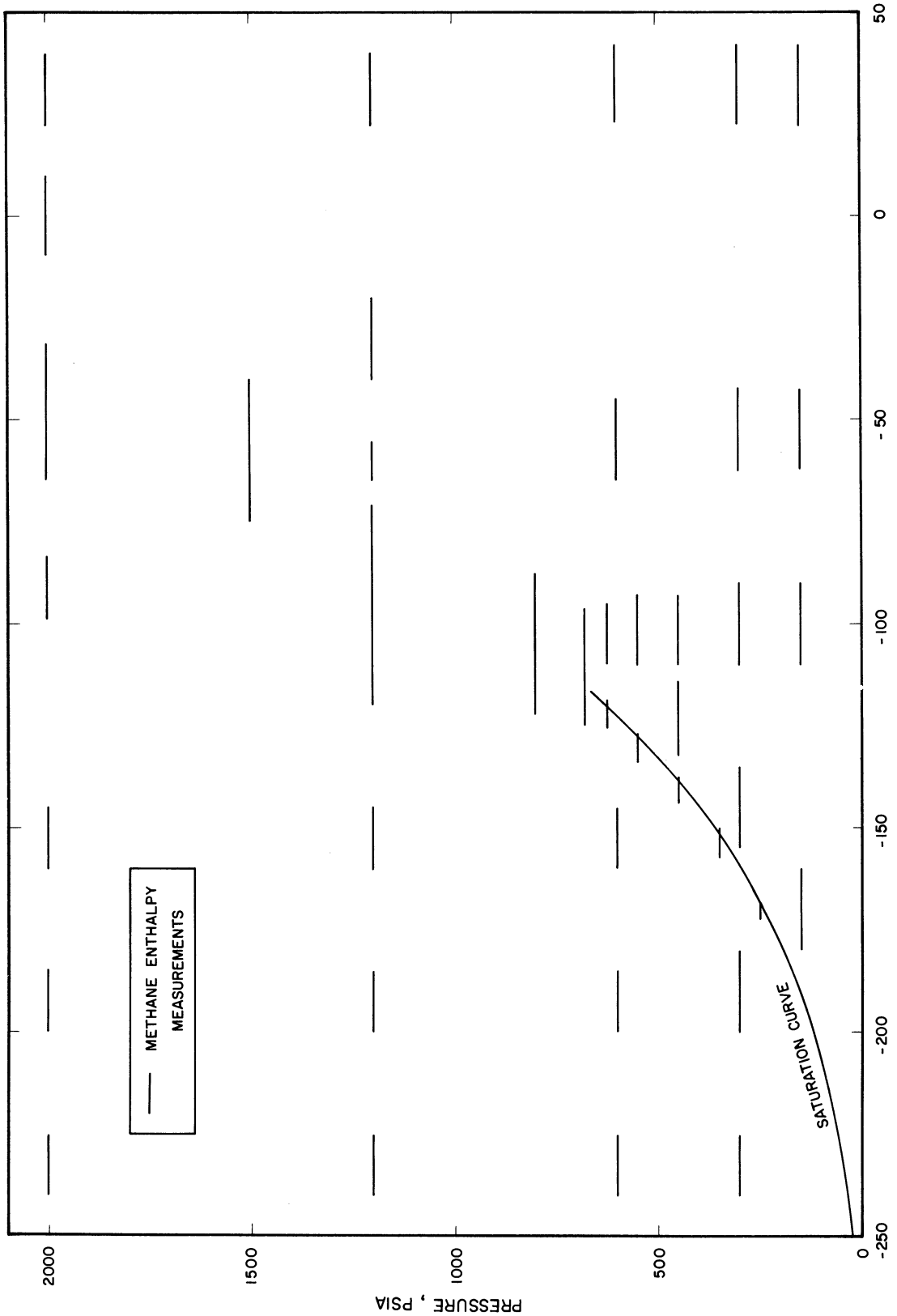

Figure 14. Pressure-Temperature Chart for Methane Indicating Conditions for Enthalpy Measurements.

TABLE VII

MEASURED HEAT CAPACITIES OF METHANE

Run	Pressure Psia	Initial Temperature °F	Final Temperature °F	Isobaric Heat Capacity, C_p Btu/lb °F
201-208	149.45	23.35	43.79	0.5377
239	149.75	-64.10	-43.29	0.5357
218	149.30	-108.81	-98.52	0.5515
		-108.81	-89.17	0.5470
238	148.70	-179.19	-166.91	0.6100
		-179.19	-156.46	0.6003
203	229.50	23.25	43.77	0.5571
240	299.67	-64.10	-43.42	0.5761
214	299.60	-109.37	-99.12	0.6322
		-109.37	-89.21	0.6232
252	299.60	-155.00	-144.93	0.8258
		-155.00	-134.67	0.7878
231	299.39	-199.28	-188.82	0.9322
		-199.28	-181.24	0.9476
227	299.18	-236.65	-221.95	0.8572
219	449.50	-108.89	-98.73	0.7803
		-108.89	-89.20	0.7558
253	449.40	-132.68	-125.13	1.0929
		-132.68	-116.71	1.0091
220	549.6	-108.90	-98.88	0.9719
		-108.90	-89.14	0.9181
204	599.53	23.25	43.55	0.6063
241	599.66	-64.10	-43.37	0.7110
235	599.0	-159.06	-147.78	1.1108
		-159.06	-137.42	1.1834
232	599.6	-199.34	-186.84	0.9114
228	599.4	-236.65	-222.65	0.8477
221	624.6	-108.88	-101.06	1.3005
		-108.88	-92.85	1.1842
209	679.6	-134.88	-127.01	1.4783
		-134.88	-122.88	1.5932
		-134.88	-120.03	1.7240
		-134.90	-117.17	1.9850
		-134.92	-116.36	2.1525
		-134.92	-115.75	2.4709
		-134.92	-115.57	2.685
		-134.92	-115.41	3.100
		-134.92	-115.15	3.689
		-134.92	-114.50	4.084
		-134.93	-112.99	4.142
		-134.93	-110.22	4.137

TABLE VII (CONT'D)

Run	Pressure Psia	Initial Temperature °F	Final Temperature °F	Isobaric Heat Capacity, C_p Btu/lb °F
222	679.7	-108.88	-101.96	1.8412
		-108.88	-93.22	1.5417
250	799.6	-99.23	-94.07	2.386
		-99.23	-86.48	1.960
223	799.7	-108.93	-106.75	5.135
		-108.93	-104.24	5.999
		-108.93	-102.19	5.810
		-108.93	-98.74	5.070
224	799.7	-118.52	-113.67	2.0505
		-188.52	-110.33	2.3564
		-118.52	-107.59	2.8378
256	999.7	-107.72	-102.81	1.7720
			-97.40	1.9855
			-92.98	2.1989
			-88.11	2.3697
			-83.90	2.4211
			-79.10	2.3861
			-72.75	2.2789
205	1199.7	23.25	43.68	0.7373
255	1199.3	-39.68	-30.90	1.0790
		-39.68	-22.16	1.0369
242	1200.65	-63.39	-58.50	1.5931
		-63.39	-53.74	1.5227
247	1199.2	-80.42	-78.22	2.066
		-80.42	-76.61	2.061
		-80.42	-74.71	2.053
		-80.42	-68.30	1.9950
226	1199.4	-99.13	-93.43	1.6365
		-99.13	-87.26	1.7349
		-99.13	-78.44	1.8574
225	1199.4	-118.59	-111.10	1.2531
		-118.59	-104.40	1.3075
		-118.59	-97.30	1.3761
236	1199.0	-159.06	-147.69	0.9739
233	1199.2	-199.34	-186.96	0.8763
229	1199.4	-238.91	-224.95	1.8298
249	1499.3	-58.30	-54.40	1.5170
		-58.30	-50.81	1.5019
		-58.30	-41.94	1.4487
248	1499.0	-74.09	-69.93	1.5183
		-74.09	-66.72	1.5311
		-74.09	-63.44	1.5349
		-74.09	-57.74	1.5382

TABLE VII (CONT'D)

Run	Pressure Psia	Initial Temperature °F	Final Temperature °F	Isobaric Heat Capacity, C_p Btu/lb °F
206	1999.5	23.25	43.67	0.9049
246	1999.3	-9.28	0.09	1.0681
		-9.28	9.84	1.0439
245	1999.5	-49.75	-45.09	1.2100
		-49.75	-39.81	1.2090
		-49.75	-32.83	1.2038
243	1999.3	-63.39	-56.56	1.1764
		-63.39	-50.19	1.1919
251	1999.5	-99.21	-81.94	1.0719
237	1999.2	-159.10	-147.65	0.8972
234	1999.3	-199.34	-186.84	0.8420
230	1999.0	-238.90	-224.80	0.8140

TABLE VIII

MEASURED LATENT HEATS OF VAPORIZATION OF METHANE

Run	Bubble Point Temperature °F	Dew Point Temperature °F	Mean Temperature °F	Pressure Psia	Latent Heat Btu/lb
216	-152.54	-150.66	-151.60	349.6	136.3
213	-138.89	-137.11	-138.00	449.3	114.6
244	-139.16	-137.64	-138.40	449.5	114.5
211	-127.99	-126.82	-127.40	549.8	87.9
212	-127.98	-126.82	-127.40	549.8	88.2
210	-120.55	-119.91	-120.23	624.6	59.5
254	-120.49	-119.86	-120.18	624.4	59.7

COMPARISON OF NITROGEN DATA

Due to the absence of published values of measurements of the heat capacity and latent heat of vaporization of nitrogen under pressure, the experimental measurements made were compared to previously published derived data. In the early experiments on nitrogen, the object of the comparison was to determine the approximate accuracy of the equipment, in order to improve the equipment such that it would produce good data. When the equipment was perfected the situation reversed, and the object of the comparison was to determine the accuracy of the published data.

Heat Capacities

The heat capacities of gaseous nitrogen measured in the present investigation are compared in Figure 15 and Table IX to values presented in NBS Circular 564[74] and to values calculated from the equation of state of Bloomer and Rao.[6] These two compilations appear to be the latest available, and the latter is quite complete, including calculated values of latent heat as well as superheated gas enthalpies. Both compilations are based on spectroscopic heat capacities, with extension to high pressure via equations of state.

Bloomer and Rao used the zero pressure heat capacity data of Goff and Gratch[28] and the equation of state,

$$P = RT\rho + (B_oRT - A_o - \frac{C_o}{T^2} - \frac{D_o}{T^4})\rho^2 + (bRT - a)\rho^3 + (\frac{c_o}{T^2} + \frac{\delta}{T^4})\rho^3 (1 + \gamma\rho^2)e^{-\gamma\rho^2} + a\alpha\rho^6 \qquad (29)$$

to tabulate enthalpies and entropies of nitrogen from -232°F to 500°F at pressure up to 1500 psia. The constants used in the equation of state are shown in Table X. The equation is similar to the Benedict-Webb-Rubin[4] equation of state. The terms D_o/T^4 and δ/T^4 were added to improve the agreement of the equation with low temperature volumetric data.

Values of heat capacity were first obtained from this data by differencing the enthalpy data versus temperature, but lack of internal consistency and difficulties in plotting showed that the inaccuracies involved might overshadow the errors produced by use of the equation of state. Further, it was desired to have some comparison at 2000 psia, which was beyond the limit of the compilations. With these factors in mind, heat capacities were calculated directly from the equation of state and the zero pressure heat capacity data. Since the equation of state is explicit in pressure, direct integration of Equation (10) would be extremely complicated. Equation (10) was not integrated directly to give heat capacity, but Equation (5) was modified to give,

$$H - H_1 = \int_{T_1}^{T} C_P^o dT + \int_{P_1=0}^{P} (V - T(\frac{\partial V}{\partial T})_P) dP = \int_{T_1}^{T} C_P^o dT$$

$$+ \int_{\rho_1=0}^{\rho} [\frac{1}{\rho}(\frac{\partial P}{\partial \rho})_T - \frac{T}{\rho^2}(\frac{\partial P}{\partial T})_\rho] d\rho \qquad (30)$$

The integrations were performed to give enthalpy as a function of temperature and density, and the equation differentiated with respect to temperature at constant pressure, by the equation,

$$C_P = (\frac{\partial H}{\partial T})_P = C_P^o + (\frac{\partial H'}{\partial T})_\rho + (\frac{\partial H'}{\partial \rho})_T (\frac{\partial \rho}{\partial T})_P \qquad (31)$$

where H' is the last term in Equation (30), the enthalpy change due to pressure.

The authors of National Bureau of Standards Circular 564[74] tabulated enthalpies, entropies and heat capacities of nitrogen from 100°K to 500°K at pressures up to 100 atmospheres. They used the virial equation of state,

$$z = \frac{PV}{RT} = 1 + B_1P + C_1P^2 + D_1P^3$$

where the virial coefficients B_1 and C_1 were obtained from an unmodified Lennard-Jones 6-12 potential, and the coefficient D_1 from an empirical equation fitted to the volumetric data. The authors state that the tables were intended for use at moderate and high temperatures, and that the equation departs considerably from the volumetric data at low temperatures.

Values for comparison were obtained from this data by plotting it versus temperature at each pressure at which values were reported. No attempt was made to obtain values at intermediate pressures either graphically or by direct use of the equation of state.

The comparisons in Figure 15 and Table IX show excellent agreement between the measured values of heat capacity and values calculated from Bloomer and Rao's equation of state. Only the measurement at 2000 psia and -150°F disagrees by more than 1%, the majority of the data agreeing to within 0.5%, the approximate accuracy of the experimental data. The values of heat capacity taken from NBS Circular 564 appear to be of the same order of accuracy as those of Bloomer and Rao for the temperature

range they used. Their values of 150 psia are considerably lower than those of Bloomer and Rao and are in better agreement with the experimental data.

Heat capacities of compressed liquid nitrogen measured in this experiment at -240°F are shown in Figure 16. No data was available from the literature for comparison.

Latent Heats of Vaporization

The latent heats of vaporization of nitrogen measured in this experiment are compared in Figure 17 and Table XI to values calculated by Bloomer and Rao[6] using the Clapeyron equation. These values were calculated using the recent vapor pressure data of Friedman and White,[25] the saturated liquid densities of Mathias, Onnes and Crommelin,[51] and the saturated vapor densities of Friedman, White and Johnston.[26] Agreement between the experimental and calculated data is good and corresponds approximately to the error of the direct measurements, $\pm 1\%$.

In determining the latent heats of vaporization, the dew point and bubble point temperature at the measurement pressure are determined from diagrams similar to Figure 12. For nitrogen, no temperature rise was detected through the two phase region, ; in keeping with the high purity of the material tested. The vapor pressure data obtained from the latent heat measurements is compared to that of Friedman and White in Table XII.

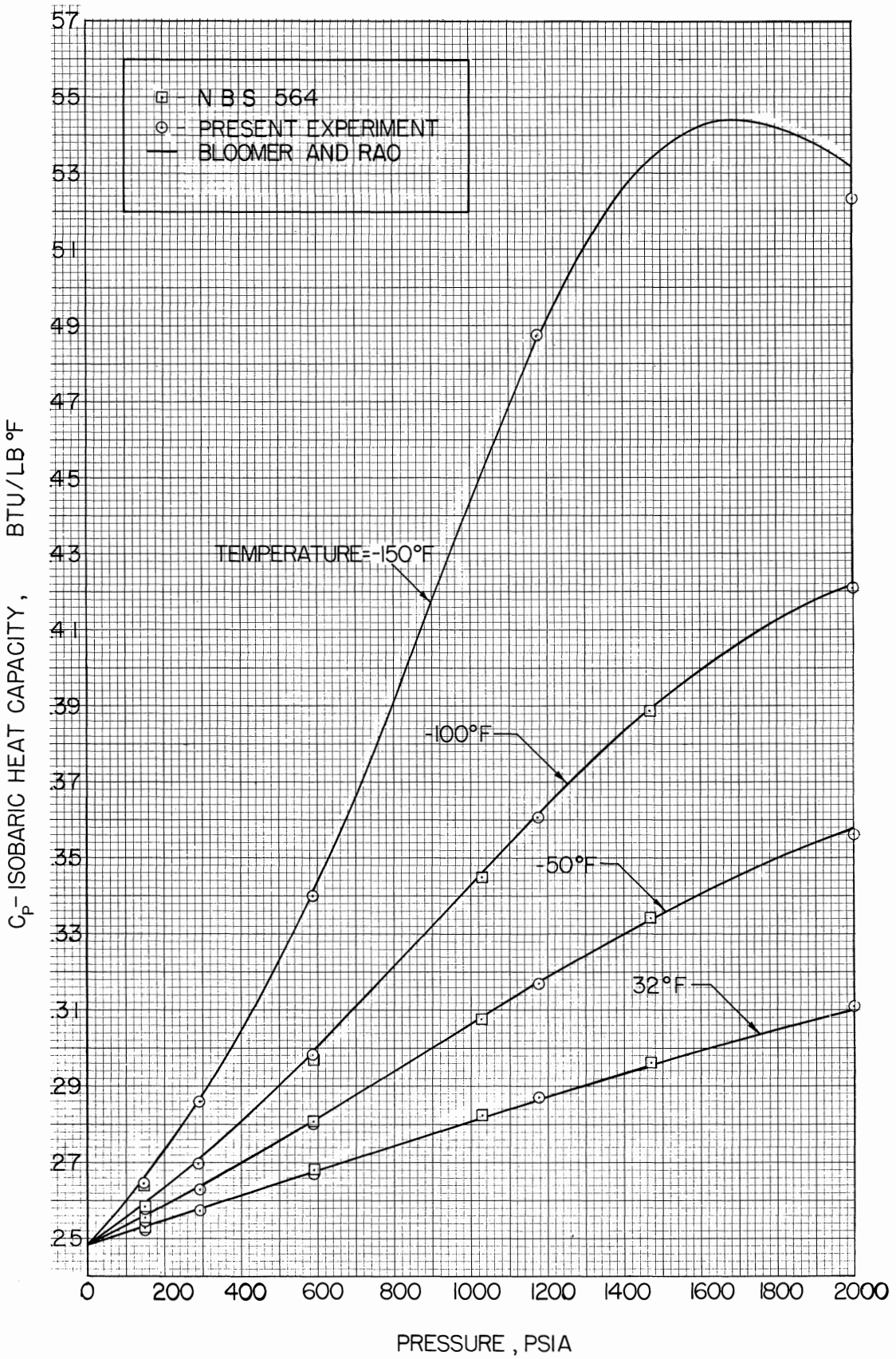

Figure 15. Comparison of Measured Heat Capacities of Nitrogen with Derived Values.

TABLE IX

COMPARISON OF MEASURED HEAT CAPACITIES OF NITROGEN

Pressure Psia	Temperature °F	Measured Heat Capacity Btu/lb°F	Bloomer and Rao: Calculated Heat Capacity Btu/lb°F	Bloomer and Rao: $\frac{Calc.C_P - Exp.C_P}{Exp.C_P} \times 100\%$	Nat. Bur. Stds. Circular 564: Calculated Heat Capacity Btu/lb°F	Nat. Bur. Stds. Circular 564: $\frac{Calc.C_P - Exp.C_P}{Exp.C_P} \times 100\%$
147	32	0.2522	0.2528	+.24%	0.2530	+.32%
147	-50	0.2547	0.2559	+.48%	0.2556	+.44%
147	-100	0.2577	0.2592	+.60%	0.2584	+.28%
147	-150	0.2645	0.2660	+.60%	0.2639	-.22%
294	32	0.2574	0.2578	+.16%		
294	-50	0.2630	0.2638	+.32%		
294	-100	0.2696	0.2711	+.20%		
294	-150	0.2859	0.2870	+.44%		
588	32	0.2673	0.2673	+.00%	0.2679	+.24%
588	-50	0.2802	0.2808	+.21%	0.2804	+.07%
588	-100	0.2982	0.2988	+.20%	0.2969	-.43%
588	-150	0.3398	0.3410	+.35%		
1176	32	0.2871	0.2868	-.10%		
1176	-50	0.3171	0.3171	+.00%		
1176	-100	0.3608	0.3615	+.20%		
1176	-150	0.4876	0.4868	-.17%		
2000	32	0.3110	0.3099	-.37%		
2000	-50	0.3562	0.3580	+.50%		
2000	-100	0.4208	0.4219	+.23%		
2000	-150	0.5233	0.5315	+1.57		

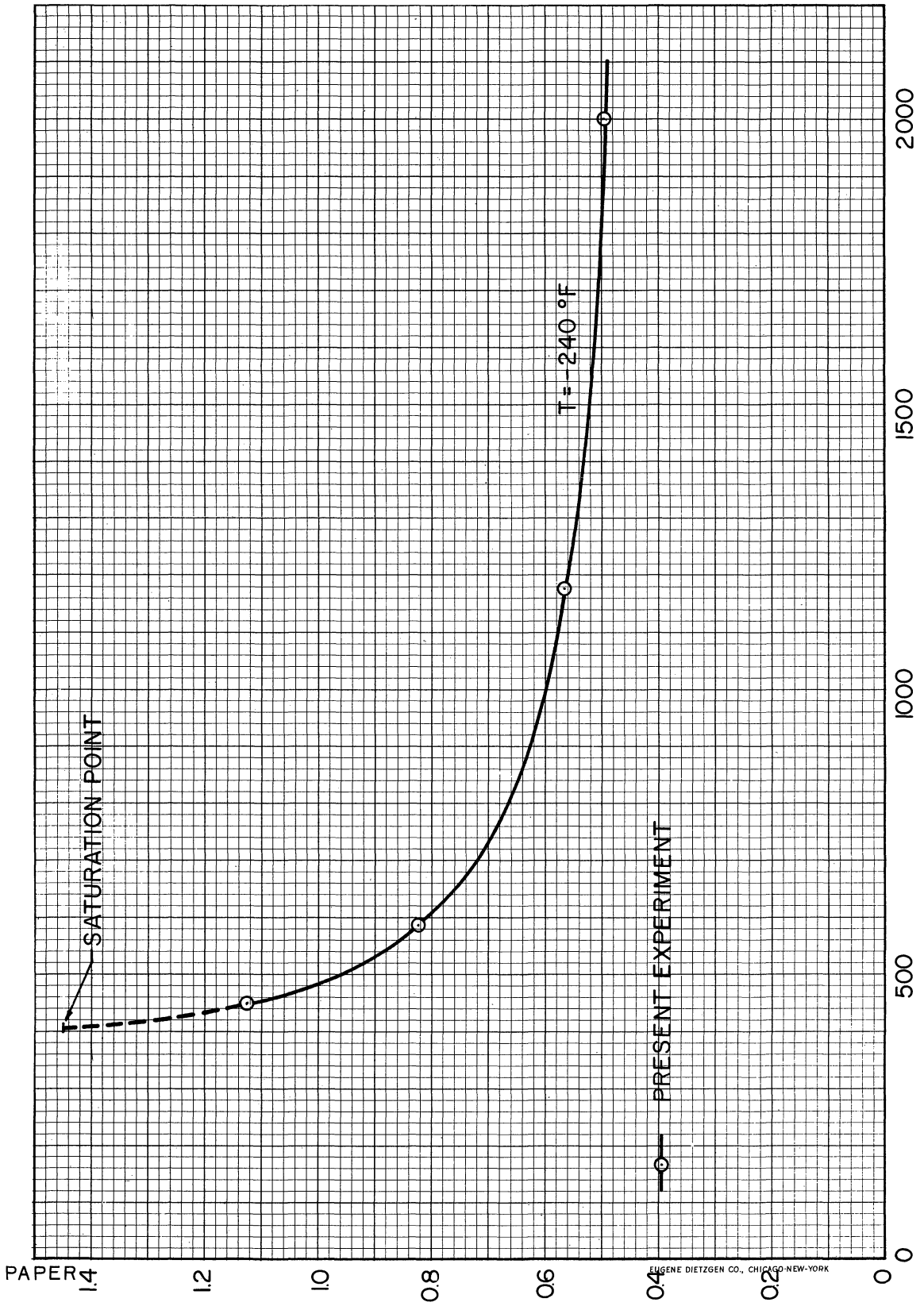

Figure 16. Heat Capacities of Compressed Liquid Nitrogen.

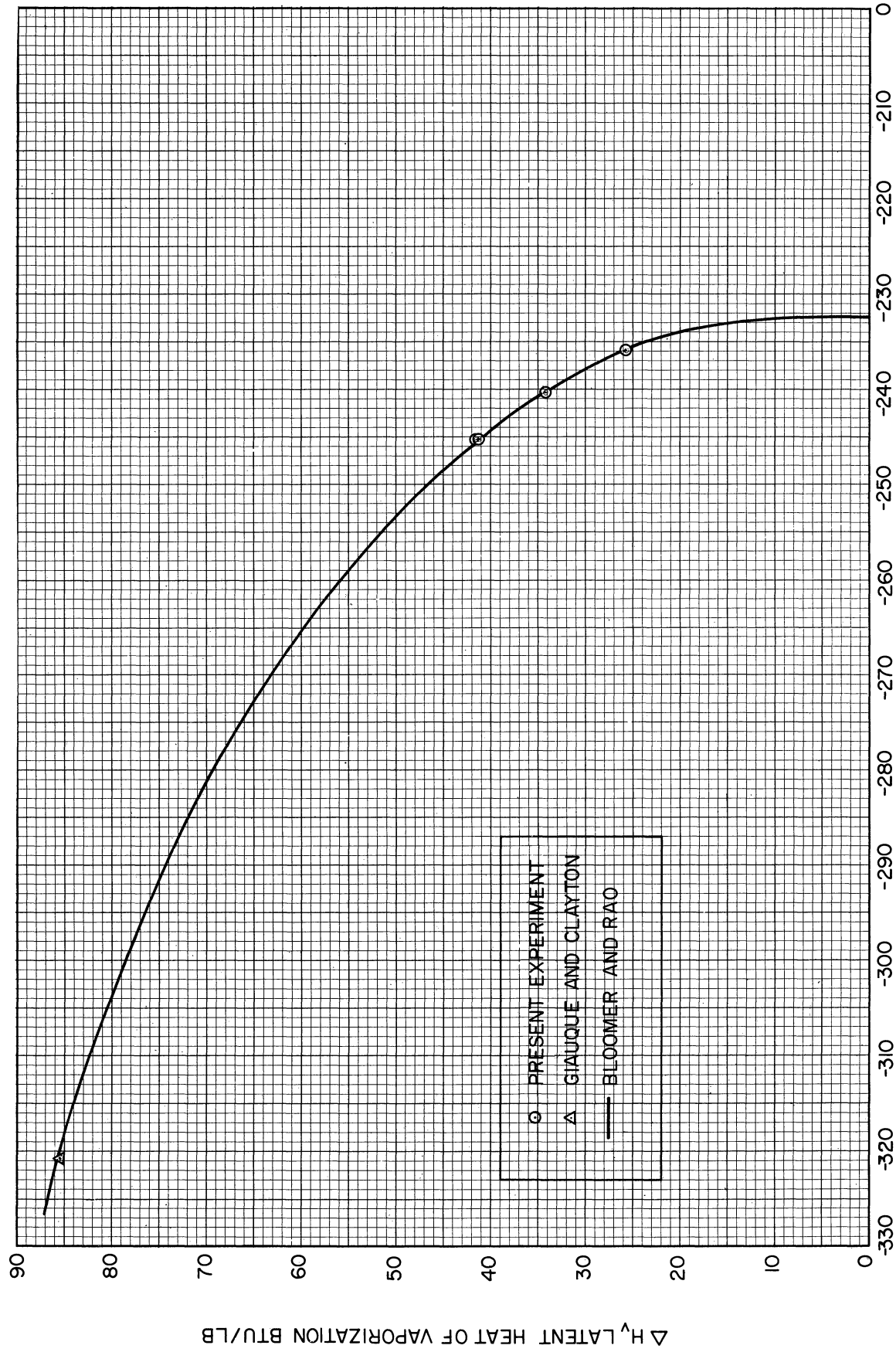

Figure 17. Comparison of Latent Heats of Vaporization of Nitrogen.

TABLE X

NUMERICAL VALUES OF CONSTANTS FOR NITROGEN
IN BLOOMER AND RAO EQUATION OF STATE

Units: Atmospheres, liters, gram moles, degrees Kelvin

Molecular Weight 28.014
Universal Gas Constant 0.08206
T°Kelvin = t(°Centigrade) + 273.16

B_o	0.0484824
A_o	1.27389
C_o	4273.00
D_o	7.61781×10^6
b	0.00232373
a	0.0178444
c	475.000
δ	0.832×10^6
γ	0.0065
a	0.00015300

TABLE XI

COMPARISON OF LATENT HEATS OF VAPORIZATION OF NITROGEN

Run	Temperature °F	Experimental Btu/lb	Bloomer and Rao Btu/lb	$\frac{\text{B\&R - Exp}}{\text{Exp.}} \times 100$
138	-245.17	41.50	41.1	-1.0%
139	-245.17	41.13	41.1	-0.1%
143	-245.22	41.69	41.2	-1.2%
140	-240.32	34.10	34.3	+0.6%
142	-235.99	25.82	26.0	+0.7%

TABLE XII

COMPARISON OF VAPOR PRESSURE OF NITROGEN

Run	Temp. Latent Ht. °F	Pressure Psia Experimental	Pressure Psia Friedman	ΔP Psi	$\frac{P_{exp.}-P_{Friedman}}{P_{exp.}} \times 100\%$
138	-245.17	349.6	349.2	+.4	+.11%
139	-245.17	349.6	349.2	+.4	+.11%
140	-240.32	399.4	399.0	+.4	+.10%
142	-235.99	449.9	449.0	+.9	+.20%
143	-245.22	349.7	348.6	+1.1	+.31%

ENTHALPY OF METHANE

The measured heat capacities and latent heats of vaporization of methane were used to define the heat capacity as a function of pressure and temperature over a good portion of the range covered, and to construct a chart of pressure versus enthalpy for methane.

Smoothed Heat Capacities

The relationship of the isobaric heat capacity of methane to pressure and temperature is shown qualitatively as a three dimensional surface in Figure 18, which was constructed from experimental measurements of the present investigation.

The methane heat capacity data was plotted versus temperature for each pressure investigated, and smooth curves were drawn through the data such that the area under the curves would equal the area under the measured heat capacity line. Figure 19 illustrates this technique for measurements made at 1200 psia. The smoothed data from these constant pressure graphs was then plotted versus pressure to give values of heat capacity at intermediate pressures, which were then used to complete the heat capacity versus temperature curves for pressures such as 680, 800 and 1500 psia, which were only investigated in regions where heat capacity changes rapidly with respect to temperature. Values taken from the heat capacity-pressure curves were also plotted versus temperature at each of the pressures at which latent heat of vaporization was measured and used, in conjunction with the liquid and vapor heat capacities obtained from latent heat measurements, to extrapolate to the values of heat capacity for the saturated liquid and vapor. Figures 20 and 21 are summaries of

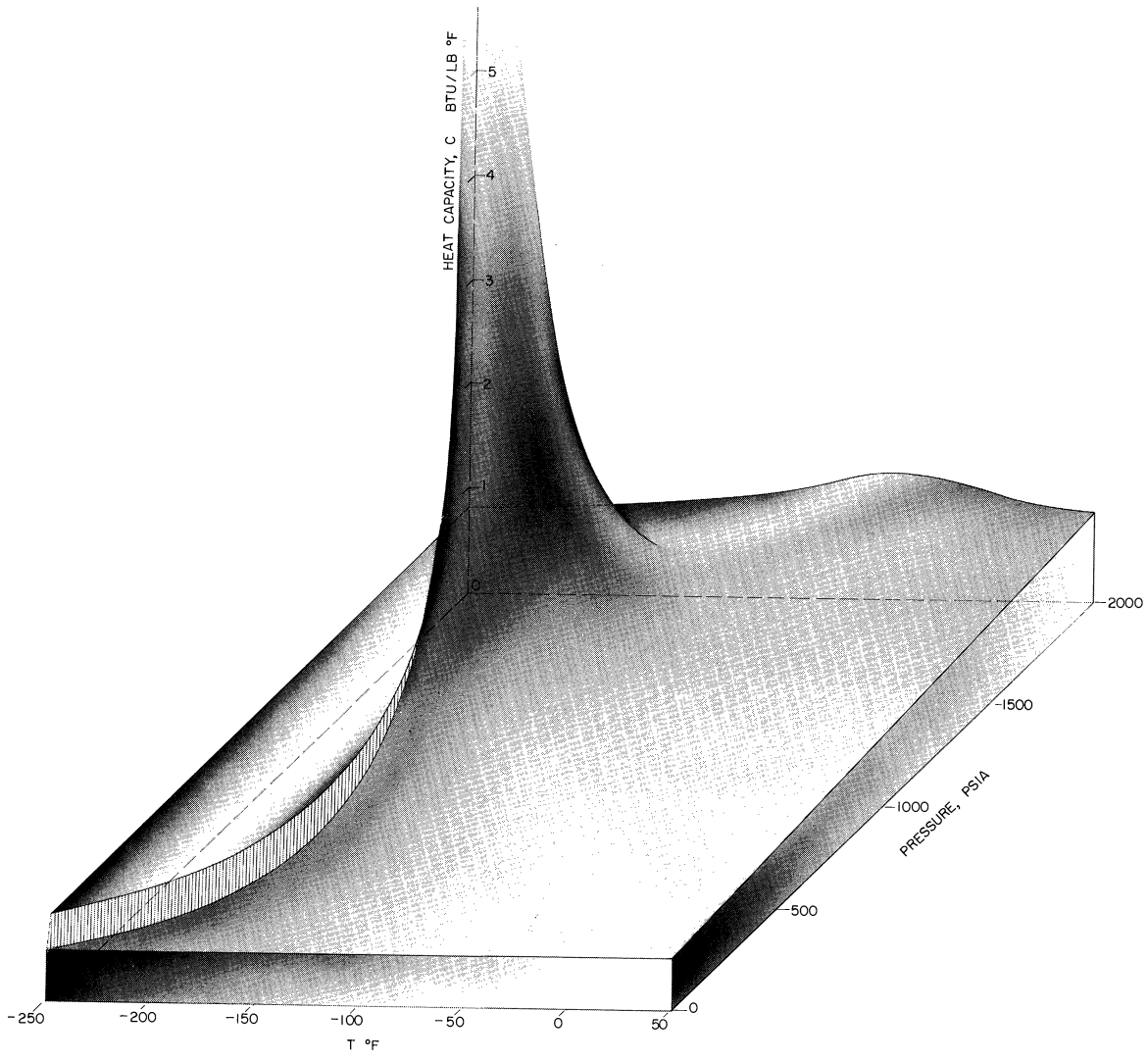

Figure 18. Heat Capacity of Methane as a Function of Temperature and Pressure.

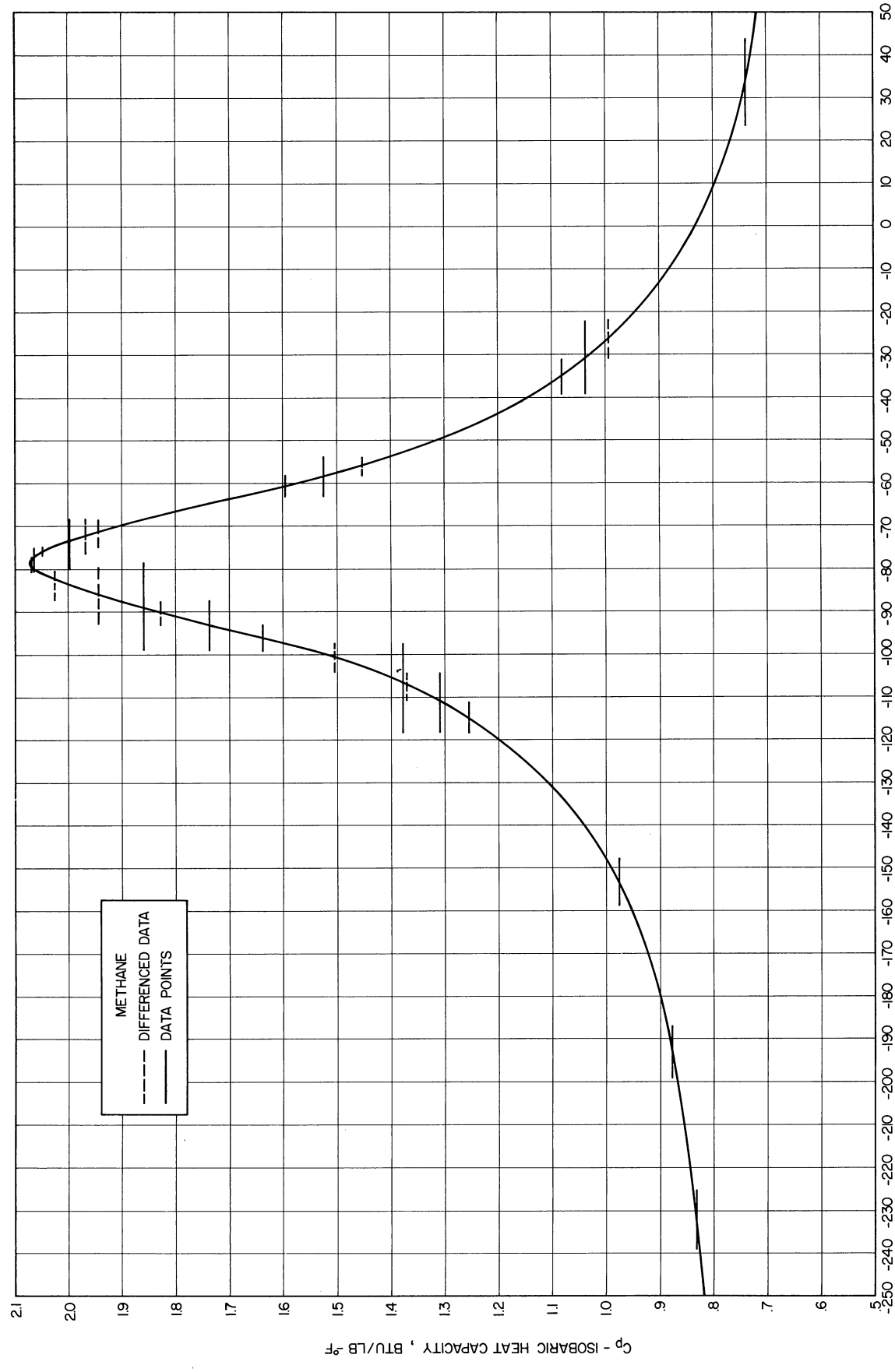

Figure 19. Heat Capacity of Methane at 1200 Psia, Illustrating Technique Used to Smooth the Data.

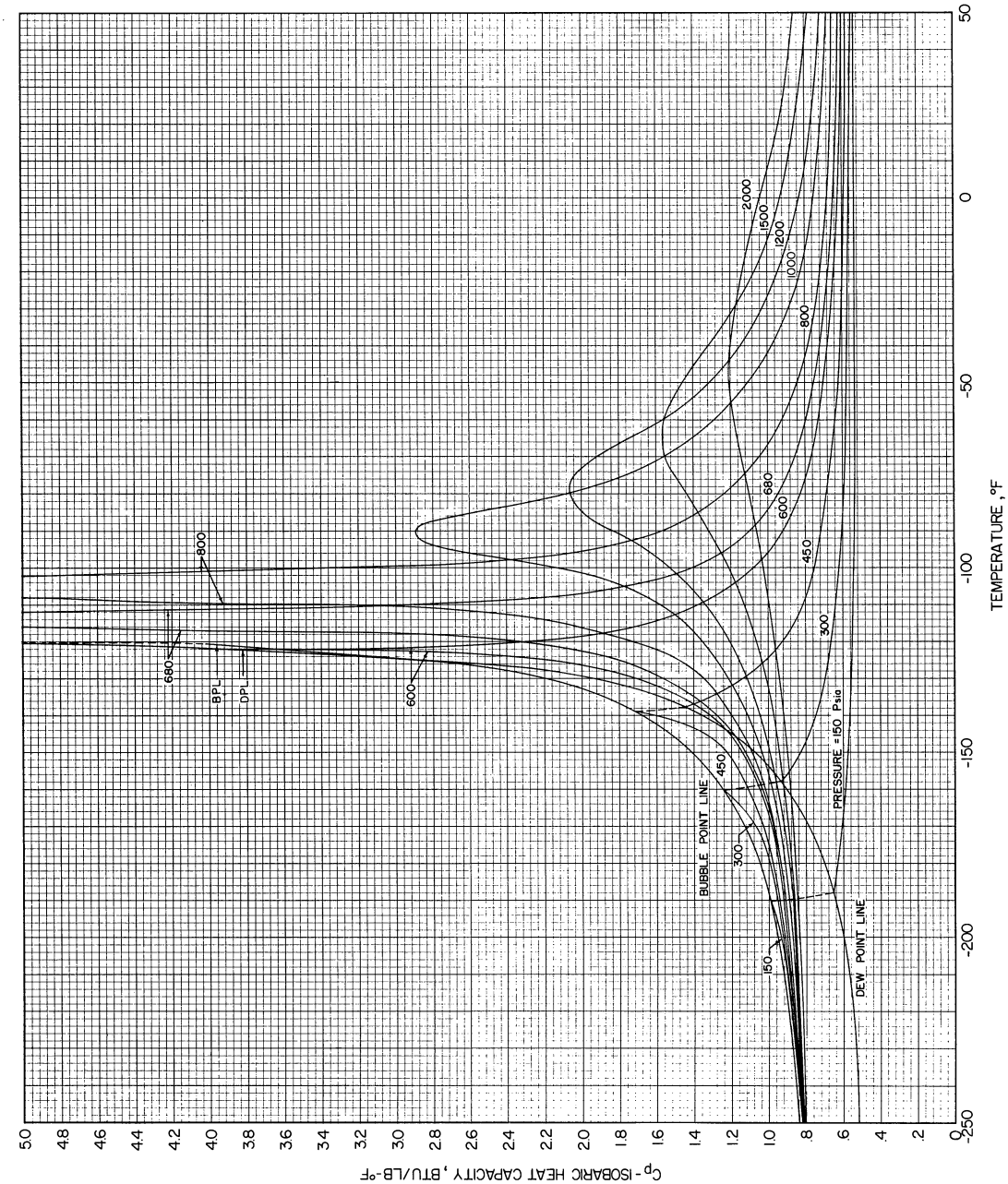

Figure 20. Smoothed Heat Capacity of Methane versus Temperature.

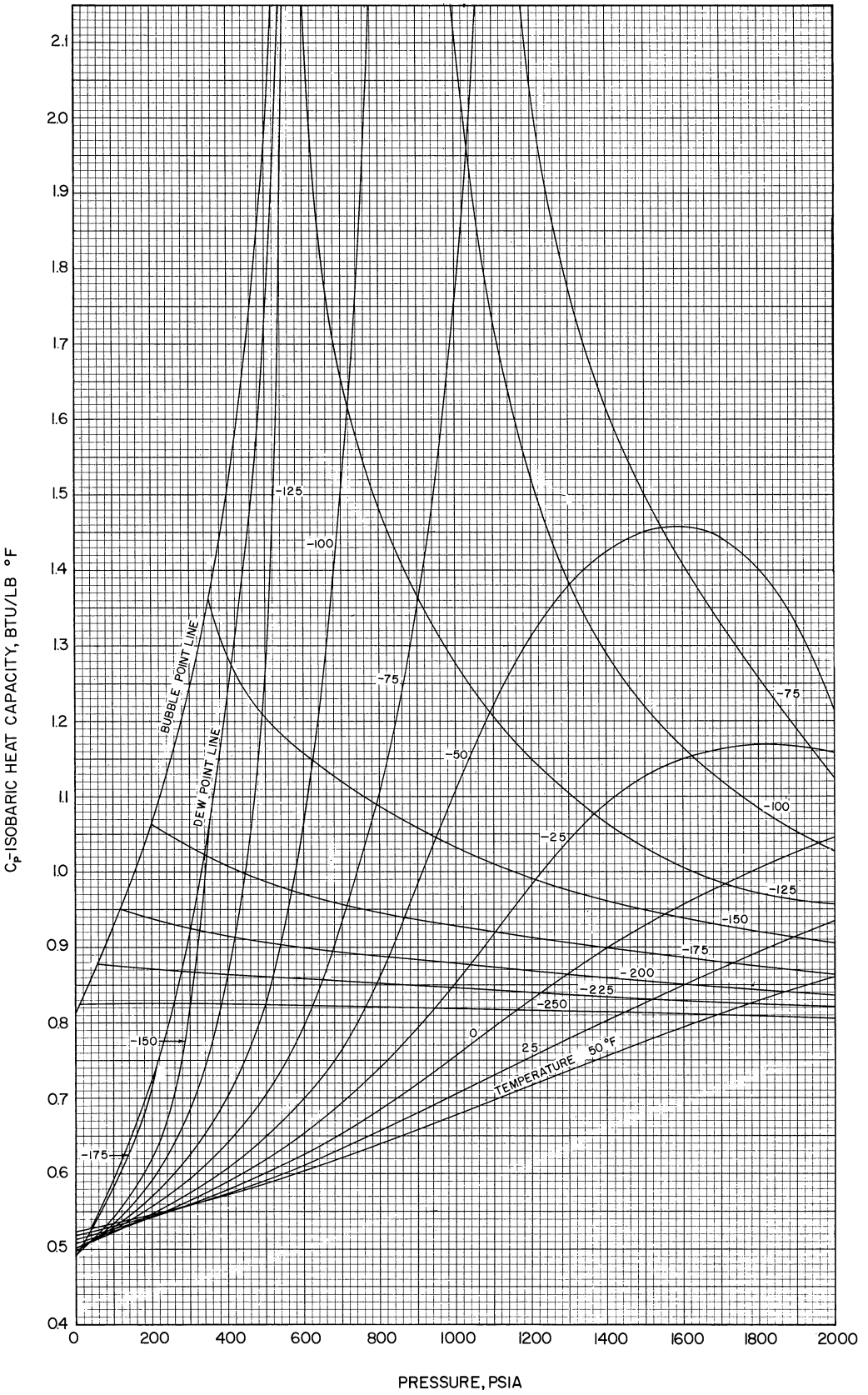

Figure 21. Smoothed Heat Capacity of Methane versus Pressure.

TABLE XIII

SMOOTHED HEAT CAPACITIES OF METHANE

Temp. °F	Pressure, Psia 150	300	350	450	550	600	625	680	800	Pressure, Psia 1000	1200	1500	2000
-250	0.825	0.824	0.824	0.823	0.822	0.821	0.820	0.820	0.819	0.818	0.817	0.812	0.804
-240	0.842	0.841	0.840	0.838	0.836	0.834	0.833	0.833	0.831	0.829	0.825	0.817	0.809
-230	0.862	0.856	0.855	0.854	0.849	0.848	0.847	0.845	0.841	0.839	0.834	0.824	0.815
-220	0.884	0.875	0.872	0.869	0.864	0.862	0.860	0.859	0.853	0.850	0.844	0.833	0.821
-210	0.910	0.895	0.892	0.888	0.885	0.881	0.878	0.876	0.871	0.861	0.854	0.842	0.827
-200	0.944	0.919	0.917	0.908	0.901	0.899	0.896	0.984	0.889	0.876	0.865	0.854	0.835
-190		0.949	0.948	0.936	0.925	0.920	0.918	0.912	0.907	0.890	0.880	0.867	0.844
-180	0.627	0.991	0.988	0.971	0.955	0.951	0.947	0.939	0.929	0.911	0.897	0.883	0.856
-170	0.603	1.062	1.040	1.021	0.998	0.996	0.988	0.975	0.962	0.939	0.919	0.901	0.870
-160	0.586		1.132	1.098	1.066	1.056	1.052	1.030	1.017	0.979	0.950	0.923	0.886
-150	0.574	0.826		1.233	1.175	1.156	1.149	1.127	1.088	1.037	0.989	0.947	0.904
-140	0.566	0.754	0.866	1.579	1.395	1.326	1.309	1.259	1.194	1.107	1.038	0.974	0.923
-130	0.560	0.705	0.785	1.117	1.972	1.703	1.628	1.532	1.336	1.207	1.106	1.099	0.945
-120	0.555	0.669	0.733	0.923	1.492	2.451	5.242	2.746	1.718	1.353	1.198	1.054	0.968
-110	0.551	0.644	0.695	0.818	1.091	1.362	1.506	2.876	3.585	1.594	1.320	1.119	0.995
-100	0.547	0.624	0.665	0.756	0.923	1.069	1.151	1.406	3.445	2.204	1.522	1.217	1.025
-90	0.544	0.608	0.642	0.713	0.830	0.922	0.977	1.122	1.653	2.900	1.831	1.347	1.056
-80	0.542	0.596	0.622	0.682	0.768	0.828	0.867	0.967	1.255	2.069	2.061	1.457	1.095
-70	0.540	0.586	0.608	0.659	0.726	0.768	0.793	0.863	1.041	1.537	1.901	1.535	1.134
-60	0.537	0.579	0.597	0.642	0.695	0.728	0.747	0.793	0.919	1.270	1.568	1.543	1.176
-50	0.536	0.573	0.589	0.628	0.671	0.698	0.711	0.749	0.841	1.103	1.309	1.454	1.209
-40	0.535	0.569	0.582	0.616	0.655	0.677	0.689	0.715	0.790	0.979	1.139	1.313	1.204
-30	0.535	0.565	0.577	0.607	0.641	0.659	0.671	0.691	0.756	0.888	1.025	1.183	1.174
-20	0.534	0.562	0.573	0.599	0.629	0.646	0.651	0.676	0.721	0.827	0.941	1.077	1.136
-10	0.535	0.560	0.570	0.593	0.619	0.636	0.642	0.660	0.699	0.785	0.879	0.994	1.092
0	0.535	0.499	0.568	0.589	0.612	0.626	0.631	0.647	0.680	0.754	0.831	0.928	1.044
+10	0.536	0.558	0.566	0.586	0.607	0.619	0.622	0.637	0.669	0.731	0.794	0.877	0.998
+20	0.537	0.557	0.565	0.583	0.602	0.611	0.616	0.628	0.659	0.712	0.765	0.840	0.954
+30	0.538	0.557	0.564	0.581	0.599	0.607	0.611	0.623	0.655	0.698	0.744	0.812	0.916
+40	0.539	0.557	0.564	0.580	0.598	0.605	0.608	0.619	0.649	0.685	0.728	0.791	0.885
+50	0.540	0.556	0.563	0.579	0.597	0.603	0.607	0.618	0.639	0.677	0.715	0.775	0.860

the heat capacities plotted versus temperature and pressure, respectively. Values from the original charts used to compile Figures 20 and 21 are listed in Table XIII.

Comparison With Literature Values

Since no direct measurements of the isobaric heat capacity of methane at low temperatures under high pressure were available from the literature, comparison was made to heat capacities obtained from derived data. The most recent and complete compilations appear to be those of Matthews and Hurd[52] and Keesom,[35] but only the former gives tabulations of enthalpy such that heat capacities may be obtained with fair accuracy by differencing the data. Matthews and Hurd calculated their enthalpies at zero pressure by statistical methods and obtained the change of enthalpy with pressure from the direct measurements of $(\frac{\partial H}{\partial P})_T$ of Eucken and Berger.[19]

The smoothed gaseous heat capacities are compared to values obtained by differencing the enthalpy data of Matthews and Hurd in Figure 22. Although agreement is fair at low pressures and moderate temperatures, it becomes poor at higher pressures and low temperatures. The largest disagreements occur at the pressure of 1500 psia, the limit of the compilation, and for lower pressures, at temperatures approaching the saturation curve.

Comparison With Equations of State

Since equations of state are frequently used to calculate the change of enthalpy or heat capacity with pressure, the accuracy to which the equations fit the heat capacity data is of considerable interest.

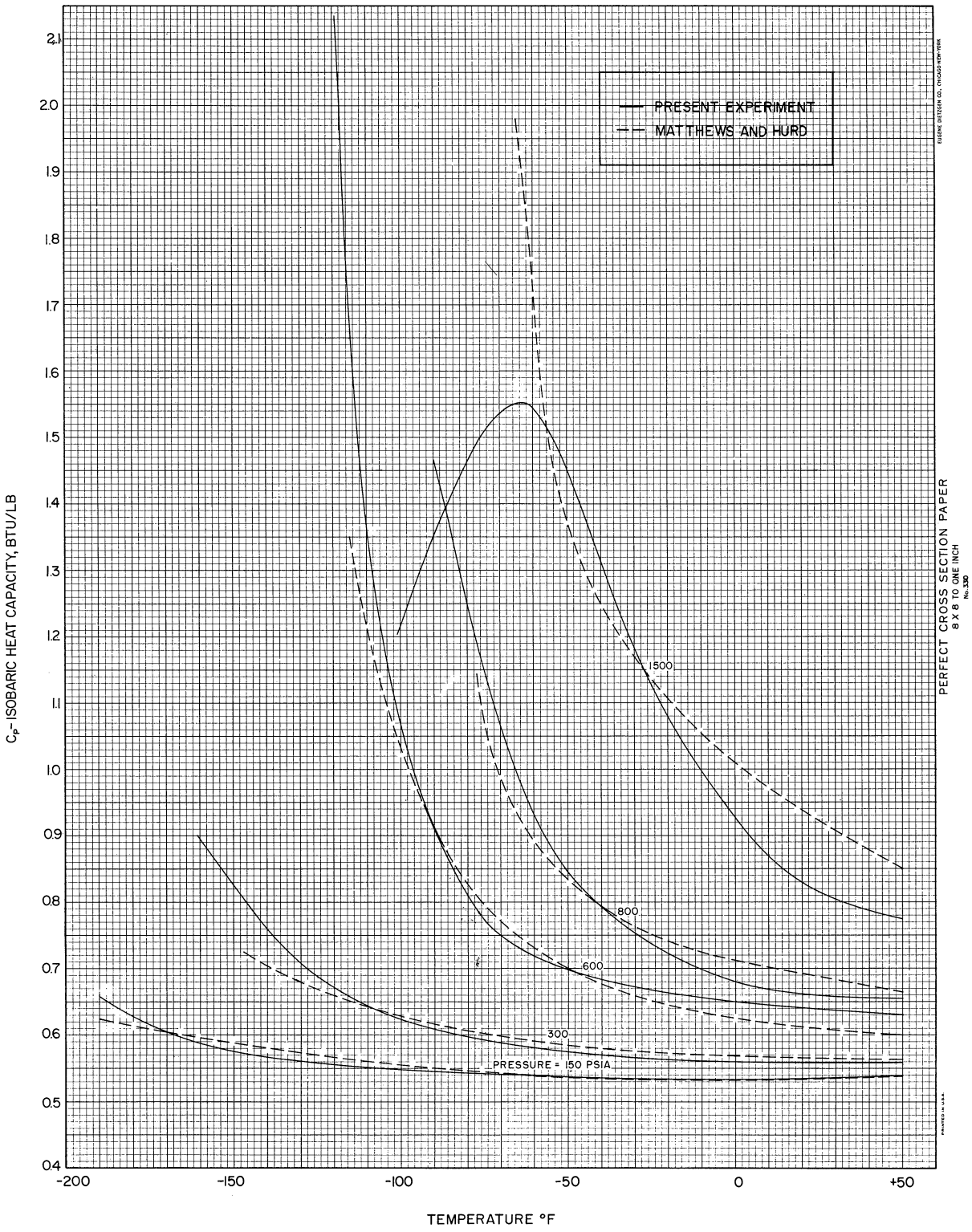

Figure 22. Comparison of Smoothed Methane Heat Capacities to Values From Matthews and Hurd.

The use of a numerical equation of state to fit heat capacity data is one of the most severe tests of the equation, since the equation must be differentiated twice.

With this in mind, isobaric heat capacities were calculated using the zero pressure heat capacities listed in API 44(2) and the equations of state of Benedict, Webb and Rubin(4) and Martin and Hou.(49) The equations of state are given as,

$$P = RT\rho + (B_oRT - A_o - \frac{C_o}{T^2})\rho^2 + (bRT - a)\rho^3 + \frac{c}{T^2}\frac{\rho^3(1+\gamma\rho^2)}{e^{\gamma\rho^2}} + a\alpha\rho^6 \quad (32)$$

$$P = \frac{RT}{V-b} + \frac{A_2+B_2T+C_2e^{-kT_r}}{(V-b)^2} + \frac{A_3+B_3T+C_3e^{-kT_r}}{(V-b)^3} + \frac{A_4}{(V-b)^4} + \frac{A_5+B_5T+C_5e^{-kT_r}}{(V-b)^5} \quad (33)$$

and the constants used are shown in Tables XIV and XV. Since no constants were available for the Martin and Hou equation from the literature, constants were fitted by the method prescribed by Martin,(48) and were then varied slightly to obtain a better fit of the available volumetric data. The sources for the data used for comparison are listed in Table XVI. Primary emphasis was given to fitting the data of Kvalnes and Gaddy(42) and Mueller,(56) since their data is in the temperature range of the present investigation.

Since both equations of state are explicit in pressure, the calculational technique used was similar to that used on the equation of state of Bloomer and Rao(19) for nitrogen. For the Benedict-Webb-Rubin equation in which pressure is given as a function of temperature and density, the equations are

$$H - H_1 = \int_{T_1}^{T} C_P^o dT + \int_{\rho_1=0}^{\rho} [\frac{1}{\rho}(\frac{\partial P}{\partial \rho})_T - \frac{T}{\rho^2}(\frac{\partial P}{\partial T})_\rho] \, d\rho \quad (30)$$

TABLE XIV

NUMERICAL VALUES OF CONSTANTS FOR METHANE
IN BENEDICT-WEBB-RUBIN EQUATION OF STATE

Units: Atmospheres, liters, gram moles, degrees Kelvin

Molecular Weight 16.042

Universal Gas Constant 0.08206

T°Kelvin = T(°Centigrade) + 273.16

B_o	0.0426
A_o	1.855
C_o	22257.0
b	0.00338004
a	0.0494
c	2545.0
α	0.000124359
γ	0.006

TABLE XV

NUMERICAL VALUES OF CONSTANTS FOR METHANE
IN MODIFIED MARTIN-HOU EQUATION OF STATE

Units: psia, cubic feet, pounds, degrees Rankin

Molecular Weight	28.014
Universal Gas Constant	0.66894

A_2	-39.681057
B_2	0.029633147
C_2	-302.25717
A_3	2.5133860
B_3	-0.0014923682
C_3	25.903247
A_4	-0.07536400
A_5	0.00019047718
B_5	0.0000028792828
C_5	0.018996954
b	0.024679167

$$C_P = C_P^o + \left(\frac{\partial H'}{\partial T}\right) + \left(\frac{\partial H'}{\partial \rho}\right)_T \left(\frac{\partial \rho}{\partial T}\right)_P \qquad (31)$$

For the Martin-Hou equation in which pressure is given as a function of temperature and volume, Equation (5) was modified to give,

$$H - H_1 = \int_{T_1}^{T} C_p^o dT + \int_{P_1=0}^{P} \left[V - T\left(\frac{\partial V}{\partial T}\right)_P\right] dP = \int_{T_1}^{T} C_{pdT}^o + \int_{V_1=\infty}^{V} \left[V\left(\frac{\partial P}{\partial V}\right)_T + T\left(\frac{\partial P}{\partial T}\right)_V\right] dV \qquad (34)$$

The integrations were performed to give enthalpy as a function of temperature and volume, and the equation differentiated with respect to temperature at constant pressure, by the equation

$$C_P = \left(\frac{\partial H}{\partial T}\right)_P = C_P^o + \left(\frac{\partial H'}{\partial T}\right)_V + \left(\frac{\partial H'}{\partial V}\right)_T \left(\frac{\partial V}{\partial T}\right)_P \qquad (35)$$

The heat capacities calculated from these equations are compared to the present data in Figure 23, which shows heat capacity versus temperature at 150, 300, 600, 1000, 1200, 1500 and 2000 psia. The present data is indicated by the horizontal bars, which represent actual data points, and by the continuous lines which represent the author's best line.

Both equations of state give fair agreement at the higher temperatures and in the regions corresponding to low reduced densities; however, accuracy decreases considerably at lower temperatures and higher densities. The Benedict-Webb-Rubin equation gives good qualitative agreement throughout the region in which it fits the volumetric data, up to about twice the critical density, but the Martin-Hou equation appears to deviate considerably from the experimental curve in regions near its limit, but where it still fits the volumetric data well. This is best shown on

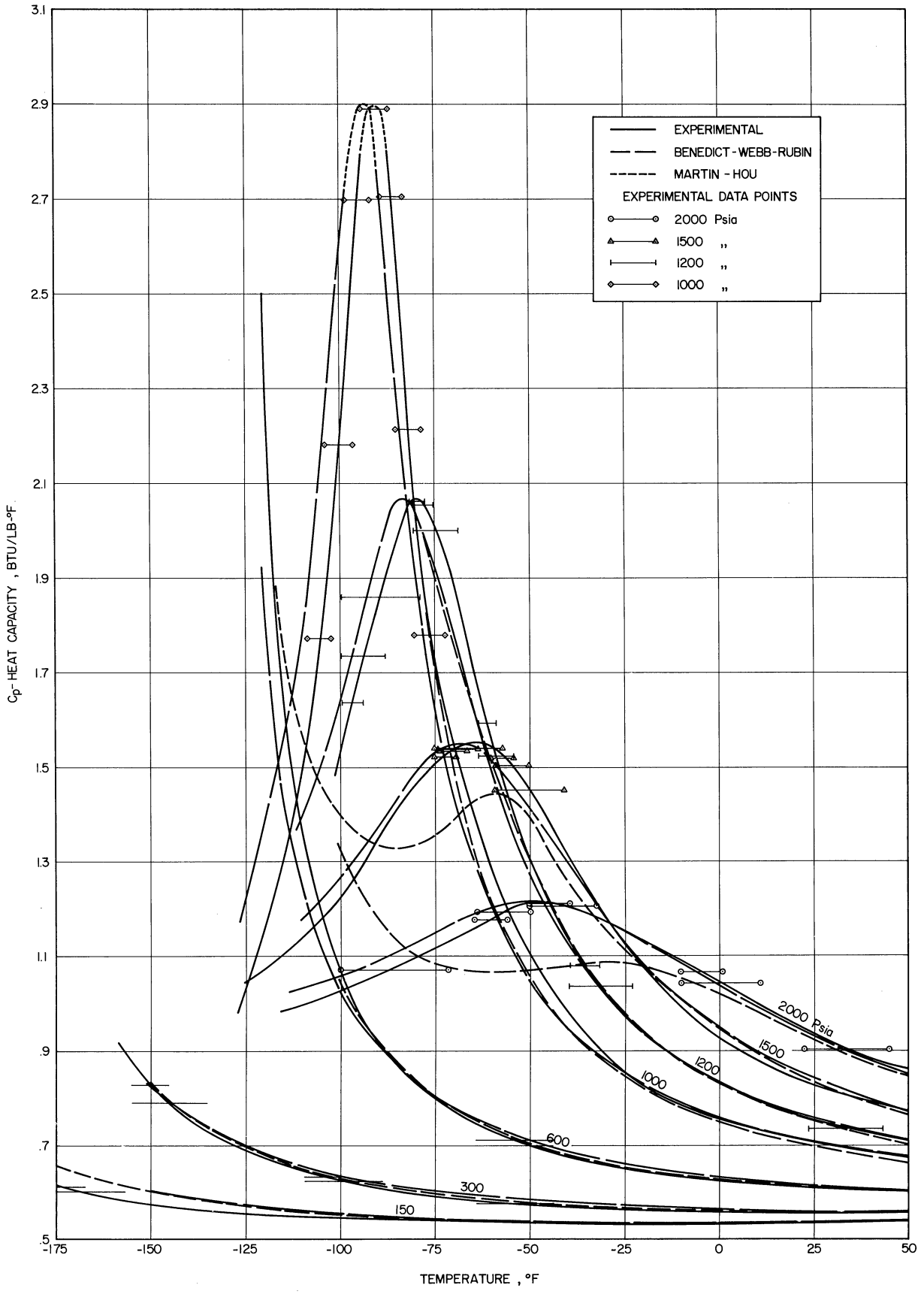

Figure 23. Comparison of Measured Methane Heat Capacities to Values Calculated from Equations of State.

TABLE XVI

REFERENCES FOR VOLUMETRIC DATA FOR METHANE

Reference	Investigators	Temperature Range °F	Pressure Range Psia
10	Cardoso	-148 to -119.2	378 to 639
39	Keyes, Burks	32 to 390	474 to 1794
42	Kvalnes, Gaddy	-100 to 390	14.7 to 5878
53	Michels, Nederbragt	32 to 300	270 to 5641
62	Mueller, Leland and Kobayashi	-200 to +50	40 to 7000
58	Olds, Reamer, Sage and Lacey	50 to 432°	5 to 10000
68	Schamp, Mason, Richardson and Altman	32 to 300	257 to 3790

the 2000 psia line. The equation fits the volumetric data to about 1.5 times the critical density corresponding to -50°F, but breaks sharply from the experimental heat capacity curve at 0°F, which corresponds closely to the critical density.

Construction of the Pressure-Enthalpy-Temperature Diagram

In constructing a pressure-enthalpy-temperature diagram for methane from the data of the present experiment, enthalpy may be determined as a function of temperature at any pressure by integration of the curves of heat capacity versus temperature and by use of the measured latent heats of vaporization. However, in order to use these

enthalpy functions to construct a P-H-T chart, either Joule-Thomson coefficients must be used to define an isenthalp throughout the pressure range of the chart, or values of $(\frac{\partial H}{\partial P})_T$ must be known at one or more temperatures throughout the pressure range. Although Joule-Thomson measurements were considered in the planning of the present experiments, it was felt that the volumetric data of methane was well known in the region near 50°F, and that values of $(\frac{\partial H}{\partial P})_T$ could be obtained using an equation of state which fits this data. In future experiments with mixtures for which the volumetric data is not well known it will be desirable to measure Joule-Thomson coefficients.

Low Pressure Enthalpies

The first step in the construction of the pressure-enthalpy chart was the setting of the data level as H = 0 for saturated liquid methane at -280°F. This is the same datum level used by Matthews and Hurd[52] and assures that all the values of enthalpy used are positive. The enthalpy of the saturated vapor was then taken as the value of the latent heat of vaporization of Frank and Clusius[24] which was corrected to -280°F. The enthalpy at -280°F and zero pressure was then determined by using the Benedict-Webb-Rubin[4] equation of state to calculate the isothermal enthalpy change at -280°F from the vapor pressure to zero pressure. Enthalpies were then charted along the zero pressure line each 10°F from -280°F to 50°F, using the values given in API 44[2]. It was apparent at this point that allowance must be made for the impurities in the methane tested. Since corrections for the impurities could be made accurately only at low pressures where the gases act ideally, it was decided that the P-H-T chart would be constructed for the gas mixture

tested, rather than for the pure component methane. With this in mind, the zero pressure enthalpies were adjusted slightly to compensate for the change in heat capacity and molecular weight. This amounted to a decrease in enthalpy change of about 0.4% along the base line, or 0.65 Btu per pound from -280°F to 50°F. This procedure provided a good set of reference data which was used in the final graph construction to extend the experimental data to low pressure. It also provided a "working datum" for gaseous methane at zero pressure and 50°F from which the chart was constructed.

The Effect of Pressure on the Enthalpy of Methane

In determining enthalpy as a function of pressure in the range of the present experiment, three sets of experimental data were available. These were the direct measurements of $\left(\frac{\partial H}{\partial P}\right)_T$ of Eucken and Berger,[19] the volumetric data listed in Table XVI and the Joule-Thomson data of Budenholzer, Sage and Lacey.[8] Although this last data is at higher temperatures, it could be easily extrapolated to the highest temperature of the P-H-T diagram, 50°F.

The required pressure-enthalpy line was determined from the volumetric data via the Benedict-Webb-Rubin equation of state, at 50°F, the highest temperature to be included in the pressure-enthalpy-temperature chart. At this temperature the equation of state not only agrees well with the volumetric data throughout the pressure range 0-2000 psia, but allows accurate calculation of the heat capacity as a function of pressure. At lower temperatures the equation of state becomes less accurate in the calculation of both volumetric properties and heat capacities. Table XVII compares the heat capacities extended from zero pressure by

use of this equation of state at 50°F to the heat capacities obtained by smoothing the data of the present experiment. Since the agreement of the equation of state with both the volumetric and heat capacity data is good, it is felt that the pressure-enthalpy line at 50°F may be determined with a high degree of accuracy using this equation of state.

Figure 24 shows the pressure-enthalpy line determined at 50°F, and compares it to the line determined from the results of Eucken and Berger,[19] and to the values calculated from extrapolated values of the Joule-Thomson coefficients of Budenholzer, Sage and Lacey.[8] The good agreement between the line calculated from the equation of state and the line predicted by Budenholzer, Sage and Lacey reinforces the conclusions that the equation of state line is of high accuracy. The data of Eucken and Berger is most probably inaccurate. We have already seen in Figure 22 that Matthews and Hurd's treatment of this data yields unreliable values of heat capacity.

Isobaric Enthalpies

The enthalpy was extended versus temperature at each pressure by integration of the graphs of heat capacity versus temperature to give values at each 10°F, and by use of the measurements of latent heats of vaporization. Numerical values of measured heat capacity and enthalpy differences were used where possible for better accuracy, along with graphical integration of the drawn curve in regions between measured points. For example, liquid heat capacity curves at the pressures at which latent heat was measured were integrated from -250°F up to the initial temperature used in the measurement of the latent heat, some 5°F

TABLE XVII

COMPARISON OF 50°F HEAT CAPACITIES
WITH VALUES DERIVED FROM B-W-R EQUATION OF STATE*

Pressure Psia	Heat Capacity, Btu/lb °F Experimental	Derived	$\frac{\text{Derived-Exp.}}{\text{Exp.}} \times 100\%$
150	.5400	.5415	+.28%
300	.5580	.5605	+.45%
600	.6048	.6042	-.10%
800	.6406	.6377	-.45%
1000	.6787	.6744	-.63%
1200	.7170	.7134	-.51%
1500	.7757	.7723	-.44%
2000	.8612	.8520	-1.07%

* Zero pressure heat capacity from A. P. I. 44(2).

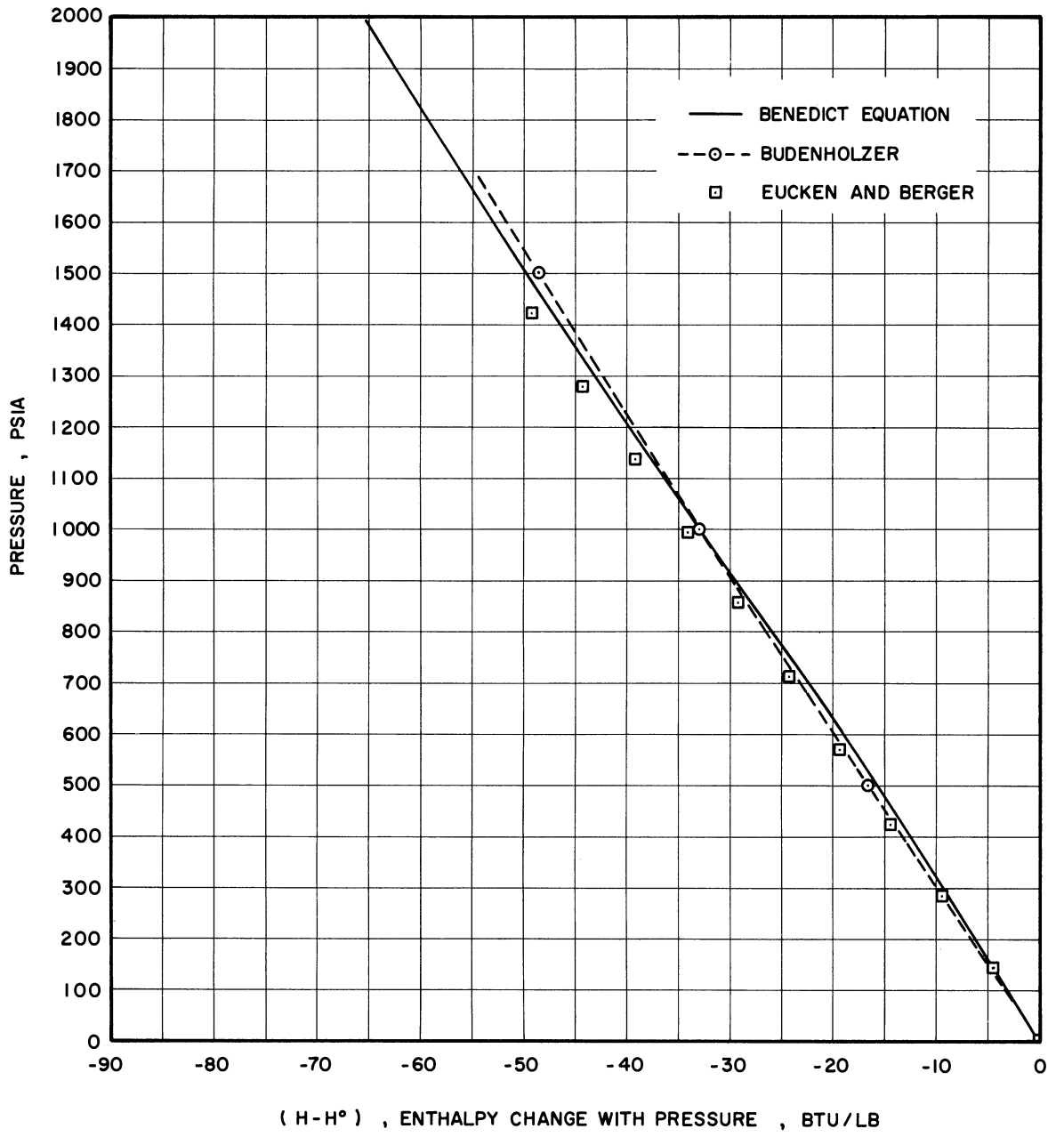

Figure 24. Comparison of Methane Enthalpy as a Function of Pressure at 50°F.

to 8°F below the bubble point. Enthalpies of the saturated liquid and vapor and the superheated gas some 2°F to 5°F above the dew point were then taken directly from charts such as Figure 12, followed by integration of the gaseous heat capacity curve to 50°F.

The integrations of heat capacity were checked for error graphically by plotting the enthalpies obtained at each pressure versus temperature, and by comparing the enthalpies at each temperature to those of other pressures on the constructed pressure-enthalpy chart. Any small deviation from smoothness of the lines drawn was checked for calculational error.

The Saturation Curve

A survey of the literature indicated that the critical pressure and temperature of methane were 669 psia and -116.6°F, respectively. These values correspond closely to the recent experimental values reported by Bloomer and Parent(5) and the values obtained from a critical review of the literature by Armstrong, Brickwedde and Scott.(3) The enthalpy at this point was calculated from the enthalpies of the saturated vapor and liquid by a method similar to the method of rectilinear diameters used for calculating critical volumes. The mean enthalpy of the saturated gas and saturated liquid for each latent heat measurement was plotted versus temperature and extended to the critical temperature to give the enthalpy of the critical point as shown in Figure 25. This value of enthalpy was checked by plotting the mean enthalpies versus pressure and extending them to the critical pressure. The two methods are equivalent, giving the same value of enthalpy at the critical point. With the critical

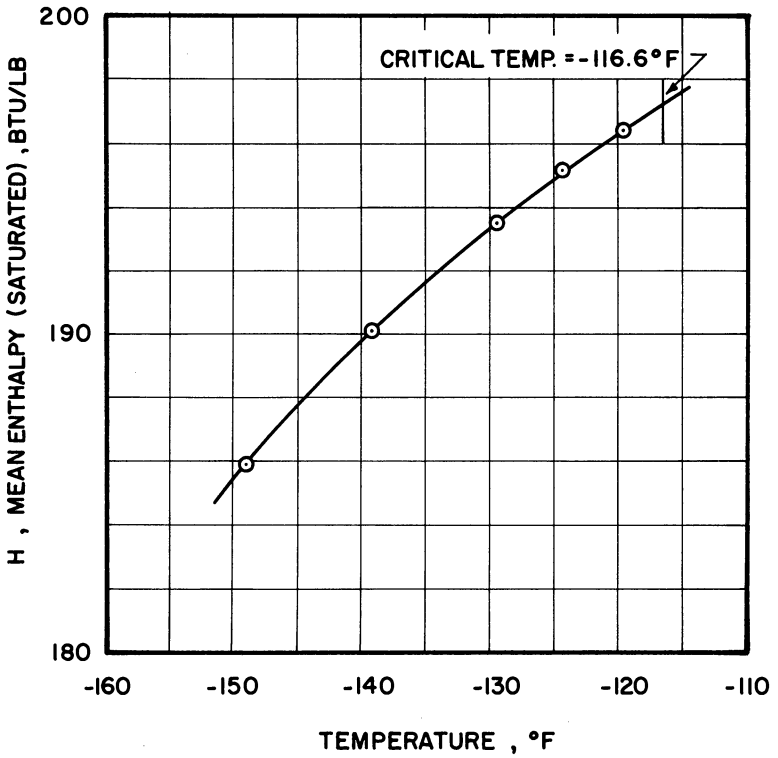

Figure 25. Plot of Average of Saturated Liquid and Vapor Enthalpies versus Temperature to Obtain Enthalpy of Critical Point.

point thus determined, the saturation curves were drawn from the dew point at 150 psia to the bubble point at 350 psia.

Final Drafting of the P-H-T Diagram

When all calculational errors had been eliminated and the saturation curve determined, smooth curves of constant temperature were fitted to the plotted points.

In general the lines agree with the plotted points to 0.1 Btu/lb, the reading error of the enlarged graph, but in the compressed liquid region below the critical point certain points disagree up to 0.7 Btu/lb.

In the gaseous region of the P-H-T diagram the constant temperature lines were extended to low pressure using the aforementioned zero pressure enthalpies. At temperatures lower than -180°F, corresponding to saturation pressures lower than 150 psia where no data was taken in the present experiment, the enthalpy of the saturated gas relative to the enthalpy of the -180°F saturation point from the data was made to agree with values from Matthews and Hurd[52] with some adjustment for smoothness and extended to the zero pressure enthalpies. In the compressed liquid region, the constant temperature lines were extended below 300 psia to the vapor pressure of pure methane to define the saturation curve. The recent vapor pressure data of Hesterman and White[30] was used.

Since the heat capacity changes only slightly with temperature in the low temperature compressed liquid region, it was felt that the P-H-T diagram could be extended to -280°F with high accuracy by extrapolating the heat capacity-temperature curves to -280°F and graphically integrating them to obtain the enthalpy data. When this was done, and the -280°F line was extended to the vapor pressure of methane, it was found that a negative correction of about 4 Btu/lb was needed to make this point agree with the original datum level of H=0 for saturated liquid methane at -280°F. The reasons for this are not clear. The disagreement is a composite of the following factors:

1. Impurities in the measured methane. Corrections would amount to one or two Btu/lb.
2. Use of the Benedict-Webb-Rubin equation of state for calculation of the isothermal enthalpy change for gaseous methane at -280°F.

3. Inaccuracy of the latent heat of vaporization at -280°F.

4. The inaccuracies inherent in the measurement of enthalpy properties in the present experiment and in the use of these properties to obtain isobaric enthalpies.

5. Inaccuracies involved in extrapolation versus temperature and pressure to -280°F saturated liquid methane.

Factors four and five are the more serious. The inaccuracy of measurement of heat capacities and latent heats of vaporization, and of integration of heat capacities to obtain isobaric enthalpies allows about 2 Btu/lb uncertainty in the very low temperature region. Although this allows accurate calculation of enthalpies as a function of temperature at any pressure in this range, it does not allow accurate calculation of enthalpy change with pressure. Extrapolation of these lines to lower pressures is expected to be inaccurate. It is unfortunate that there is no volumetric data for methane in the low temperature compressed liquid region which would allow calculation of pressure-enthalpy lines, which would be more accurate than those presented here; however, volumetric data may be calculated from that of other substances by using reduced volume techniques with fair accuracy.

Figure 26 compares the -250°F pressure-enthalpy line of the present experiment to that calculated by Keesom[35] using reduced volumes of ethylene, and illustrates the problems encountered at low temperatures. The points plotted were determined from the data, and show a degree of precision much higher than would be expected from the accuracy of the data. The experimental pressure-enthalpy line could be drawn through the points and extrapolated in a number of ways to obtain various results,

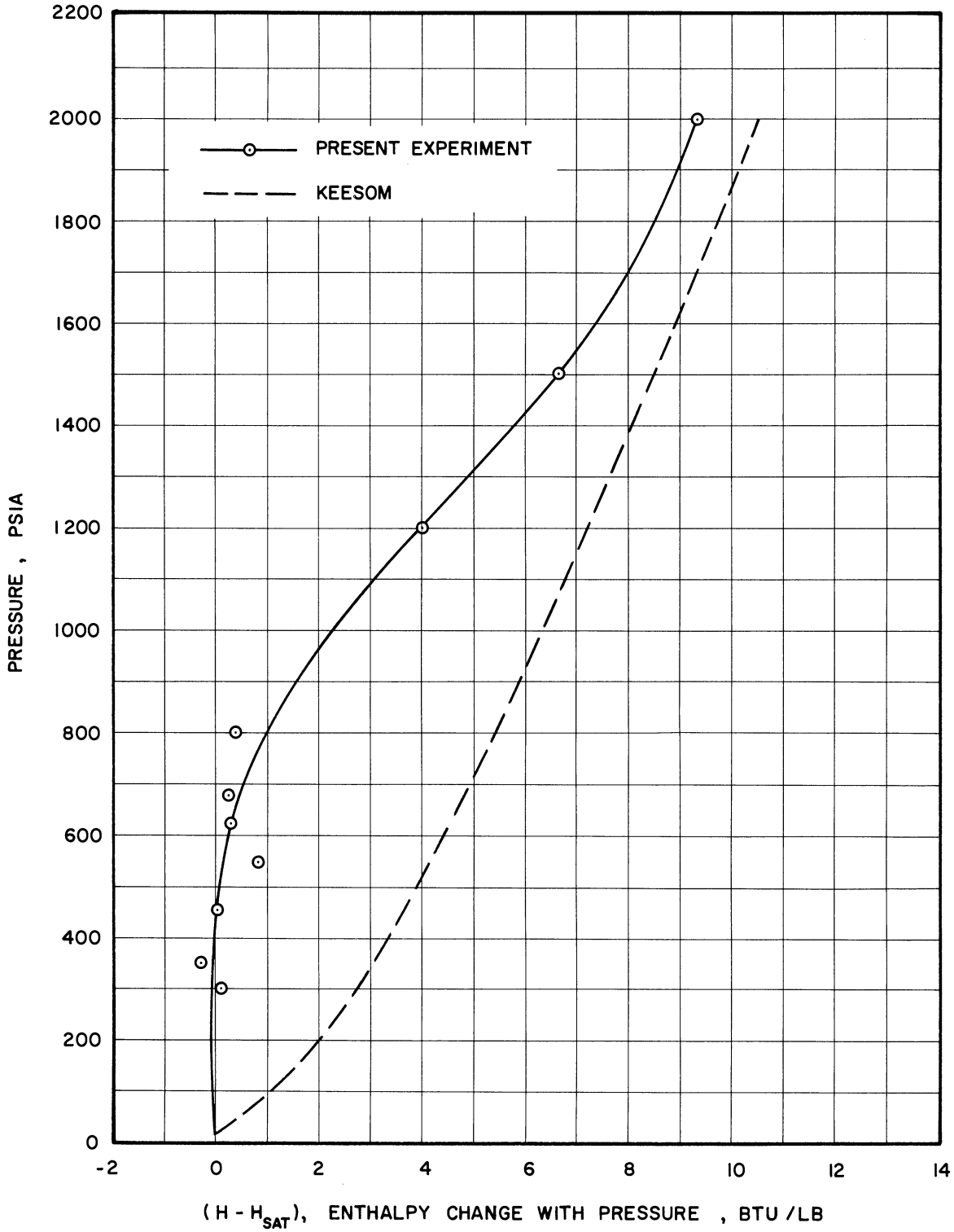

Figure 26. Comparison of Experimental Pressure-Enthalpy Line at -250°F with Derived Values.

but it would be difficult to draw this line with any degree of confidence such that it would agree well with the Keesom's line.

In constructing the P-H-T diagram the pressure-enthalpy lines were drawn through the data as shown in Figure 26, in such a way as to maintain the internal consistency of the diagram. The enthalpies determined were decreased by 4 Btu/lb to make the extrapolated enthalpy for -280°F saturated liquid be equal to zero, and slight adjustments were made in the saturated vapor enthalpies at low pressure in order to correct for the use of the Benedict equation of state, and in order to smooth the latent heats of vaporization.

The final pressure-enthalpy-temperature diagram is shown in Figure 27. Rectangular coordinates were used for both pressure and enthalpy in order to illustrate the behavior of methane under high pressure in more detail than possible on a diagram of the logarithm of pressure versus enthalpy. In order to increase the accuracy of enthalpy calculations, the values taken from the diagram are tabulated in Table XVIII. These tabulated values were differenced with respect to temperature and adjusted slightly where necessary such that the differenced values agreed with the heat capacity curves. All such adjustments were within the reading error of the diagram.

It is felt that enthalpy differences at constant pressure may be obtained from the P-H-T diagram to an accuracy of 1% or 0.5 Btu/lb, whichever is larger. The exceptions are that enthalpy differences for liquids below 300 psia and superheated gases below -180°F are of considerably lower accuracy.

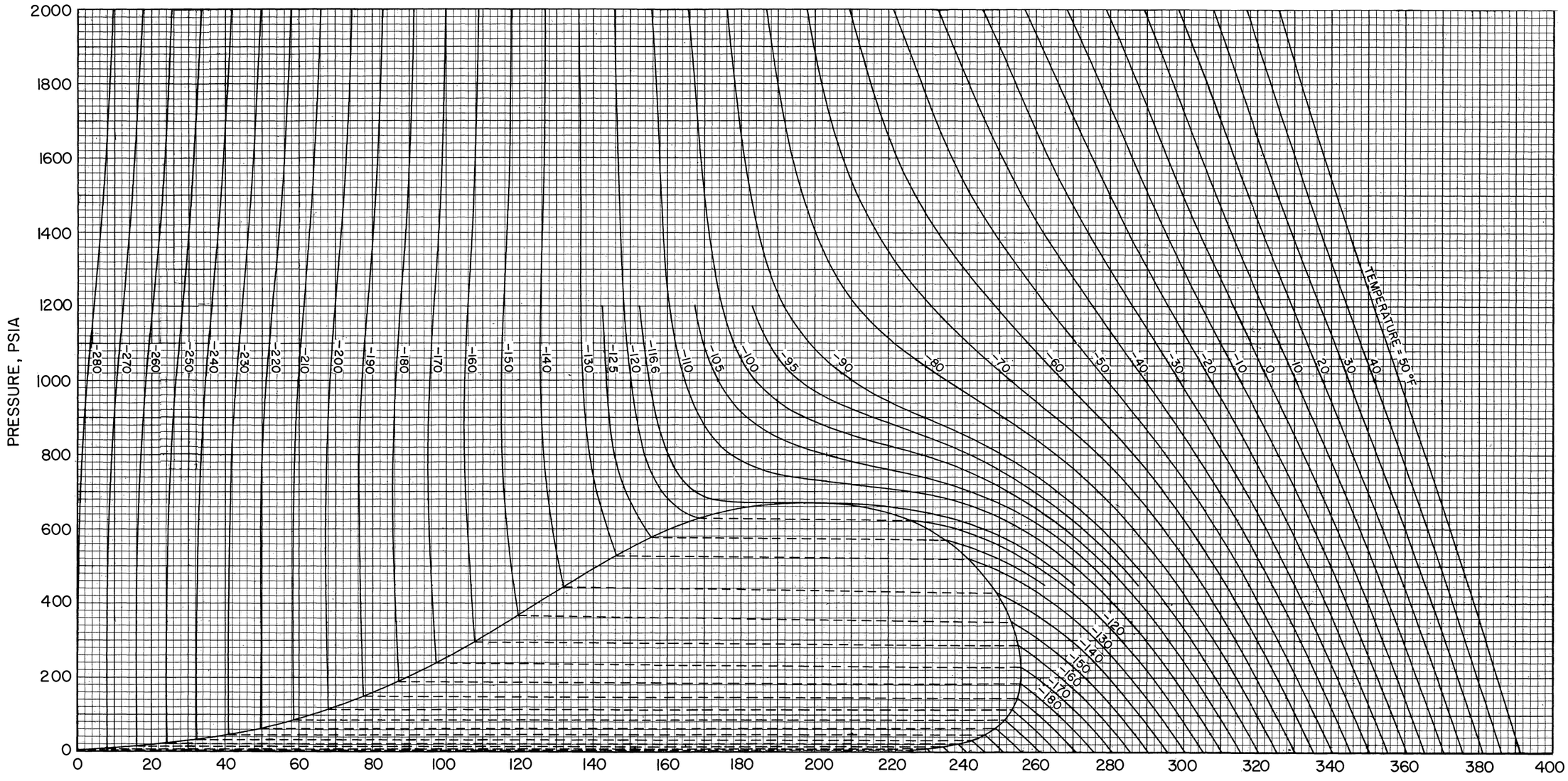

Figure 27. Pressure-Enthalpy-Temperature Diagram for Methane.

TABLE XVIII

ENTHALPY OF METHANE

Pressure Psia	Temperature °F (Methane)	Bubble Point Temperature °F	Dew Point Temperature °F	Saturated Liquid Enthalpy Btu/Lb	Saturated Vapor Enthalpy Btu/Lb	Latent Heat of Vaporization Btu/Lb.
5	-280			0	226.0	226.0
9	-270			8.1	230.5	222.5
14	-260			16.1	234.8	218.7
22	-250			24.3	238.8	214.5
31	-240			32.6	242.7	210.1
46	-230			41.1	246.1	205.0
65	-220			49.8	249.0	199.2
87	-210			58.7	251.6	192.9
115	-200			68.0	253.6	185.6
149	-190			77.5	255.0	177.5
190	-180		-178.4	87.2	255.8	168.6
240	-170		-168.5	97.3	255.8	158.5
298	-160		-159.6	107.9	254.6	146.7
367		-150	-148.1	119.6	252.5	132.9
443		-140	-138.5	132.0	248.1	116.1
530		-130	-129.0	146.6	240.3	93.7
579		-125	-124.2	155.8	234.4	78.6
631		-120	-119.3	168.3	224.5	56.2
669		-116.6	-116.6	197.2	197.2	0

Temp. °F	Pressure Psia	0	50	100	150	200	250	300	350	400	450	500	550	600	625	680	700	800	900	1000	1200	1500	2000
Sat. Liq.			44.2	63.6	77.7	89.2	99.4	108.4	117.0	125.2	133.3	141.6	150.3	160.6	167.2								
Sat. Gas			246.7	252.6	255.0	255.8	255.4	254.6	253.0	250.8	247.7	243.5	238.3	231.3	226.3								
-280	226.4	0.0	0.0	0.0	0.0	0.0	0.0	0.0	0.1	0.1	0.1	0.2	0.3	0.4	0.4	0.6	0.7	1.1	1.7	2.4	4.3	6.9	9.5
-270	231.3	8.0	8.0	8.0	8.0	8.0	8.0	8.0	8.1	8.1	8.1	8.2	8.3	8.4	8.4	8.6	8.7	9.1	9.7	10.4	12.3	14.9	17.5
-260	236.3	16.1	16.1	16.1	16.0	16.0	16.0	16.1	16.1	16.1	16.1	16.2	16.3	16.4	16.4	16.6	16.7	17.1	17.7	18.4	20.3	22.9	25.5
-250	241.2	24.3	24.3	24.2	24.2	24.2	24.2	24.3	24.3	24.3	24.3	24.4	24.5	24.6	24.6	24.8	24.9	25.2	25.8	26.5	28.3	30.9	33.5
-240	246.1	32.6	32.6	32.5	32.5	32.5	32.5	32.6	32.6	32.6	32.6	32.7	32.8	32.9	32.9	33.1	33.2	33.4	34.0	34.7	36.4	39.0	41.6
-230	251.0	41.1	41.1	41.0	41.0	41.0	41.0	41.1	41.1	41.1	41.1	41.2	41.2	41.3	41.3	41.4	41.5	41.7	42.3	42.9	44.6	47.1	49.7
-220	256.0	250.8	49.8	49.7	49.7	49.7	49.7	49.7	49.7	49.7	49.7	45.8	49.8	49.8	49.8	49.8	49.9	50.0	50.6	51.2	52.9	55.4	57.9
-210	260.9	255.8	58.7	58.6	58.6	58.6	58.6	58.5	58.5	58.5	58.5	58.4	58.4	58.4	58.4	58.4	58.5	58.6	59.2	59.7	61.4	63.8	66.1
-200	265.8	260.8	255.4	68.0	67.9	67.8	67.6	67.5	67.5	67.5	67.5	67.4	67.3	67.3	67.3	67.3	67.3	67.3	67.9	68.4	70.0	72.3	74.4
-190	270.7	266.0	260.8	77.5	77.3	77.2	77.0	76.9	76.8	76.8	76.8	76.5	76.3	76.2	76.2	76.2	76.2	76.2	76.8	77.2	78.7	80.9	82.8
-180	275.7	271.2	266.3	260.1	87.1	86.8	86.6	86.4	86.1	86.1	86.1	85.7	85.6	85.5	85.5	85.4	85.4	85.4	85.9	86.3	87.6	89.7	91.3
-170	280.6	276.4	271.8	266.3	260.1	97.2	96.9	96.7	96.4	96.2	95.8	95.5	95.3	95.2	94.9	94.9	94.9	94.9	95.3	95.6	96.7	98.6	99.9
-160	285.5	281.6	277.2	272.4	266.9	260.6	107.9	107.3	107.0	106.8	106.4	106.0	105.7	105.5	105.0	105.0	104.8	104.8	105.1	106.1	107.7	108.7	
-150	290.4	286.8	282.6	278.2	273.3	267.9	261.4	253.5	119.2	118.3	117.7	117.2	116.6	116.3	115.8	115.6	115.2	114.9	114.9	115.7	117.0	117.7	
-140	295.4	292.0	288.0	283.9	279.5	274.8	269.3	263.0	254.9	131.8	130.7	129.9	129.0	128.7	127.9	127.4	126.5	125.9	125.6	125.7	126.6	126.8	
-130	300.3	297.1	293.3	289.6	285.6	281.2	276.6	271.2	264.7	257.0	247.0	145.7	143.8	143.1	141.5	140.9	138.9	137.9	137.2	136.6	136.6	136.1	
-125										262.3	253.8	242.1	154.1	152.6	149.4	148.7	145.7	144.3	143.4	142.2			
-120	305.3	302.2	298.6	295.2	291.5	287.5	283.3	278.7	273.2	267.1	259.8	251.3	238.2		160.2	158.5	153.7	151.6	150.1	148.1	147.1	145.7	
-116.6										270.3	263.9	256.3	245.8	239.1	172.6	167.6	160.1	156.8	154.9	152.2			
-110	310.3	307.3	303.9	300.7	297.3	293.6	289.9	285.7	281.0	275.9	270.3	264.0	256.0	251.4	236.5	225.0	177.2	168.8	164.9	160.6	158.1	155.5	
-105										279.9	274.9	269.2	262.4	258.3	247.8	242.1	203.2	181.3	173.6	167.4			
-100	315.3	312.4	309.2	306.2	303.1	299.6	296.3	292.5	288.3	283.8	279.1	273.9	267.9	264.3	255.6	252.1	229.0	196.9	183.5	174.8	169.9	165.6	
-95										287.6	283.2	278.3	272.9	269.8	262.2	259.3	242.0	215.8	195.6	182.9			
-90	320.3	317.5	314.5	311.7	308.7	305.4	302.4	299.0	295.1	291.2	287.1	282.5	277.7	274.8	268.2	265.8	251.0	229.6	209.9	191.6	182.6	176.0	
-80	325.3	322.6	319.8	317.1	314.3	311.2	308.4	305.2	301.7	298.2	294.5	290.6	286.3	284.0	278.6	276.7	265.4	250.9	235.3	211.3	196.7	186.7	
-70	330.3	327.7	325.0	322.5	319.8	317.0	314.2	311.3	308.1	304.9	301.5	298.1	294.3	292.3	287.8	286.1	276.7	265.1	252.9	231.5	211.7	197.9	
-60	335.3	332.8	330.2	327.8	325.3	322.7	320.0	317.3	314.4	311.4	308.3	305.1	301.8	300.0	296.1	294.5	286.5	276.8	267.0	248.9	227.2	209.5	
-50	340.3	337.9	335.4	333.2	330.8	328.3	325.8	323.2	320.5	317.7	314.8	311.9	308.9	307.3	303.8	302.4	295.3	287.2	279.0	263.1	242.2	221.4	
-40	345.3	343.0	340.7	338.6	336.3	333.9	331.5	329.1	326.5	323.9	321.2	318.6	315.8	314.5	311.1	309.8	303.4	296.7	289.4	275.3	256.1	233.4	
-30	350.3	348.1	346.0	343.9	341.8	339.5	337.2	335.0	332.5	330.1	327.5	325.1	322.4	321.1	318.1	316.9	311.1	305.0	298.7	286.1	268.6	245.4	
-20	355.3	353.3	351.2	349.2	347.2	345.0	342.8	340.7	338.4	336.1	333.7	331.4	328.9	327.7	325.0	323.8	318.5	312.8	307.3	295.9	279.9	256.9	
-10	360.4	358.4	356.4	354.5	352.6	350.5	348.4	346.4	344.2	342.0	339.7	337.6	335.3	334.2	331.7	330.6	325.6	320.4	315.3	305.0	290.3	268.1	
0	365.5	363.5	361.7	359.9	358.0	356.0	354.0	352.1	350.0	347.9	345.7	343.8	341.6	340.5	338.1	337.1	332.5	327.8	323.0	313.6	299.9	278.8	
10	370.6	368.7	367.0	365.2	363.4	361.5	359.6	357.8	355.8	353.8	351.7	349.9	347.8	346.8	344.5	343.6	339.2	334.8	330.4	321.6	308.8	289.0	
20	375.7	373.9	372.3	370.6	368.8	367.0	365.2	363.5	361.6	359.6	357.6	355.9	354.0	353.0	350.8	350.0	345.8	341.8	337.6	329.4	317.4	298.7	
30	380.9	379.2	377.6	376.0	374.2	372.5	370.8	369.1	367.3	365.4	363.5	361.9	360.0	359.1	357.1	356.3	352.4	348.6	344.7	337.0	325.7	308.1	
40	386.1	384.5	382.9	381.4	379.6	378.0	376.3	374.7	373.0	371.2	369.4	367.9	366.0	365.2	363.3	362.5	358.9	355.3	351.6	344.4	333.7	317.1	
50	391.3	389.8	388.2	386.7	385.0	383.5	381.9	380.3	378.7	377.0	375.3	373.8	372.0	371.3	369.5	368.7	365.3	361.9	358.4	351.6	341.5	325.8	

Isothermal enthalpy changes with pressure include not only the experimental error of the present data, but error in the 50°F pressure-enthalpy curve. However, with respect to this curve, isothermal enthalpy changes are accurate to about 1% or 0.5 Btu/lb in the superheated gas region above -180°F, and in the fluid region above the critical temperature. The accuracy with which enthalpy changes with pressure may be calculated in the compressed liquid range is felt to be about 0.5 Btu/lb down to -160°F, but decreases considerably at lower temperatures.

Comparison of Enthalpies

The enthalpy data obtained from the data of the present experiment should be particularly useful to engineers and scientists working with methane at low temperatures and high pressures. It is felt that the pressure-enthalpy-temperature diagram presented represents a considerable improvement on previous compilations of thermodynamic properties of methane. Comparisons of the basic measurements and some of the enthalpy data have been presented in previous sections, in order to give the reader an idea of the accuracy and reliability of these measurements and the charts obtained from them. In the following, the enthalpies are compared to those from previous compilations or calculated from previous data.

Saturated Liquid Enthalpies

The enthalpy of saturated liquid methane from -280°F to the critical point is compared in Figure 28 to enthalpies calculated from the saturated heat capacity data of Wiebe and Brevoort[76] and Hesterman and White.[30] The values shown for Wiebe and Brevoort were taken directly from their publication, and changed slightly to agree with the basis H=0

at -280°F. The values shown for Hesterman and White were obtained by integration of Equation (17),

$$\Delta H_{sat} = \int_{T_1}^{T_2} C_{SL} dT + \int_{P_1}^{P_2} V dP \qquad (17a)$$

where the first integral was obtained by graphical integration of the data and the second taken from Wiebe and Brevoort. Since Hesterman and White's measurements went only to -260°F, lower values were assumed to be the same as those of Wiebe and Brevoort.

The values of the present experiment agree well with those of Wiebe and Brevoort throughout the temperature range investigated except that the enthalpy of the critical point differs by about 9 Btu/lb. Hesterman and White are considerably higher than the present experiment. It should be noted that the liquid enthalpies of the present experiment below -160°F are dependent upon extrapolation of the integrated data as described in the previous section. They cannot be considered of high accuracy, and part of the 3 Btu/lb difference between the present enthalpy and that of Hesterman and White at -160°F could be due to the extrapolation of the present data. However, Hesterman and White's values continue to be higher and reach a maximum of 7 Btu/lb greater than the present experimental values at -125°F. Part of the disagreement may be because the methane used by Hesterman and White was considerably purer than that of the present experiment, but still the disagreement seems unusually high.

Latent Heats of Vaporization

The smoothed latent heats of vaporization from the enthalpy chart, and those obtained by direct measurement are compared in Figure 29

to the direct measurements of Frank and Cluzius[24] and Hesterman and White[30] and those calculated by Matthews and Hurd[52] and Keesom.[35] The latent heats measured in the present experiment are slightly lower than the others, and agree well with the measurements of Hesterman and White. The smoothed values from the pressure-enthalpy-temperature heat are in agreement with Hesterman and White's measurements, but tend to be about 1% low at the lower temperatures. This is primarily due to the difficulty in extrapolation of enthalpies of the compressed liquid to low pressure at these temperatures.

In measuring the latent heats of vaporization, the bubble point and dew point lines were determined as a function of pressure and temperature for the methane used. This data is compared to the vapor pressure data of Hesterman and White for pure methane in Figure 30.

Enthalpy Differences

Table XIX compares selected enthalpy differences from the present experiment to those of Matthews and Hurd[52] and Keesom.[35] It is apparent from this comparison that both compilations contain serious inaccuracies. Both give accurate values of enthalpy differences for gases at low pressures, and Keesom's values at higher temperatures (0 to 50°F) appear to be in good agreement up to 2000 psia, the limit of the present experiment. Matthews and Hurd show considerable disagreement in all temperature ranges at pressures above 600 psia. The most serious disagreements in both compilations appear to be at high pressures and low temperatures near the critical temperature.

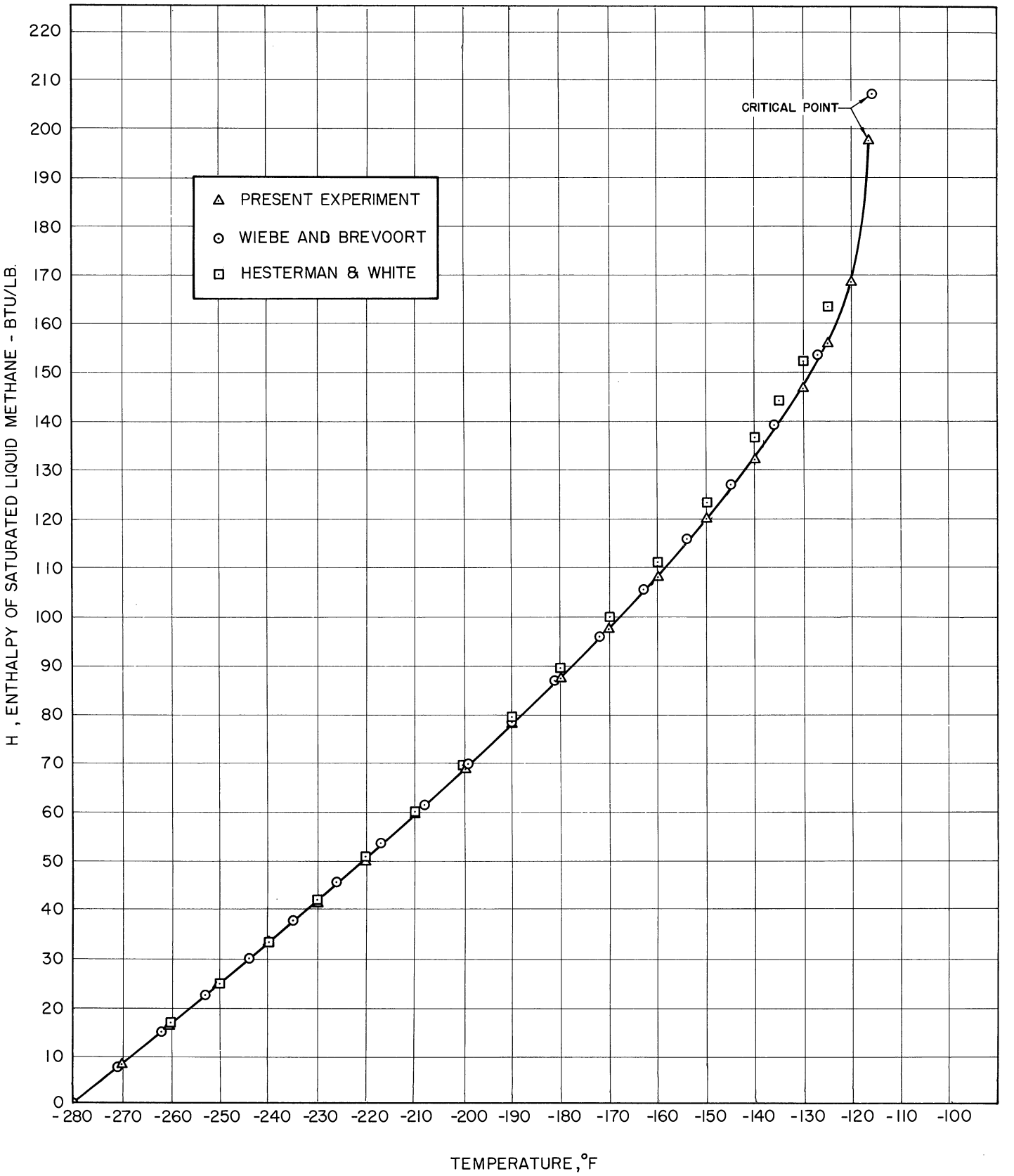

Figure 28. Comparison of Saturated Liquid Enthalpies of Methane

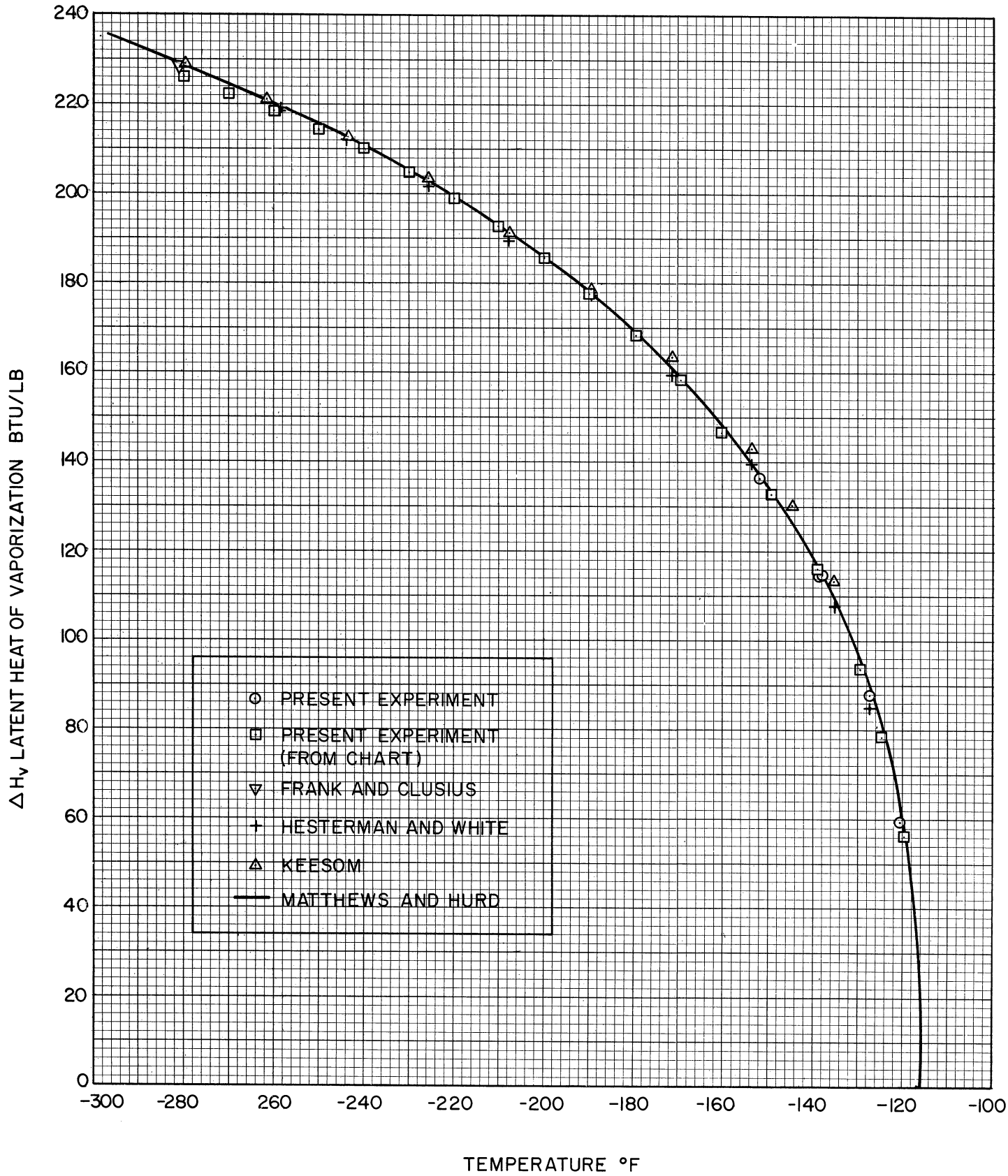

Figure 29. Comparison of Latent Heats of Vaporization of Methane.

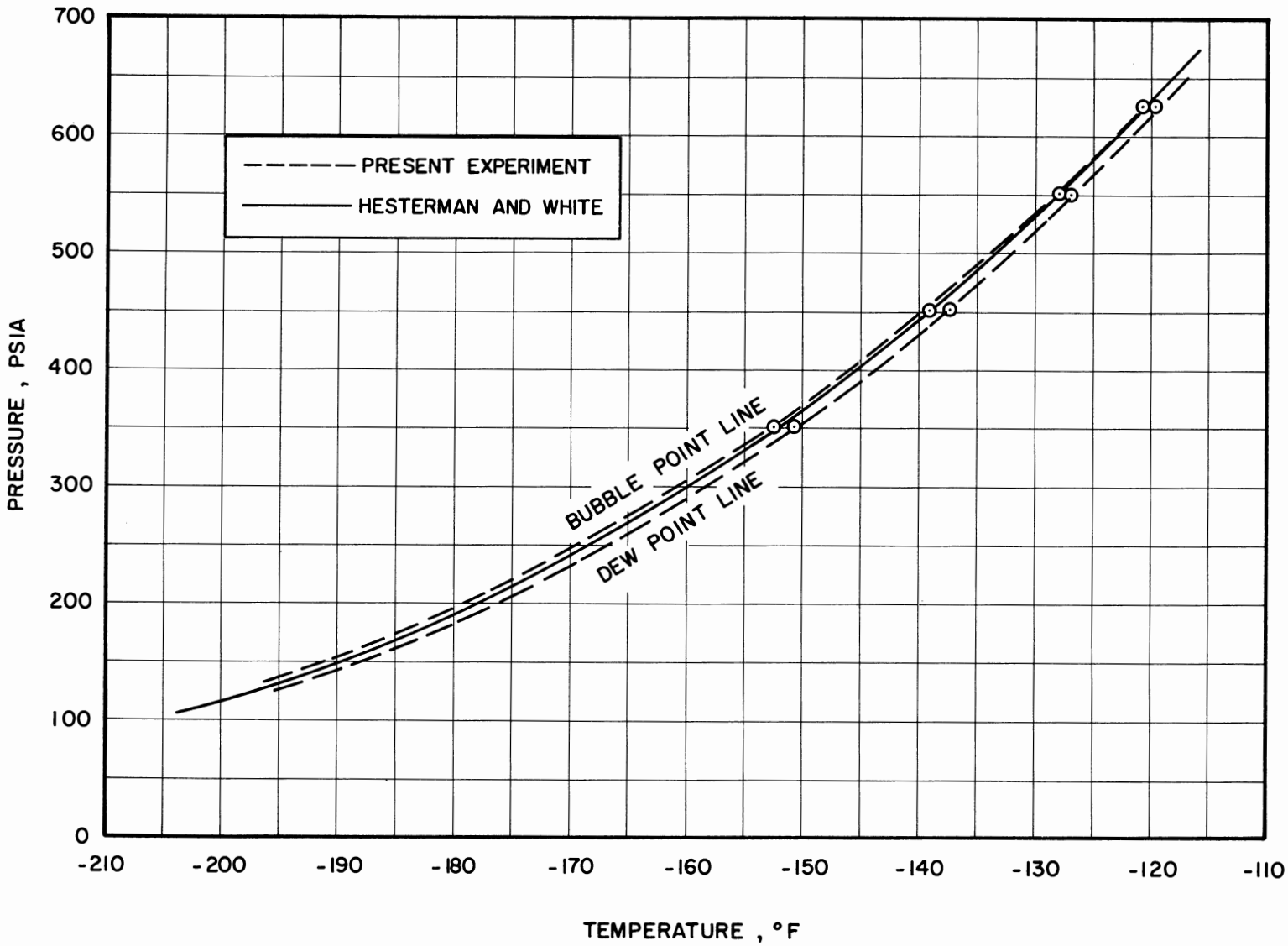

Figure 30. Comparison of Vapor Pressure of Methane.

TABLE XIX

COMPARISON OF ISOBARIC ENTHALPY DIFFERENCES OF METHANE

Pressure Psia	Temperature T_1 °F	Temperature T_2 °F	Experimental Enthalpy Diff. Btu/lb	Matthews and Hurd Derived Enthalpy Diff. Btu/lb	Matthews and Hurd $\left(\frac{\text{Der.}-\text{Exp.}}{\text{Exp}}\right)\times 100\%$	Keesom Derived Enthalpy Diff. Btu/lb	Keesom $\left(\frac{\text{Der.}-\text{Exp.}}{\text{Exp}}\right)\times 100\%$
150	-250	-200	43.8			43.4	-0.9
	-180	-100	46.1	46.5	0.9	45.9	-0.4
	-100	0	53.7	54.1	0.7	54.0	0.6
	0	50	26.9	26.9	0.0	26.8	-0.4
300	-250	-170	72.7			69.3	-4.7
	-150	-50	64.4	63.8	-0.9	63.1	-2.0
	-50	50	56.1	57.2	2.0	56.0	-0.2
600	-250	-200	42.7			40.7	-4.7
	-200	-130	76.5			74.7	-2.5
	-110	-50	52.9	51.2	-3.2	49.3	-6.8
	-50	50	63.1	65.4	3.7	63.0	-0.2
800	-250	-150	90.0			88.0	-2.2
	-150	-100	113.8			113.5	-0.3
	-100	-50	66.3	59.4	-10.4	59.7	-10.0
	-50	+50	70.0	71.7	2.4	69.9	-0.1
1000	-250	-150	88.4			86.5	-2.1
	-150	-90	95.0			101.5	6.8
	-90	0	113.1	105.1	-7.1	106.9	-5.5
	0	50	35.4	37.2	5.1	35.2	-0.6
1500	-250	-150	86.1			83.7	-2.8
	-150	-70	94.7			98.4	3.9
	-70	0	88.2	94.1	6.7	87.5	-0.8
	0	50	41.6	46.3	11.3	41.6	0.0
2000	-250	-150	84.2			80.6	-4.3
	-150	-100	47.9			50.8	6.1
	-100	-50	55.8			59.0	5.7
	-50	0	57.4			56.3	-1.9
	0	50	47.0			46.9	-0.2

RECOMMENDATIONS FOR FUTURE WORK

1. The equipment should be modified to eliminate the pressure fluctuations presently encountered in the measurement of liquid heat capacities and latent heats of vaporization at pressure below 300 psia. Since these fluctuations lessen with lower flow rates, perhaps the best approach would be the enlargement of passages where liquefaction or vaporization occur, including the heating baffles within the calorimeter.
2. Joule-Thomson equipment should be perfected in order to define enthalpy as a function of pressure at a greater number of places than possible in the present experiment.
3. The pressure balance used to determine the pressure of the measurement should be modified or replaced inorder to provide higher accuracy and faster response to pressure changes.

SUMMARY AND CONCLUSIONS

1. Flow calorimetric equipment was perfected to the extent that measurements of isobaric heat capacity (C_p) and latent heat of vaporization of light gases and their mixtures may be measured reliably to $\pm 0.5\%$ and $\pm 1\%$, respectively at temperatures from -250°F to 50°F, at pressures from 150 to 2000 psia. The only serious problem remaining is that liquefaction and vaporization of gases in the system cause instabilities which interfere greatly with the measurement of liquid heat capacities and latent heats of vaporization at pressures below 300 psia.
2. Measurements were initially made on nitrogen, and included the latent heat of vaporization at 350, 400 and 450 psia, gaseous heat capacities from 150 to 2000 psia at 32, -50, -100 and -150°F, and compressed liquid heat capacities at -240°F from 400 to 2000 psia.
3. The latent heat of vaporization of methane was measured at 350, 450, 550 and 625 psia. The heat capacity of methane was measured throughout the temperature range -250°F to 50°F at pressures to 2000 psia. Particular emphasis was placed on the critical region and other areas where heat capacity changes greatly with pressure and temperature.
4. The experimental values of latent heat of vaporization agree well with previously measured and derived values. Equations of state which fit the volumetric data allow calculation of gaseous enthalpies under pressure with good accuracy at the higher reduced temperatures; however, they appear to give results of poor accuracy for dense gases at high reduced densities, particularly in the critical region.

5. The experimental data for methane was used in coordination with certain properties from the literature to construct a new pressure-enthalpy-temperature diagram for methane, which allows calculation of enthalpy differences to about $\pm 1\%$. Recent compilations of thermodynamic properties show good agreement with this diagram at higher temperatures and moderate pressures, but are shown to allow inaccuracies of 5 to 10% in calculations of enthalpy differences at low temperatures and high pressures, and in the region of the critical point.

APPENDIX A

ACCURACY OF THE RESULTS

The accuracy of data of the types obtained in the present experiments is difficult to evaluate. In the following sections the many factors involved in obtaining a reasonable estimate of this accuracy are discussed in detail, with respect to both the measurements and the treatments applied. In general the discussion will be centered upon the results for methane, the discussion being applicable to the earlier results for nitrogen.

Accuracy of the Measurements

The accuracy of each measurement is directly dependent upon the measurements of heat input, temperature rise and flow rate, and less directly dependent upon the measurements of pressure and calorimeter bath temperature.

Heat Input

The quantity of heat introduced into the calorimeter is determined with the highest accuracy of any major measurement. Heat input is calculated by the equations,

$$Q = \frac{E_c I_c}{17.581} \text{ watt/Btu/Min} \tag{36}$$

where

$$I_c = \frac{E_{L1}}{R_1} - \frac{E_{L2}}{R_5} \tag{37}$$

$$E_c = \frac{E_{L2}}{R_5} (R_5+R_8+R_9) \tag{38}$$

For the purpose of errors calculation, these equations may be rewritten as

$$I_c = \frac{E_{L1}}{R_1} \tag{39}$$

$$E_c = E_{L2}\left(\frac{R_8+R_9}{R_5}\right) \tag{40}$$

which contain only the major terms.

Since the accuracy of each of the resistors is 0.01%, the wide limits of accuracy due to the resistors is 0.01% for the current, I_c, and 0.02% for the voltage, E_c.

In each of these equations, additional error is added by the potentiometer readings, E_{L1} and E_{L2}. For the typical reading the values would each be about 40,000 microvolts, measurable to $\pm$(0.01% + 2μV) or 0.015%, as given in the specifications for the medium range of the potentiometer in Table XXXII, Appendix E. It is apparent that for lower heat inputs the accuracy would be lower, and for higher heat inputs accuracy would approach 0.01%. Nevertheless, 0.015% is a value which covers the majority of cases.

The wide limit of error, then, is the addition of the errors due to the resistors and the potentiometer readings: % error = 0.01% + 0.02% + 0.015% + 0.015% = 0.06%.

It is difficult to justify further treatment of this measurement by use of statistical methods, but it is felt that a more realistic evaluation of the error involved may be obtained by compounding the errors due to the resistors and the potentiometer as though they were the standard deviations of a number of determinations. The necessary

equations are presented and/or derived in a good number of books on statistical methods such as Volk[75] or Wilson,[77] regarding compounding of errors. The primary equation with which we are concerned is,

$$\sigma(y) = \left\{ \sum_{i=1}^{n} \left[\frac{\partial y}{\partial x_i} \sigma(x_i) \right]^2 \right\}^{1/2} \tag{41}$$

where σ is the standard deviation (or in this case the guaranteed accuracy) and y is a measurement related to the components x_i by the relation,

$$y = y(x_1, x_2, \ldots, x_n) \tag{42}$$

Equation (41) may be used for percentage or fractional errors by dividing through by y, to give

$$\frac{\sigma(y)}{y} = \left\{ \sum_{i=1}^{n} \left[\frac{1}{y} \frac{\partial y}{\partial x_i} \sigma(x_i) \right]^2 \right\}^{1/2} \tag{43}$$

Treating the function Q and its components with this equation, we have,

$$\begin{aligned} \frac{\sigma(Q)}{Q} &= \left[\left(\frac{\sigma(E_{L1})}{E_{L1}}\right)^2 + \left(\frac{\sigma(R_1)}{R_1}\right)^2 + \left(\frac{\sigma(E_{L2})}{E_{L2}}\right)^2 + \left(\frac{\sigma(R_5)}{R_5}\right)^2 \right. \\ &\quad \left. + \left(\frac{\sigma(R_8)}{R_8+R_9}\right)^2 + \left(\frac{\sigma(R_9)}{R_8+R_9}\right)^2 \right]^{1/2} \\ &= \left[(0.015)^2 + (0.01)^2 + (0.015)^2 + (0.005)^2 + (0.005)^2 \right]^{1/2} \\ &= 0.026\% \end{aligned} \tag{44}$$

Considering the above, and the fact that about 0.01% uncertainty may be added due to instability of the power supply, the accuracy of the heat input measurement is taken as $\pm 0.05\%$.

Temperature Rise

The calibrations of the thermocouples used to measure the temperature rise through the calorimeter are shown in Table XXXI. Thermocouple G25691T was used in most of the experiments and will be considered here.

There is no way to obtain a really accurate estimate of the accuracy of the measurement of temperature rise through the calorimeter. The cubic equation used to fit the calibration data appears to be satisfactory, and fits the data to an average of one microvolt. Since the large majority of temperature rises measured produced emfs of the order of 1000 to 2000 microvolts, it could be implied from Table XXXI, Appendix E that the thermocouple is capable of accuracy of the order of 0.05 to 0.1%. However, more uncertainties are added by factors other than the calibration. A slight error may be caused by the thermocouple measuring a temperature other than the true temperature of the gas, due to heat transfer or kinetic effects, but calculations show that errors due to these effects are extremely small. However, in order to eliminate the effects due to heat transfer through the thermocouple wires, it was necessary to work the wires around various tubes or objects at the appropriate temperatures, tie them in place, and contact them thermally by use of Apiezon grease or epoxy resin. This treatment undoubtedly caused some stress and deformation of the constantan wires, which in turn would cause the thermocouple to deviate from its calibration. The fact that the thermocouple is six-junction will reduce this effect to some extent, but the uncertainties caused are indeterminate. Osborne, Stimson and Sligh[60] showed that temperature differences of the order of 10°C may be measured

to about 0.2% with carefully calibrated one-junction copper constantan thermocouples, and it is felt that the present thermocouple is of high enough quality to surpass this accuracy. Erros due to reading the emfs generated with the potentiometer is $\pm(0.01\% + 0.2\mu V)$ which corresponds to $\pm 0.03\%$ for a 1000 μV reading and $\pm 0.02\%$ for a 2000 μV reading.

Overall accuracy for the measurement of temperature rise is felt to be within 0.15 to 0.2% from the above considerations. It should be noted, however, that the precision with which any one temperature difference may be measured corresponds approximately to the error of the potentiometer, $\pm 0.03\%$. This means that in the correction for heat leakage where measured heat capacity is plotted versus reciprocal flow rate at constant temperature rise through the calorimeter, error of the thermocouple will be constant, and only the error of the potentiometer will enter into the extrapolation to infinite flow rate.

Flow Rate Measurement

The flow metering data was correlated by the equation

$$\frac{\rho_m \Delta P_m}{\mu F} = a_o + a_1\left(\frac{F}{\mu}\right) + a_2\left(\frac{F}{\mu}\right)^2 + a_3\left(\frac{F}{\mu}\right)^3 \qquad (23)$$

where $\rho_m \Delta P_m$, μ and F are the density, pressure drop, viscosity and flow rate of the gas through the meter, and a_o, a_1, a_2 and a_3 are calibration constants obtained by a least squares fit of the data. The errors may best be analyzed by inspection of the term $\frac{\rho_m \Delta P_m}{\mu F}$, which is shown in Figure 8, plotted versus $\frac{F}{\mu}$. The errors of measurement involved in the flow calibration are listed in Table XX and are felt to be good estimates of the standard deviations of the various measurements. When the